Optimisation of bipedal walking motion with unbalanced masses.

Mahmoodi, Pooya

Optimisation of Bipedal Walking Motion with Unbalanced Masses

Pooya Mahmoodi

College of Engineering
Swansea University

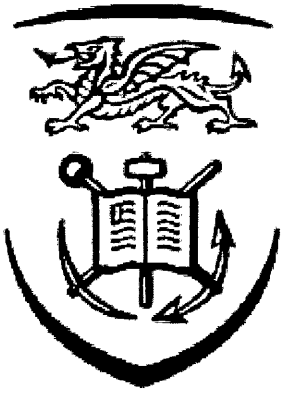

Swansea University
Prifysgol Abertawe

Submitted to Swansea University in fulfilment of the requirements for the degree of Doctor of Philosophy

August 2014

ProQuest LLC.
789 East Eisenhower Parkway
P.O. Box 1346
Ann Arbor, MI 48106 – 1346

Declaration

This work has not previously been accepted in substance for any degree and is not being concurrently submitted in candidature for any degree.

Signed ... . (candidate)

Date .....08/02/2014.....

STATEMENT 1

This thesis is the result of my own investigations, except where otherwise stated. Where correction services have been used, the extent and nature of the correction is clearly marked in a footnote(s).

Other sources are acknowledged by footnotes giving explicit references. A bibliography is appended.

Signed .. .. (candidate)

Date .....08/02/2014.....

STATEMENT 2

I hereby give consent for my thesis, if accepted, to be available for photocopying and for inter-library loan, and for the title and summary to be made available to outside organisations.

Signed ... . (candidate)

Date .....08/02/2014.....

Acknowledgments

First, I would like to thank my supervisor, Dr Rajesh Ransing for his endless help, encouragement, patient, support, and most importantly, his friendship throughout my research work. I would also like to thank Prof Mike Friswell for his expertise and support during the time and a special thanks to Dr Nick Owen for his help with the experiments.

I would like to thank everyone in College of Engineering at Swansea University for creating very friendly and supportive research Environment in which to work.

Thanks also go to my wonderful friends for providing fun times.

A huge thank you goes to my family, especially to my parents and my sister for their unbounded help and encouragement.

Last and foremost, I want to thank my wife, Farzaneh for her love and support over the years.

Summary

Commercial prosthetic feet weigh about 25% of their equivalent physiological counterparts. The human body has a tendency to overcome the walking asymmetry resulting from the mass imbalance by exerting more energy.

A two link passive walking kinematic model, with realistic masses for prosthetic, physiological legs and upper body, has been proposed to study the gait pattern with unbalanced leg masses. The 'heel to toe' rolling contact has significant influence on the dynamics of biped models. This contact is modelled using the roll-over shape defined in the local co-ordinate system aligned with the stance leg. The effect of roll-over shape curvature and arc length has been studied on various gait descriptors such as average velocity, step period, inter leg angle (and hence step length), mechanical energy. The bifurcation diagrams have been plotted for point feet and different gain values. The insight gained by studying the bifurcation diagrams for different gain and length values is not only useful in understanding the stability of the biped walking process but also in the design of prosthetic feet.

It is proposed that the stiffness and energy release mechanisms of prosthetic feet be designed to satisfy amputee's natural gait characteristics that are defined by an effective roll-over shape and corresponding ground reaction force combinations. Each point on the roll-over shape is mapped with a ground reaction force corresponding to its time step. The resulting discrete set of ground reaction force components are applied to the prosthetic foot sole and its stiffness profile is optimised to produce a desired deflection as given by the corresponding point on the roll-over shape. It is shown that the proposed methodology is able to provide valuable insights in the guidelines for selection of materials for a multi-material prosthetic foot.

TABLE OF CONTENTS

List of Figures

List of Tables

Chapter 1 Introduction

1.1 Introduction

Once a human learns to walk in childhood, the walking becomes one of the main body locomotion and helps the human to move from one place to another. Very soon the ability to achieve stable walking is taken for granted. While at first glance walking may appear simple but in reality the computational modelling of a stable walking process is a challenging task. Investigation of the stable walking becomes even more complex when body has a tendency to walk asymmetrically e.g. in situations faced by lower limb amputees.

1.2 Lower limb amputees walking motion

Amputees with a unilateral transtibial and transformal amputation have approximately 20-30% more metabolic cost of walking than able-bodied persons (Gailey et al., 1994, Waters and Mulroy, 1999) and also, they preferred to walk 30-40% slower (Hsu et al., 2006). Several researchers have proposed that the metabolic cost needed for locomotion during the single support phase is minimised by reducing the inertia of the prosthetic leg (Royer and Martin, 2005, Gitter et al., 1997, Czerniecki et al., 1994, Donn et al., 1989, Kurz et al., 2008, Mattes et al., 2000). However, the inertial asymmetry affects the symmetry of gait (Mattes et al., 2000). The lower limb amputees power their physiological and prosthetic legs differently during walking (Engsberg et al., 1991) and the resulting asymmetric load can lead to joint degeneration and pain so that up to 71% of lower limb amputees have complained of lower back pain (Burke et al., 1978b, Hurley et al., 1990, Hurwitz et al., 2001, Radin et al., 1973). Lower limb amputees have poor stability when they walk on an inclined surface due to limit range of ankle motion and ankle power generation that lead to reduced ground reaction forces, speed and single support phase time in the prosthetic leg (Vickers et al., 2008).

It is reported in the literature that lower limb prosthesis users expend 16% more metabolic cost (VO_2) and heart rate (HR) per unit distance during walking than abled participants (Gailey et al., 1994). There is evidence that clinical conditions such as

diabetes, stroke, hemiplegia or even old age influence the gait profile. The gait speed and step length (step period) influences the stability and increases the risk of falls (Espy et al., 2010). A method to capture forefoot, midfoot and hindfoot motion during different gait tasks has been proposed (Sawacha et al., 2009) and it showed statistically significant differences in forefoot kinematics parameters over the full gait cycle. The kinematic and kinetic gait profiles in individuals with chronic stroke have been studied (Kim and Eng, 2004) and it was found that the magnitude and pattern of these profiles related to gait performances. Distinctly different walking patterns as characterised by roll-over shapes in patients with hemiplegia following a stroke have been reported in the literature (Fatone and Hansen, 2007).

In summary, there is strong evidence in the literature that for lower limb amputees significant number of external factors including kinematic and kinetic parameters affect person's gait characteristics that can make walking inefficient, and in certain situations, unstable. The effects of these factors must be accounted for in a computational model for bipedal walking motion.

1.3 Bipedal walking motion

The three-dimensional bipedal motion is normally defined in three planes namely sagittal, frontal and transvers planes while the motion of a planar biped is described as occurring in a sagittal plane. The sagittal plane divides the body into right and left portions. The frontal plane is the plane perpendicular to the sagittal plane that divides the body into front and back sections. The transverse plane is perpendicular to both the frontal and sagittal planes and separates the body into upper and lower portion (See Figure 1.1).

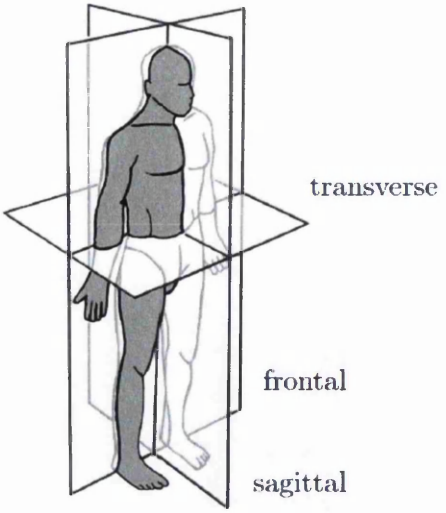

Figure 1.1. Description of transverse, fontal and sagittal planes (Westervelt, 2003).

A stable gait has been classified into three categories: namely a statically, quasi-statically and dynamically stable gait (Westervelt et al., 2007).

- **Statically stable gait:** The biped gait is said to be statically stable if the projection of Centre of Mass (COM) remains within the convex hull of the foot support area (Goswami, 1999) during the single or double support phase. In double support phase both legs are in contact with the ground at the same time.

- **Quasi- statically stable gait:** The biped gait is said to be quasi-statically stable if the Centre of Pressure (COP) of the biped remains inside the support polygon. The COP is also known as the Zero Moment Point (ZMP). The concept of ZMP was presented by Vukobratovic and Juricic (1969) and is widely used as a criterion to control biped walking so that the ZMP does not leave the foot support area. ZMP is a point on the ground where the net moment of the inertial forces and the gravity forces has no component along the horizontal axes (Vukobratovic and Borovac, 2004).

- **Dynamically stable gait:** The biped gait is said to be dynamically stable if the COP remains on the boundary of the convex hull of the foot support area for at least part of the cycle while the walking is still stable (Westervelt et al., 2007). Human gait is not statically and quasi-statically stable as during a significant part

of the human gait cycle the projection of the human's COM is outside the support area and also the position of the human's COP is on the boundary of the support polygon. Therefore, ZMP can't be used to study the stability of the bipedal walking.

In order to simplify a computational model, the number of degrees of freedom (DOF) of the body that correspond to the number of joints are normally reduced. For example, during the single support phase, the stance leg remains almost straight so that the knee joint can be ignored and the whole leg can be considered as a single link. Figure 1.2 shows bipeds that are modelled with one DOF (Figure 1.2a) to a very high number of DOF (Figure 1.2e). Biped is modelled with a single mass and an inverted pendulum in Figure 1.2a to estimate the stance leg motion trajectory and is compared with experimental data (Gard and Childress, 2001). Figures 1.2b and c (Garcia et al., 1998, Freidovich et al., 2009) describe a biped model with two links (2-DOF) and an upper body mass on hip joint and the leg's mass for Figure 1.2b is assumed to be very small while the model in Figure 1.2c has more realistic leg's mass. Both models were passive and could walk down a shallow inclined surface without using any active elements. However, they assume point feet and hence are unable explain the effect of rolling motion of the feet during walking. In Figure 1.2d upper body is modelled as a link namely torso that is connected to the hip joint (La Hera et al., 2013). The biped is actuated at the hip joint to control the stability of the posture during walking on level ground. Figure 1.2e shows a 9-DOF (the five joint angles and two feet plus the Cartesian coordinates of the hips) active biped with knee joint and a lumped mass located on each link (Hurmuzlu et al., 2004). However, the model is not able to present the rolling motion of the foot.

As shown in Figure 1.2a-e, the biped locomotion is normally studied as an open kinematic chain consisting of legs and often an upper body segments. The Legs and the Upper body is represented by one or multiple links that depend on the number of joints that take part in the motion analysis such as knee joint, ankle joint and shoulder joint. One or both legs may be in contact with the ground during walking that divides a walking cycle into two phases namely single support phase and double support phase respectively.

The double support phase usually takes only about 10-20% of the human walking cycle and it depends on the walking speed. The percentage of the double support phase throughout a walking cycle decreases with increase in the walking speed and it diminishes during running. Therefore for simplicity, the double support phase is regularly assumed to be instantaneous. It is also true that most of the researchers described the single support phase as a continuous single support phase so that the body swings about a pivot point and a set of differential equations analyse the biped motion and describe the dynamics (Asano et al., 2005, Garcia et al., 1998, Goswami et al., 1996, Goswami et al., 1998, McGeer, 1990, Srinivasan et al., 2009).

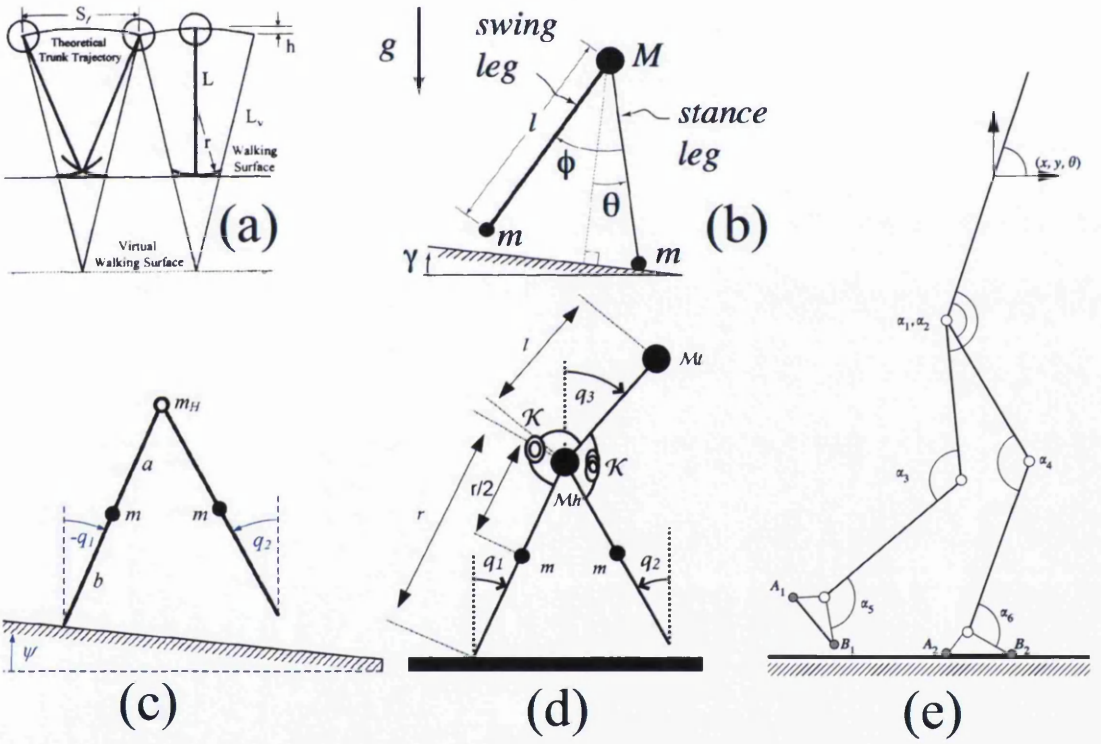

Figure 1.2. Biped models configurations with different DOF. (a) Biped motion modelled with an inverted pendulum (1-DOF). (b) and (c) show 2-DOF biped model with very small legs mass and more realistic mass respectively. Kneeless 3-DOF biped model with torso is presented in (d). (e) shows a 9-DOF biped model with knee, ankle and hip joints (Garcia et al., 1998, Gard and Childress, 2001, Freidovich et al., 2009, Hurmuzlu et al., 2004, La Hera et al., 2013).

These assumptions, however, do not take into account the contribution from the ankle kinematic and feet into the equation of motion. The contact event during double support phase leads to a discontinuity in motion. These issues must be addressed whether the walking cycle is modelled as a passive or active motion.

1.4 Scope and objectives of the work

The musculoskeletal system of the human body in gait simulation has been studied in recent years although it seems that many of the interactions between the body segments, including the ankle-foot system (Hansen, 2002), and the strategy that a human body takes to have a stable walking on a level surface to an uneven surface is neither fully understood nor applied in computational models.

The aims of this research study are as follows:

1. To develop a kinematic model of a biped configuration using laboratory data on human ankle-foot motion.
2. To study the effect of ankle/foot mechanism on the walking symmetry and stability.
3. To develop a numerical method for computation of dynamics of the biped configuration
4. To optimise the prosthetic foot design using the numerical model.

All of these objectives were achieved and the research has resulted into the following publications:

- P Mahmoodi, RS Ransing & MI Friswell, Amputee specific initial alignment of a prosthetic foot based on the optimal roll-over shape. *(under preparation)*

- S Aristodemou, P Mahmoodi, RS Ransing & MI Friswell, Prosthetic Foot Design Optimisation Based on Roll-Over Shape and Ground Reaction Force Characteristics. *(under preparation)*

- P Mahmoodi, RS Ransing & MI Friswell, 2013. Modelling the Effect of 'Heel to Toe' Roll-over Contact on the Walking Dynamics of Passive Biped Robots. *Applied Mathematical Modelling* 37, 7352-7373.

- P Mahmoodi, RS Ransing & MI Friswell, Understanding the Influence of Input Variables on the Stability of a Two Linked Robot. *UK National Conference on Computational Mechanics in Engineering,* Southampton University, 29-31 March 2010.

1.5 Layout of the thesis

Chapter 1 Introduction: The background, research need and the objectives of the research are introduced in this chapter.

Chapter 2 Literature Review: The existing commercial prosthetic foot designs are reviewed and their weaknesses and strengths discussed. This comparison is useful as one of the objectives of the research is to explore how the knowledge discovered in this research can be used to enhance the existing prosthetic foot designs. During the initial literature review, a concept of roll-over shape, which was used by the experimental community to characterise the human gait, was discovered. The applicability of the roll-over shape is reviewed in detail as this concept has been used in this research to mimic the ankle-foot kinematics. The literature review that relates to Chapters 3, 4 and 5 is written in the respective chapters.

Chapter 3 Modelling the Effect of 'Heel to Toe' Roll-over Contact on the Walking Dynamics of Passive Biped Models: This chapter begins with a review of kinematic models used for simulating biped walking in robotic as well as biomechanics applications. A novel roll-over contact model has been proposed and to the best of author's knowledge, the proposed model has, for the first time, allowed modelling of the rolling motion of a stance leg foot during level walking. In order to discover inherent trends and relationships among various kinematic and kinetic parameters on the stability of biped walking process, a passive walking model with a heel to toe non-circular rolling contact has been proposed. The effect of roll-over shape on the stability of biped locomotion is studied using bifurcation diagrams and the phase plane limit cycles. The effect of bipedal parameters on gait descriptors such as mechanical energy, average velocity, step period and inter- leg angle is also investigated.

Chapter 4 Optimising the 'Heel to Toe' Roll-over Shape for Symmetric Passive Bipedal Walking Motion With Unbalanced Masses: This chapter extends the passive bipedal model suggested in Chapter 3 with realistic legs mass and length with an upper body mass located on the hip joint. The model developed in Chapter 3 assumed equal masses for both legs. However, most of the commercially available prosthetic feet weigh just over quarter of their biological counterparts. This mass imbalance has direct influence on the respective positions of the centre of masses and subsequently on the walking stability. For a given roll-over shape at the physiological foot, the proposed mathematical formulation allowed determination an optimal roll-over shape for the prosthetic foot. The passive model, again, allowed visualising inherent relationships and trends among various kinematic and kinetic parameters. Bifurcation diagrams and phase plane limit cycles provided further insights.

Chapter 5 Prosthetic Foot Design Optimisation Based on Roll-Over Shape and Ground Reaction Force Characteristics: It is proposed in this chapter that an optimally determined roll-over shape be used to compare the foot deflection of a prosthetic foot when subjected to transient ground reaction forces. The roll-over shapes and the corresponding ground reaction forces were measured experimentally and used to optimise the stiffness profile of three prosthetic feet. The literature review has indicated that the proposed approach and the recommended design guidelines in this chapter are novel and original.

Chapter 6 Conclusion and Future Work: Every chapter has its own conclusions, however, the overall conclusions of this research are highlighted in this chapter and future research tasks and challenges are also discussed.

Chapter 2 Literature Review

2.1 Introduction

Walking is one of the major daily activities of humans. The analysis of a human gait is still an active area of research. The research on analysing biped walking normally focuses on enhancing the understanding of how body parts interact with each other during walking. The benefit of this research is transferable to many applications e.g. improving comfort levels of tanstibial and transformal amputees during walking, designing biped robots, improving able or disable athletes performance and etc. The effect of various gait parameters on the gait stability is still not fully understood and with the advances in the prosthetic industry the need for advanced computational models is ever growing. A concept of roll-over shape or effective rocker has recently been proposed by many researchers (Hansen and Childress, 2009, Hansen et al., 2004a, Knox, 1996, Ren et al., 2010) to model the effective feet shape by simplifying the complexity of ankle motion during a walking step. Therefore, it is felt appropriate to review the state-of-the-art on commercially available **prosthetic feet** and the experimental findings on the **roll-over shape concept** before presenting the research undertaken in this thesis.

2.2 Prosthetic feet

The evolution of prosthetics has a long and storied history. Some of the reasons for amputations in the past were Reynaud's phenomenon, leprosy, frostbite and trauma and in the Middle East, punishment for crimes was the most common reason for amputation. Lower limb amputation is still an option for dire medical emergency and historically, in some parts of the world, a severe form of punishment (Friedmann and Lawrence, 1972). In Peru, amputating feet as a punishment date from about 300 B.C. (Friedmann and Lawrence, 1972). There are reports of well known persons who have also received prosthetic devices during Persian and Roman times. Herodotus, in his History, written in 484 B.C., tells of a Persian soldier, Hegesistratus, captured by the enemy, imprisoned in the stocks, and encased by his foot. He escaped by cutting off part of his foot, and replaced it later with a wooden prosthesis (Wilson, 1972).

In the recent years, the prosthetic technology has advanced significantly thereby improving the comfort, control and aesthetics of prosthetic feet and minimising the psychological impact on using these feet (Plettenburg, 1998) and individualising the prosthetic feet for amputees with different level of activity (Postema et al., 1997). Historically, proesthetic foot are designed to imitate the human physiological foot in form and function (Romo, 1999).

Amputees rely more on their physiological leg than their prosthetic leg during walking, which lead to asymmetry gait, greater physiological leg ground reaction forces, joint powers and joint moments. This asymmetric gait and loading of the physiological and prosthetic legs can lead to osteoporosis in the prosthetic leg, osteoarthritis in the physiological leg and lower back pain in amputees (Burke et al., 1978a, Engsberg et al., 1991, Gailey et al., 2008, Kulkarni et al., 2005). Prosthetic feet have been developed over years to enhance the activities of the amputees and aid them to walk more naturally. They are classified in three categories namely Conventional Feet (CF), Energy-Storing-and-Returning (ESAR) feet, and recently Bionic feet (Versluys et al., 2008).

2.2.1 Conventional feet

Prior to the early 1980s, conventional prosthetic feet were designed with the goal of restoring basic walking and simple occupational tasks.

Conventional prosthetic feet are passive devices constructed by a rigid wooden keel, surrounded by a combination of foam and other materials and they can't fully represent mechanical characteristics of the able-bodies lower leg biological system. In spite of conventional prosthetic leg limitations, they can still allow individuals with lower leg amputation to return to many functional activities (Sinitski et al., 2012).

In the past the Solid Ankle Cushion Heel (SACH) foot have been the most common designs in the conventional prosthetic foot. A SACH foot has been used for years in the United States and Britain (Cuiham EC et al, 1984; Doane NE et al, 1983; Goh JCH et al, 1984), and because it is inexpensive and robust, it's still prescribed frequently especially in low income countries (Rino Versluys et al, 2008).

The Jaipur foot is also a conventional foot which is waterproof, durable with high tensile strength and high impact resistance, low-cost, and also can be used with or without shoes. Jaipur foot is helping over 1.2 million amputees in the world. The SACH foot has a better shock absorption capacity than the Jaipur foot as the heel consists of a rubber wedge while the performance of the Jaipur foot is more natural and sense of limping is less as compared to the SACH foot (Arya et al., 1995, Adalarasu et al., 2011).

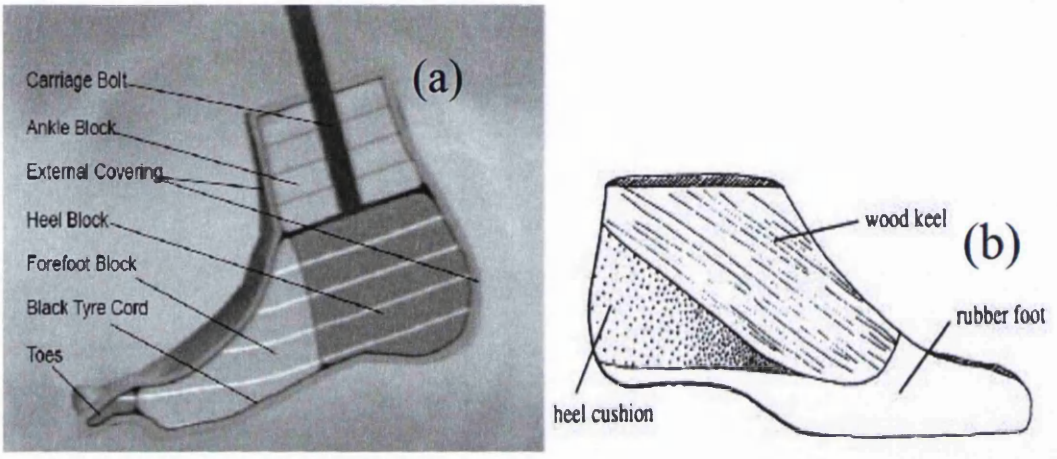

Figure 2.1. A sagittal section of the Jaipur foot (a) and the SACH foot (b) (Adalarasu et al., 2011).

2.2.2 Energy-Storing-and-Returning (ESAR) feet

Energy storing and returning (ESAR) feet have been developed due to the development of elastic lightweight materials, improvement of amputee gait and also the desire for amputees to participate in athletics and sport. ESAR feet are made of a lightweight carbon fibre construction and vary in cost and complexity (Romo, 1999). ESAR feet deflect due to ground reaction force and return to its original shape when the load is removed.

According to Ventura et al. (2011), understanding the influence of energy return and ankle dorsiflexion on amputee gait are important to design prosthetic feet that aid amputees in achieving natural gait motion. Elasticity and flexibility of the ESAR feet can decrease skin problems although they don't seem to decrease stump pain (Alaranta et al., 1994).

The keel of the conventional feet are rigid and prevent the prosthetic foot dorsiflexion while the keel of ESAR feet have springs which allow sufficient dorsiflexion, thereby decreasing the load on the sound side.

Most of the energy in the conventional feet is dissipated in the material, whereas ESAR feet assist the propulsion of the body as it is designed to store and release energy during single support phase and toe off (beginning of the next single support phase) respectively (Versluys et al., 2008). Differences between conventional and ESAR prosthetic feet are often studied using kinematics and stride characteristics (Postema et al., 1997).

The literature indicates that the amputee gait with ESAR foot is improved as compared to conventional foot in the following ways: the self-selected walking speed is increased (Snyder et al., 1995), prosthetic leg stride length and propulsive forces are increased (Perry and Shanfield, 1993, Powers et al., 1994), ankle dorsiflexion and energy storage and return of the prosthetic foot is increased (Ventura et al., 2011) and peak vertical ground reaction forces (GRFs) on the physiological leg are decreased (Lehmann et al., 1993, Perry and Shanfield, 1993, Powers et al., 1994, Snyder et al., 1995). However, more active and less body weight amputees have more benefit of using ESAR feet than the other amputees (Alaranta et al., 1994) thereby, for markedly overweight amputees the SACH foot can be a better choice (Wirta et al., 1991).

Ernest M. Burgess developed the first ESAR foot namely the Seattle foot in 1985. In order to improve running performance, the foot used a patented spring, called a monolithic keel, made of a strong and lightweight material called Delrin®, a DuPont product. The spring helped the patient push off in taking a step. It did so by storing energy when the foot initially stepped down, and then releasing that energy when the heel left the ground as the step is completed. The result was a more natural, springy step than is possible with a conventional prosthetic foot (http://www.washington.edu/research/pathbreakers/1985a.html). The Seattle foot is the heaviest solid ankle design commercially available and it's constructed for the moderate to higher activity ambulatory and aims at mobility rather than stability (Drongelen, 2000).

The Flex-Foot is another type of the ESAR foot composed of a carbon and fibreglass shaft, which store energy during heel contact and extends during toe off (Romo, 1999). There are no differences in walking speed for moderately active transtibial amputees during walking with Flex-Foot and SACH foot although Flex-Foot improved the symmetry of walking and the range of ankle joint motion during late stance (Wagner et al., 1987). Lehmann et al. (1993) presented that walking with Flex-Foot as compared to SACH foot had longer midstance phase, greater ankle angle range and greater forward movement of the centre of pressure. Although the use of the flex foot enhanced the push-off power and the plantarflexor moment for the prosthetic feet as compared to the conventional feet, these values are still less than the physiological leg (Underwood et al., 2004).

Prosthetic foot still has limited mechanical energy return e.g. SACH foot 39%, Seattle foot 71% and Flex foot 89% while the human foot returns 246% mechanical energy (Gitter et al., 1991).

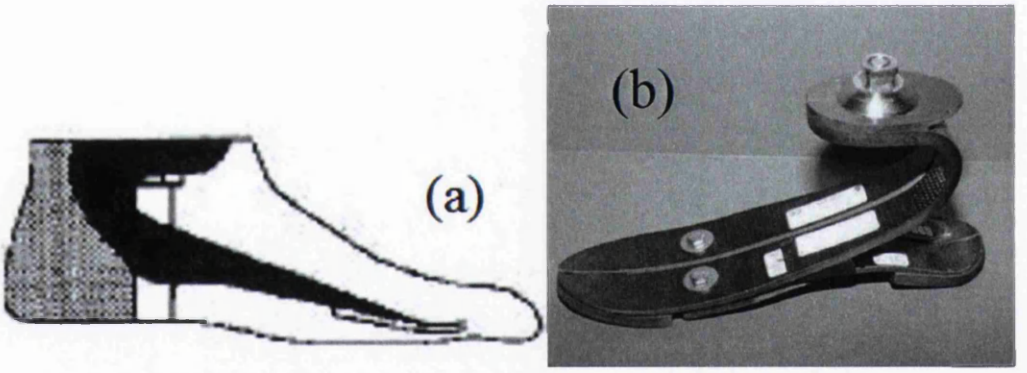

Figure 2.2. A cross section of the Seattle foot (a) (Hafner et al., 2002) and the Flex-Foot (b) (Underwood et al., 2004).

2.2.3 Bionic feet

A human body with 80 kg weight at 0.8Hz walking rate requires 36 Joules of energy and 250W of peak power per step (Hitt et al., 2007). Conventional and ESAR foot use passive components and return much less mechanical energy as compared to the physiological foot as the physiological ankle produces more energy than it absorbs. Active components have been developed to improve the efficiency of the prosthetic

feet as they become more comparable with the physiological leg (Bergelin and Voglewede, 2012).

Bionic feet are defined as mechanical devices with an active component that are worn by a transtibial amputee. Most of the Bionic feet are currently at a research stage and they can be categorised based on their electronically driven devices, pneumatically driven devices and actuation principle (Versluys et al., 2009).

Ossur Proprio-Foot is one of the first bionic feet (Versluys et al., 2009). The technology behind the PROPRIO FOOT consist of three steps namely Sense (Sensor Technology), Think (Artificial Intelligence) and Act (Active Ankle Motion). Angle sensor records ankle motion in every millisecond and also detects the moment of heel strike (when the swing prosthetic feet contacts the ground). The motion data is then analysed to identify whether the amputee is walking, stationary or seated as well as type of walking surface such as inclined surface, level surface and stairs. In the next step, the motion data is input to a patented form of artificial intelligence called Terrain Logic. Terrain Logic determines the most appropriate prosthetic foot ankle flexion for a walking step based on the ankle motion trajectory from previous stride. In the final step a lightweight, precision stepper motor moves the prosthetic foot components so that the ankle flexion matches with the desired flexion and adjust the heel height regarding to the shoe height (http://www.ossur.com/?PageID=15736). Although Ossur Proprio-Foot has active elements it's considered to be a passive design as active elements don't generate energy during prosthetic leg stance phase (Bergelin and Voglewede, 2012).

SPARKy prosthetic leg is another type of bionic feet which is developed at Arizona State University with the aim of bringing physiological ankle function to transtibial amputees (Bellman et al., 2008). SPARKy uses a robotic tendon actuator to actively stretch springs when the ankle rolls over the foot, thereby allowing the springs to provide its users with 100% of the push-off power required for walking. This is comparable to able body's gait while maintaining gait kinematics (Hitt et al., 2007). Robotic tendon actuator reduces the peak power required for an electric lightweight motor to provide the power required for gait by adjusting the position of a finely tuned spring (Hitt et al., 2009). Inspite of energy efficiency of the SPARKy foot, the

design of the foot as shown in Figure 2.3b is rather large as compared to the physiological leg as well as the amputated leg profile.

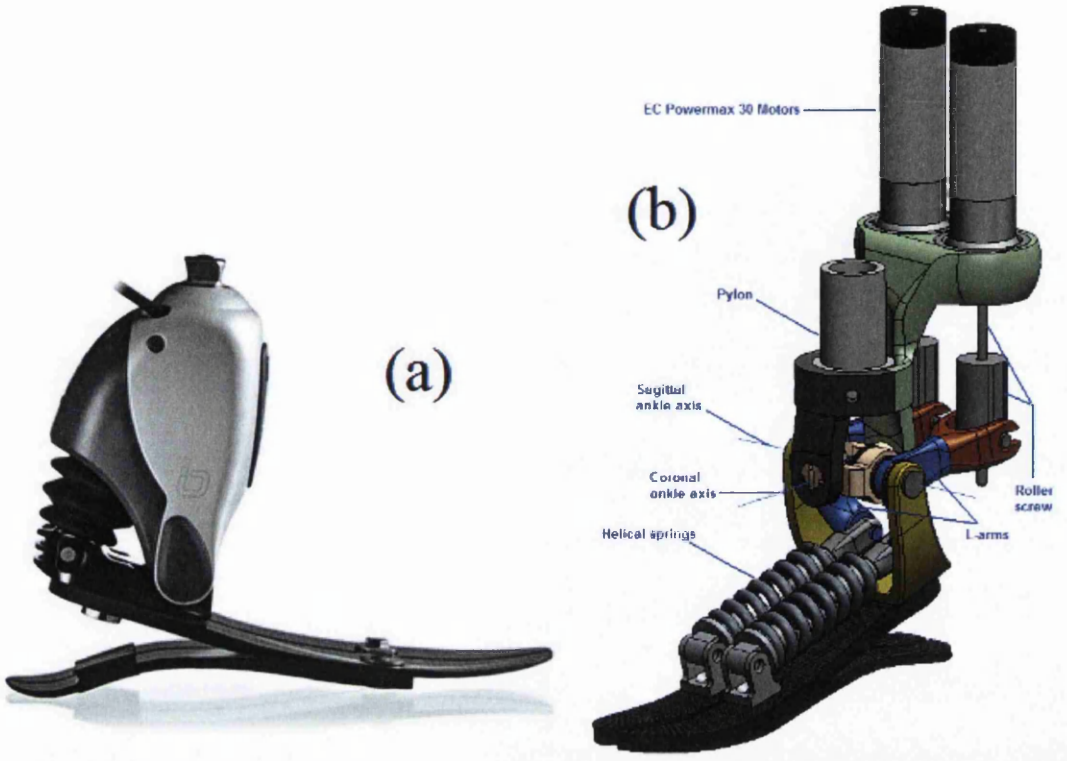

Figure 2.3. A PROPRIO FOOT (a) (http://www.ossur.com/?PageID=15736) and the SPARKy foot (b) (Bellman et al., 2008).

2.3 Roll-Over Shapes

A roll-over shape is a very useful tool to analyse ankle and the whole body kinematics. Figure 2.4 describes the basic premise of roll-over shape measurement by determining the location of contact points of a wheel with a rolling surface. In the global coordinate system, a series of contact points produces a straight line on a rolling surface (Hansen et al., 2004a). However, the points present a rolling geometry around the wheel if the locations of same points are determined with respect to a coordinate system fixed on the wheel as shown in Figure 2.4. The rolling wheel in this example was rigid and the locations of contact points in wheel-based coordinate system could be easily measured by tracing the circumference of the wheel. However, this method can be used to measure a roll-over shape of a flexible object such as prosthetic foot. Roll-over shape presented by Hansen et al. (2000) is a locus

of centre of pressure in a local co-ordinate system so that its origin is located on ankle joint system with x and y-axis perpendicular (in the direction of toe) and aligned to the shank (towards the hip) during the rolling motion of the single support phase. Adamczyk et al. (2006) defined roll-over shape as a rigid arc which is identified by measuring the deformation of the human foot/ankle system and capturing the position of the body at the same time. In their experiments, subjects wore seven wooden arc shaped boots of varying radius and they found a geometric relationship between COM work and the amount of angle of COM velocity changes before and after swing leg impact. Finally they found that the COM velocity change and step-to-step transition work are a function of foot radius of curvature so that the centre of mass work decreases by increasing arc radius. Bar-Cohen and Breazeal (2003) is also described the roll-over shape as an effective rocker geometry that the human locomotor system conforms during the stance phase of walking.

Regarding the definition of the local coordinate system, Hansen et al. (2002 and 2004a) classified the roll-over shape in four categories namely Foot roll-over shape, Ankle-Foot (AF) roll-over shape, Knee-Ankle-Foot (KAF) roll-over shape and Hip-Knee-Ankle-Foot (HKAF) roll-over shape.

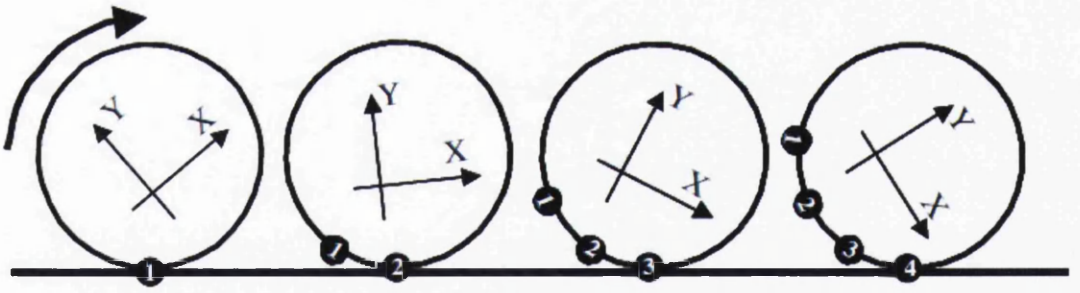

Figure 2.4. The location of contact points of a rolling wheel with ground are on a straight line in the coordinate system of the rolling surface. However, at the same time the points of contact reflect the geometry of the wheel in a wheel-based coordinate system (X-Y) (Hansen et al., 2004a).

2.3.1 Foot Roll-over shape

Hansen et al. (2004a) measured roll-over shape experimentally using a foot-based coordinate system. Heel, forefoot and ankle markers were used to determine the foot-based coordinate system so that the origin is presented by the ankle marker and the

X-axis is defined to be in the direction of a vector starting at the heel marker and going through the forefoot marker (see Figure 2.5a).

2.3.2 Ankle-Foot (AF) Roll-over shape

The origin of the local coordinate system of the AF roll-over shape is located on ankle joint and its y-axis is parallel to the shank. Hansen (2002) determined the local coordinate system experimentally by using two markers located on the ankle and the knee respectively and then the roll-over shape was measured by determining the location of centre of pressures with respect to their corresponding local coordinate system from heel contact to opposite heel contact (see Figure 2.5b).

2.3.3 Knee-Ankle-Foot (KAF) Roll-over Shape

In order to measure the KAF roll-over shape two markers were used to determine the trajectories of an ankle joint and a hip joint. The first one was located on ankle joint same as the AF roll-over shape and the second one located on hip joint. The y-axis of the local coordinate system is defined as a line which is passed through the ankle joint and the knee joint (see Figure 2.5c).

2.3.4 Hip-Knee-Ankle-Foot (HKAF) Roll-over Shape

The HKAF roll-over shape is measured in a similar manner as the KAF and AF roll-over shape. The trajectory of the body centre of mass (BCOM) is determined by using a marker which is approximated as the centroid at any instance of the left ASIS (anterior superior iliac spine), the right ASIS, and the sacral markers (Hansen, 2002). The other marker is located on ankle joint so that a line which connects the BCOM and the ankle joint describes the y-axis of the local coordinate system (see Figure 2.5d). Positions of the centre of masses for all types of roll-over shape are identical and are found in global coordinate system. During the single support phase of able-bodied normal walking, knee joint remains almost straight and the AF, KAF and HKAF roll-over shape are very similar to each other.

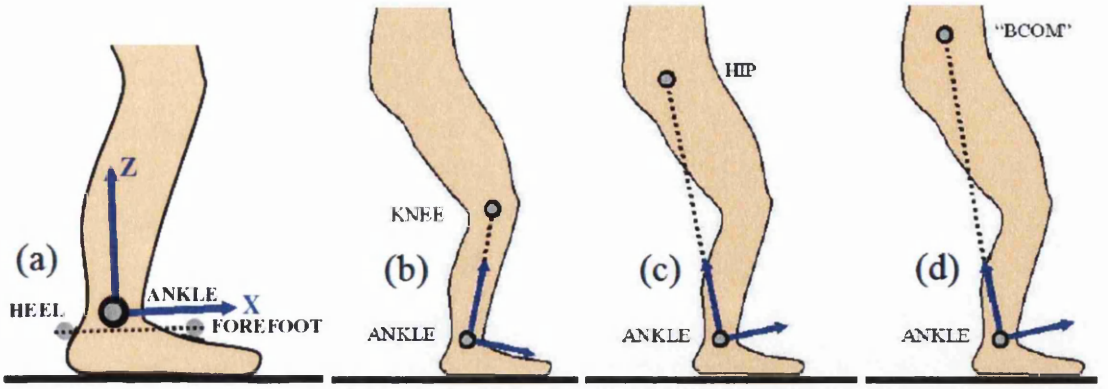

Figure 2.5. a,b, c and d describe the local coordinate system for Foot, Ankle-Foot (AF), Knee-Ankle-Foot (KAF) and Hip-Knee-Ankle-Foot (HKAF) systems respectively (Hansen, 2002, Hansen et al., 2004a). The origins of all local coordinate systems are located on ankle joint. The x-axis of Foot system is parallel to a line which connects the heel marker to forefoot marker and the y-axis of AF, KAF and HKAF starts from the ankle marker towards knee marker, hip marker and body centre of mass (BCOM) marker respectively.

2.3.5 Effect of various walking conditions on the roll-over shapes

Knowledge of physiological roll-over shape characteristics on different walking conditions such as walking with different speeds, heel heights and on inclined surfaces may help in development of new generation of prosthetic feet that can adapt to the changes automatically. As a result the published literature on this topic is reviewed next.

The effect of walking speed on roll-over shape

In order to study the effect of walking speed on roll-over shape Hansen et al. (2004a) performed an experiment on 24 able-bodied subjects (14 female and 10 male) with five speed ranges. The results presented that the roll-over shape does not change significantly as the walking speed of a subject decreases or increases (see Figure 2.6). However, Hansen et al. (2004a) found that the walking speed slightly affects the arc length, the vertical and horizontal positioning of the radii of the arc and the vertical and horizontal positioning of the arcs. This is however considered as statistically insignificant.

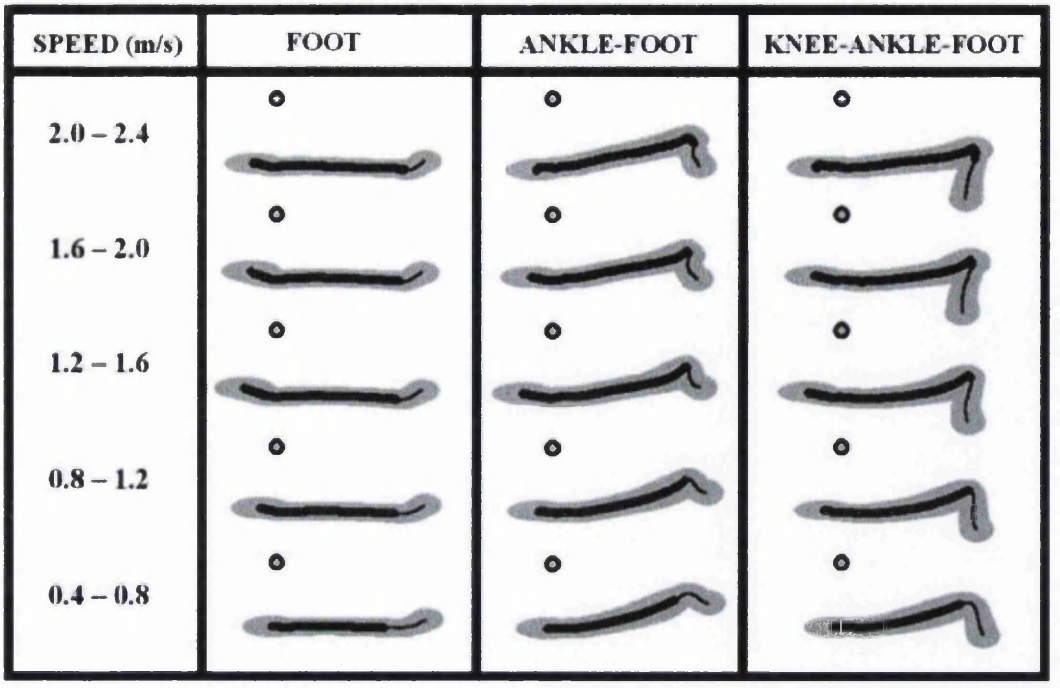

Figure 2.6. Foot, AF and KAF roll-over shape for five different range of walking speed (Hansen et al., 2004a).

The effect of added weight on roll-over shape

Carrying heavy objects is another human daily task which might affect the roll-over shape. Hansen and Childress (2005) studied the effect of added weight on roll-over shape by performing an experiment on 10 young able-bodied subjects (five female and five male) with various weight starting from 51.1 kg to 100.9 kg. The roll-over shape is measured for each subject at three different speed (slow, normal and fast) while the subjects carried an added weight of 00.0kg, 11.5kg and 23.0kg.

The results presented that the roll-over shape did not change during walking when the subjects carried different weights. It is observed that the able-bodied human can maintain the roll-over shape irrespective of added weights by powering the body joints as necessary (see Figure 2.7).

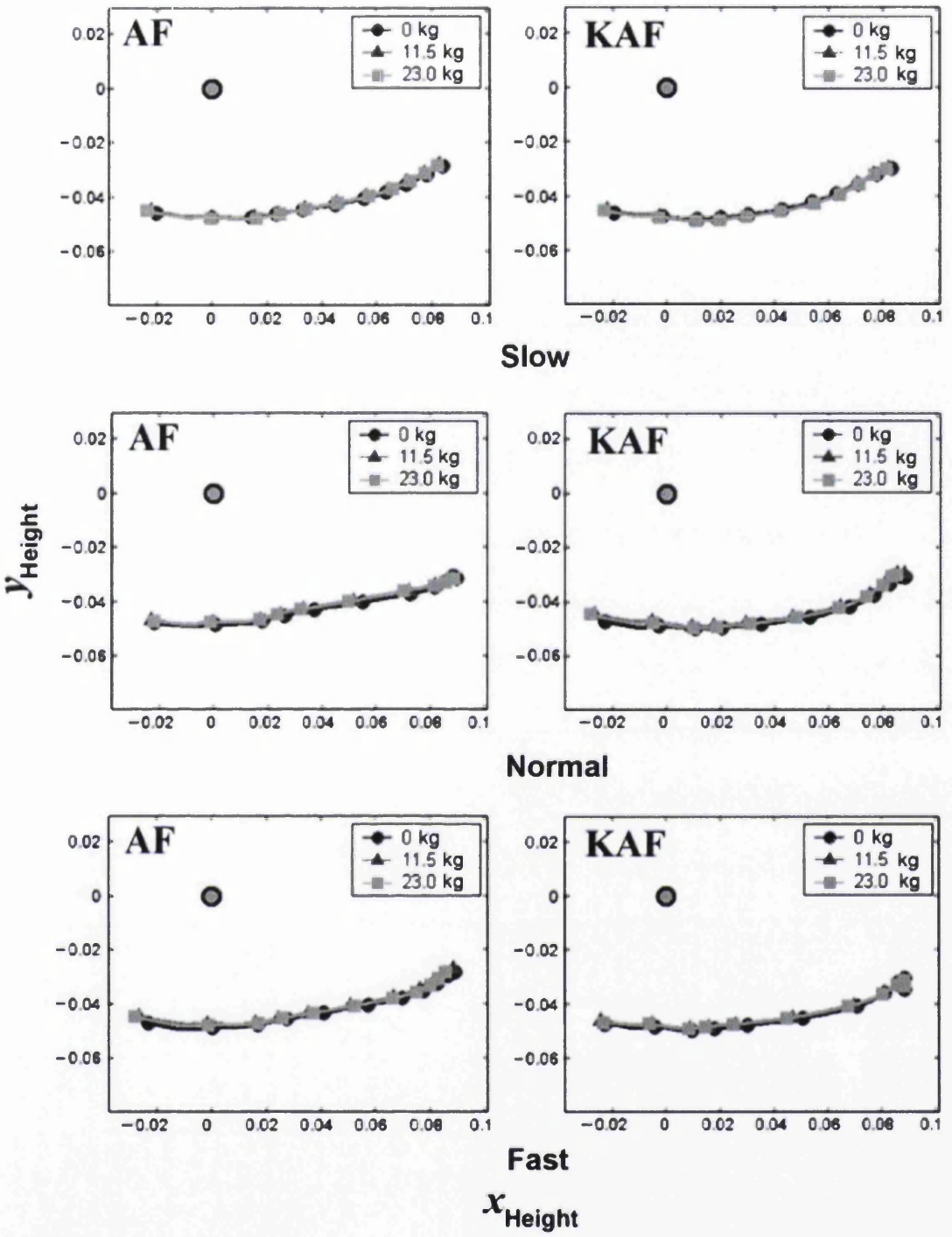

Figure 2.7. AF and KAF roll-over shape for walking with 0 kg, 11.5 kg and 23 kg added weight (Hansen and Childress 2005).

The effect of shoe heel height on roll-over shape of physiological and prosthetic feet

A common observation is that able bodied individuals often wear shoes of different heel heights without experiencing much difference in the overall stability during the walking process (de Lateur et al., 1991, Opila-Correia, 1990). The most probable reason for this observation is that able-bodied individuals are able to adapt their ankle motion in conjunction with other subtle changes at the knee to compensate for the effects introduced by different shoe heights. Choi et al. (2005) studied the effect of shoe heel height on roll-over shape of five able female volunteers who walked on a level surface. Each subject wore four pairs of shoes with different heel heights so that it started from 0 (no heel) to 9 cm heel height.

The results performed by Choi et al. (2005) show that the roll-over shape for different shoe heel height remained almost constant although by decreasing the heel height the distance between the rolling contact points and ankle joint decreased and therefore, the roll-over shape moved upwards (See Figure 2.8). It can be concluded from this observation that the able-bodied persons are able to adjust their ankle motion so that the roll-over shape remains almost constant for different heel height. The same results have been also observed by Hansen and Childress (2009).

A recent study by Hansen and Childress (2009) examined the effect of shoe heel height on the roll-over shapes of prosthetic ankle foot systems (see Figure 2.8b). They used seven prosthetic feet and plotted the corresponding roll-over shapes. The length and the slope of the forefoot part of the roll-over shape were noticeably different in each case. It was observed that the orientation of the roll-over shape changed for a prosthetic foot for different shoe heights and the prosthetic foot was unable to adapt to the ankle motion on its own. However, it was possible to align the roll-over shape by manually adjusting the heel height of the prosthetic shoe.

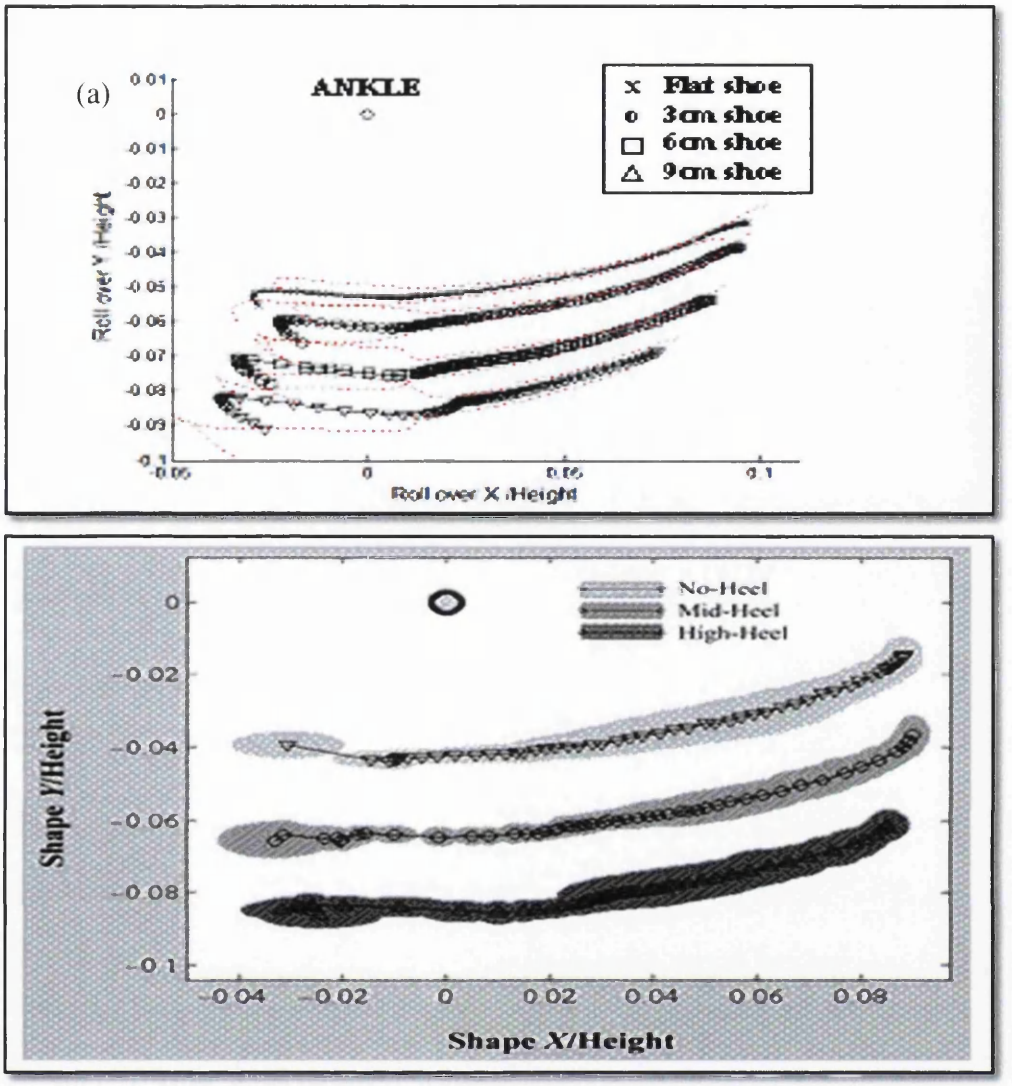

Figure 2.8. (a) and (b) present roll-over shapes of able-bodied persons with different show heel height and are studied by Choi et al. (2005) and Hansen and Childress (2009) respectively. The roll-over shapes in both graphs remained almost constant as the shoe heel height changed.

The effect of inclined surface on roll-over shape

Hansen et al. (2004b) studied the effect of changing the slope angle of a surface on the roll-over shape by performing an experiment on ten subjects who walked on a level surface, a 5^{o} surface and a 10^{o} surface at their normal self-selected speed. The roll-over shape of ankle foot (AF) and knee-ankle-foot (KAF) systems were measured and the results show that AF and KAF roll-over shape are oriented corresponding to levels of inclination for uphill walking while for downhill walking

just the KAF roll-over shape oriented and the AF retained the level walking orientation (see Figure 2.9). The orientation of KAF roll-over shape for uphill and downhill walking is anti-clockwise (dorsiflexion) and clockwise (plantarflexion) respectively.

The effect of prosthetic forefoot flexibility on roll-over shape

The effect of prosthetic forefoot flexibility was further studied by Klodd et al. (2010) in a double blind randomised cross over study to determine the effects of forefoot flexibility on the gait of 14 unilateral transtibial prosthesis users. It was discovered that when prosthetic feet had excessively flexible forefoot sections, they provided shorter effective foot lengths, reduced ankle moments on the prosthetic side and introduced a 'drop off' effect when the body weight was transitioned from the prosthesis to the intact limb. However, the forefoot flexibility does not influence the oxygen intake of persons with unilateral trans-tibial amputations. Hansen et al. (2006) also studied the effect of the roll-over shape arc length on the gait of unilateral trans-tibial prosthetic users. It was found that participants experienced higher loads on their sound limbs at various walking speeds when the roll-over arc length of the prosthetic foot was shortened. There was also an indication of a reduction in step length.

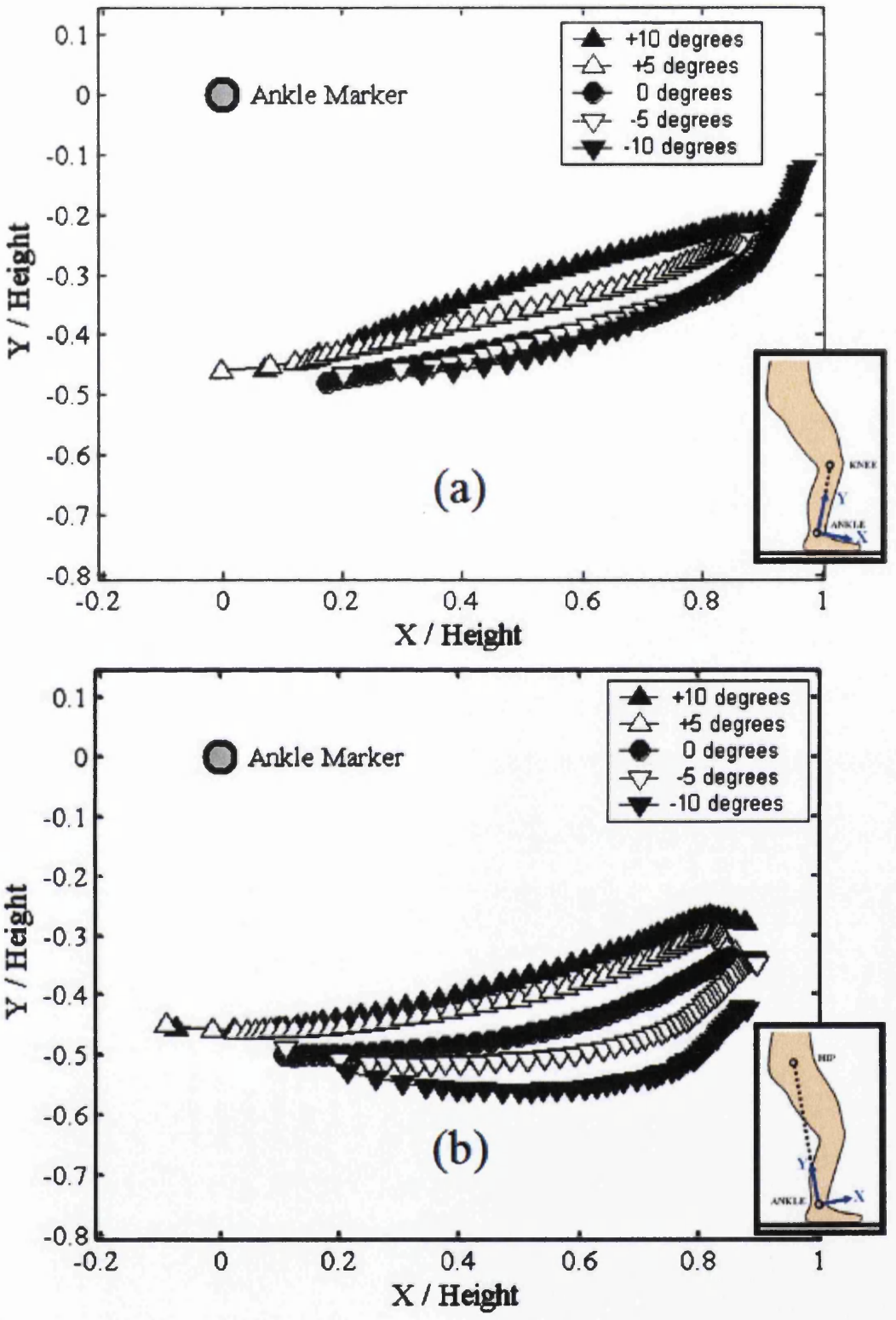

Figure 2.9. The AF (a) and KAF (b) roll-over shape for downhill, level and uphill walking (Hansen et al., 2004b). The roll-over shape of AF system is oriented for uphill walking while the KAF roll-over shape oriented with all different levels of inclination.

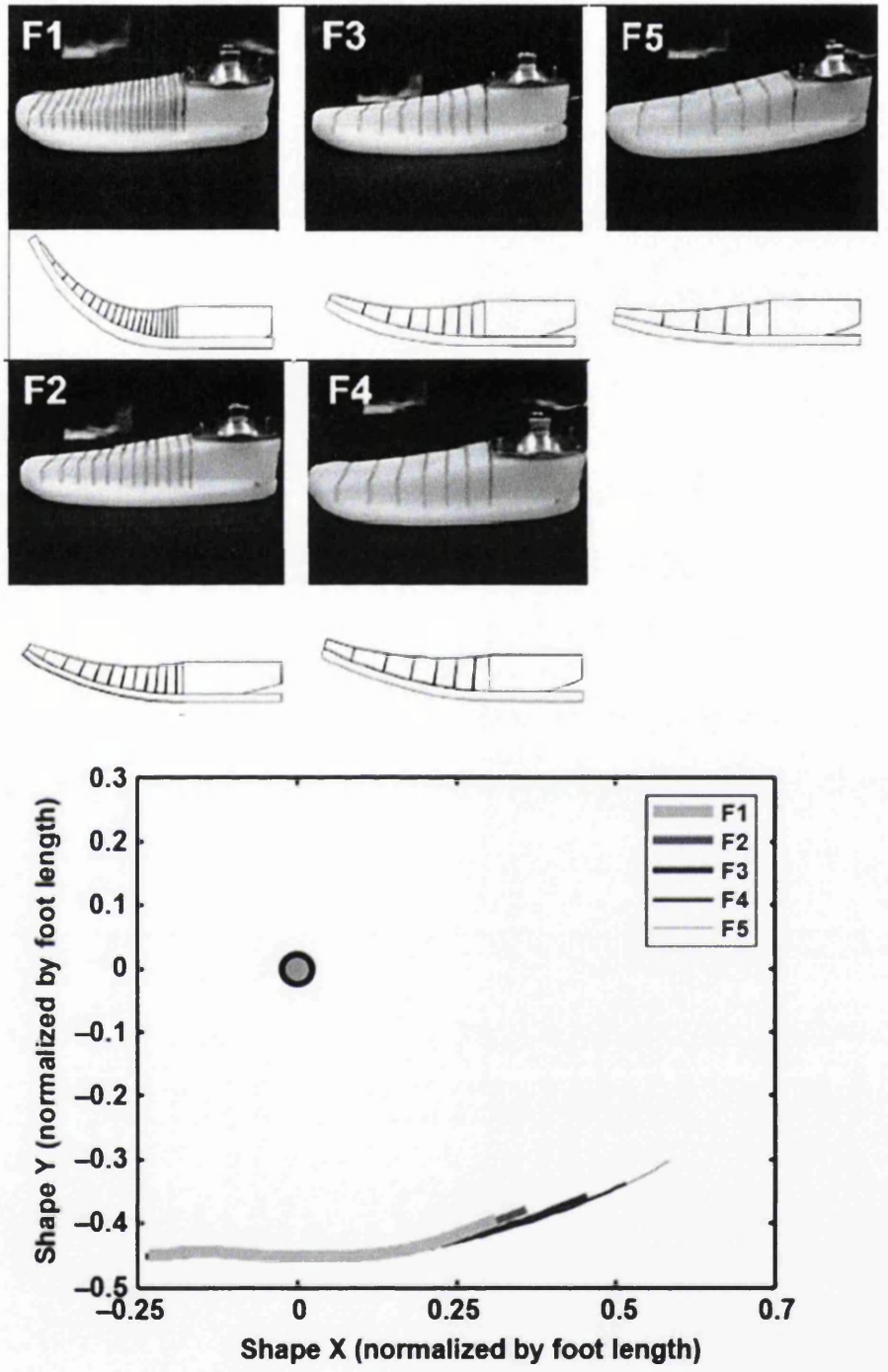

Figure 2.10. roll-over shape of five different prosthetic feet with different flexibility (Klodd et al., 2010).

The effect of stair ascent/decent on roll-over shape of physiological and prosthetic feet

The effect of roll-over shapes based on stair ambulation was performed experimentally by Sinitski et al. (2012). The data collected from the experiment was used to determine the human kinematics and kinetics, torque-angles, and lastly the effective roll-over shapes during each condition for each subject that took part in the experiment. The subjects underwent a single biomechanical gait assessment while walking on a level ground, and up and down a custom 16-step instrumented staircase. The results obtained from the experiment are illustrated in Figure 2.11. The black line, the dark gray line and the light gray line represent the level ground, stair ascent and stair descent roll-over shape respectively and the ankle joint is located on origin and is shown by a circle. Each roll-over shape consists of a solid line and an extended dotted line. The solid line presents the roll-over shape during single support phase and the dotted line describes the roll-over shape when both legs are in contact with the ground (double support phase).

When prosthetic limb individuals had to walk up the staircase constructed it was found that they were unable to power the prosthetic leg as compared to the able bodied persons. Walking down the stairs the prosthetic limbs had limited dorsiflexion and plantarflexion motions. In summary, the prosthetic limbs were unable to mimic the roll-over shapes recorded for the able-bodies during stair ascent amputations (see Figure 2.11).

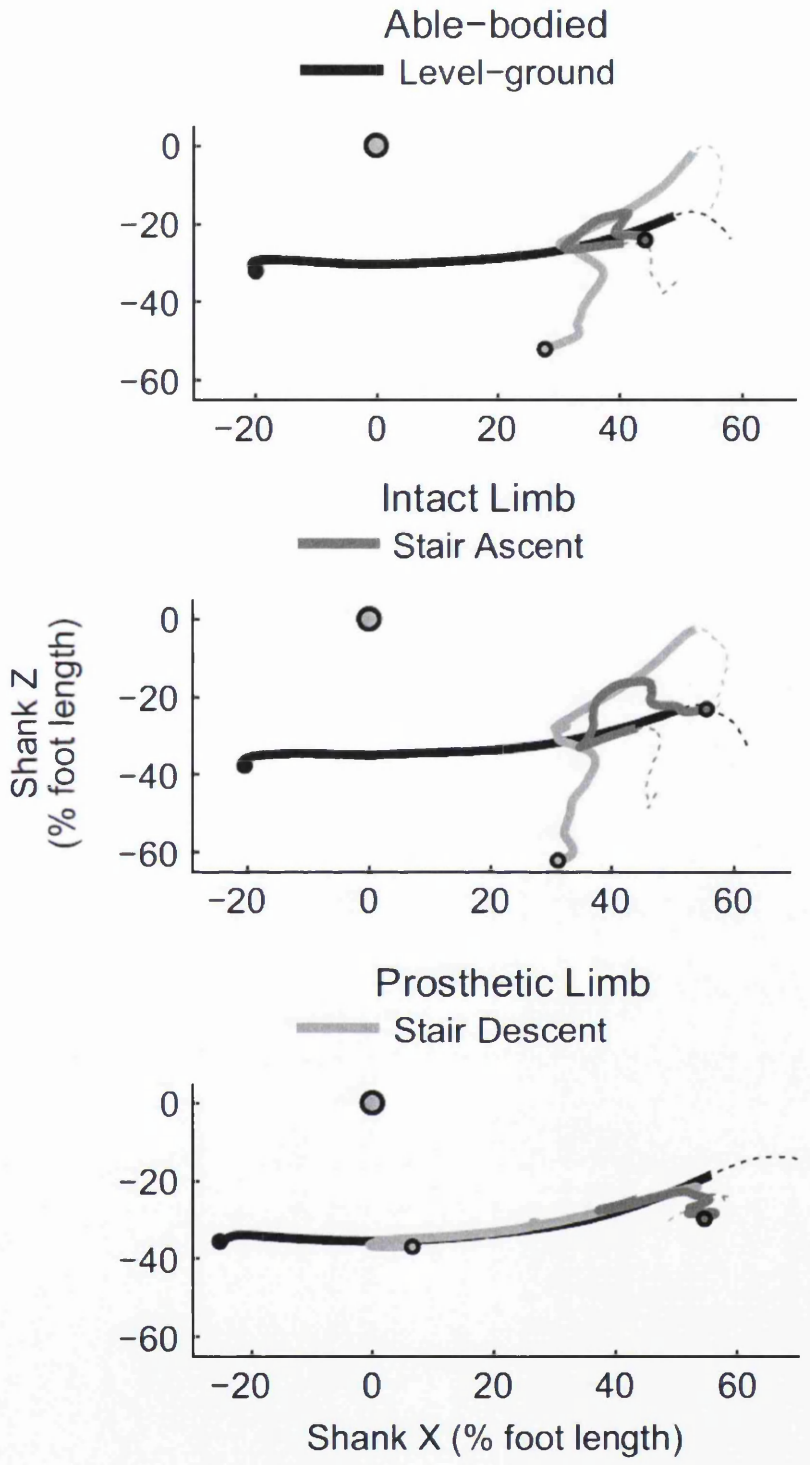

Figure 2.11. Roll-over shapes for able-bodied, intact limb and prosthetic limb persons at level ground and stair ascent/descent walking conditions (Sinitski et al., 2012).

Circular or Non-circular roll-over shapes

Majority of the roll-over shapes studies reviewed in this chapter were assumed the shapes to be circular. However, as demonstrated by Curtze et al. (2009) this is not always true. The authors designed an experiment to investigate the roll-over characteristics of a number of prosthetic feet in combination with different shoes. It was found that the roll-over shapes created by human feet did not have constant curvature. The experiments showed that the forward travel does not progress linearly as predicted by circular feet with a constant radius of curvature. The research implied that the roll-over shape is characterised by three regions with a mid region being flat or with a large instantaneous radius of curvature. It was observed that the forward travel and the associated roll-over shapes were completely different for various prosthetic feet. Major et al. (2011) have also used multiple reference points to characterise the non-linear variation of a roll-over shape.

2.4 Conclusions

The historical development of various prosthetic feet, including the state of the art development on prosthetic feet, has been reviewed. The information discovered has helped this research effort in designing prosthetic foot geometries for the SACH and ESAR feet in Chapter 5. It also helped to shape the future work, as discussed in Chapter 6, in identifying opportunities for improving bionic feet.

The use of roll-over shape concept has also fundamentally altered the initial research direction undertaken for modelling foot kinematics. The complexities of modelling ankle motion along with its muscular support system are simplified by incorporating the roll-over shape in the mathematical model. However, the accuracy of capturing the human gait motion was not sacrificed. The observation that the generic shape of a roll-over shape is perhaps non-circular has influenced the choice of the polynomial function used in characterising roll-over shapes. This is described in detail in Chapter 3 of this thesis. It is pointed out that this insight is one of the most fundamental assumptions of this research and the mathematical models and design guidelines proposed in Chapters 3-5 are based on this assumption.

Chapter 3 Modelling the effect of 'heel to toe' roll-over contact on the walking dynamics of passive biped models

3.1 Introduction

Human like feet are complex shaped and capturing the roll-over phase of the stance leg requires understanding of the knee-ankle-foot kinematics along with the effect of the foot curvature. The foot for a biped has been modelled as either a point, a flat or a curved/circular foot, even though it is generally known that the foot shape has direct influence on the stability of the walking process along with step period, inter-leg angle or step length, average velocity and energy.

Parallel to the robotics research, a 'roll-over shape' concept has been evolved over the last decade within the prosthetics research community. This shape is representative of the knee-ankle-foot kinematics and the curvature of the foot shape. One of the advantages of the roll-over shape is that it can be determined experimentally and hence can be input into the computational model.

The computational modelling of the human walking process is a complex phenomenon. Analysing passive dynamic walking to provide insights into human walking behaviour is a reasonable analogy. Collins et al. (2001 and 2005) extended McGeer's (McGeer, 1990) passive walking robot to a human like biped robot and showed that its efficiency is comparable to that of a human. Hansen et al. (2004a) compared the overall leg rocker radius in their experiment with the radius predicted by McGeer (1990) for human walking even though McGeer's biped robot's circular arc feet replaced the knee-ankle-foot roll-over shape derived in their experiment.

McGeer (1990) defined the concept of passive walking for biped robots on a sloping surface. Exploring the usefulness of this technique, extending it to multi-link biped robots, and understanding the linearisation process of the dynamic equations of a robot about an equilibrium point, are areas of active research (Asano et al., 2005, Geng et al., 2006, Goswami et al., 1998, Hass et al., 2006, Hobbelen and Wisse, 2008, Kuo, 1999, Kwan and Hubbard, 2007, Wisse et al., 2007). Remy et al. (2009)

extended the biped robot theory to quadrupeds. However, all of these publications have either used point, flat or circular arc shaped feet.

Recent publications have modelled a flat foot with a segmented foot allowing rotation at the ankle and toe joints (Huang et al., 2010, Wang et al., 2010). Li et al. (2010) proposed an arched foot (inverted circular arc) along with circular arc and flat feet. Narioka et al. (2009) replaced a circular arc foot with a flat foot that would create a circular roll-over shape. Their analytical model was an over simplified model with a single body mass, a weightless leg, an ankle joint and a flat foot which contacts the ground at the heel and the toe. However, they also constructed a robot and verified that for the same roll-over shape the robot's stability was insensitive to the variation in the body mass. Ren et al. (2010) used an actual roll-over shape with variable curvature. The analytical foot roll-over model was designed to predict ankle kinematics i.e. to predict the positions of ankle joints and the centre of pressure positions. The model for passive walking dynamics was not developed.

Replacing circular feet with roll-over shapes with variable curvature and maintaining the continuity of angular velocity of the swing leg during the roll-over phase requires re-development of the equations from first principles, as described by McGeer (1990) and Goswami et al. (1998). In order to model the influence of variable curvature of roll-over shapes and the continuous angular velocity of the swing leg during the roll-over phase, a simple two linked biped robot has been considered in this chapter, with a point leg mass located at a user defined location on the leg, and a point hip/body mass being located at the intersection of legs. The roll-over shape is discretised with a discrete pivot point model and the concept of the stance leg transition phase has been introduced to model a situation when two pivot points are in contact with the sloping surface. Between two subsequent stance leg transition phases, the stance leg pivots around a single pivot point and the dynamics of the swing leg (single support phase) is modelled with the point feet double pendulum model described by Goswami et al. (1998).

A schematic diagram of foot motion during the human walking process is shown in Figure 3.3. The walking step starts when a foot makes a heel contact with the ground (heel strike). Subsequent to the heel strike, the foot (also referred to as the stance leg foot) rolls over while the other leg (referred to as the swing leg) takes the next step.

The roll-over phase continues until the toe pushes off the stance leg (toe off). At the same time, the swing leg makes the heel contact and becomes a stance leg for the next foot step.

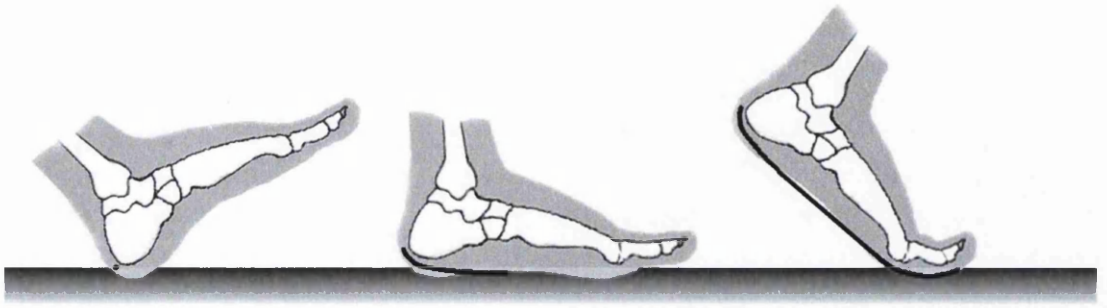

Figure 3.1. Foot movement during human walking process and the resulting roll-over shape.

The understanding of walking dynamics and mechanics of the foot-ground contact is important, particularly in the design of prosthetic feet. One of the objectives of prosthetic feet design is that the prosthetic foot closely matches its biological counterpart. The key design criteria are stability, energy requirements and walking speed. Although a large number of prosthetic foot types are commercially available, there are significant gaps in the clinical knowledge regarding the effects of different prosthetic components on various aspects of human mobility e.g. making transfers, maintaining balance, changing walking speed, negotiating ramps and obstacles (Van der Linde et al., 2004). Clinical gait analysis focuses on an assessment of a patient with walking disorders. The analysis usually consists of five elements: videotape examination, measurement of anthropometric parameters, kinematic analysis, kinetic measurement and electromyography. Until the mid-nineties the gait parameters did not include 'roll-over shapes' as a clinically relevant parameter (Whittle, 1996). However, it appears that at the same time the effective shape of prosthetic feet with ankle motion was studied by Knox (1996). The effective shape was referred to as the 'roll-over' shape of the foot. In other words, it is the path followed by the centre of pressure described in a coordinate frame attached to the prosthetic shank. The initial study discovered that the roll-over shape was insensitive to the walking speed

making it an important parameter in the design and alignment of the prosthetic foot (Hanson et al., 1999).

Experimental determination of 'heel to toe' roll-over shapes is not easy and techniques to determine the approximate shape have only emerged in recent publications. With the experimental evidence reviewed in Section 2.3 of this thesis, it has become clear that understanding the effect of roll-over shapes on the walking dynamics of less able bodied individuals is indeed an important research area and must not be overlooked. The variation among roll-over shapes for different feet is significant. It is observed that the overall shape can be characterised by three parts, namely the hindfoot, the midfoot and the forefoot, with different lengths and slopes (Meier et al.).

There is no evidence in the literature that suggests the effects of complex roll-over shapes on the walking dynamics of biped robots have been modelled computationally. A novel discrete pivot point rolling model coupled with the continuous angular velocity assumption for the swing leg is proposed in this chapter to accurately model the complexities of roll-over shapes. A discrete pivot point rolling model to take into account the effect of variable curvature in the roll-over shapes is described in Section 3.2. The roll over shape is input to the proposed model and is reproduced by fitting three quadratic polynomials. The rolling contact is discretised with discrete pivot points. The influence of the impact after each pivot contact is modelled by introducing a transition phase so that the corresponding conditions in the swing and stance leg dynamics are updated accurately. The procedure is described in Section 3.3. This method can be used for any roll-over shape. The existence of a stable trajectory of the biped motion is defined by the robot parameters. The accuracy of the discrete pivot point model is investigated in section 3.3.5. Results are discussed in Section 3.4 and the chapter is concluded in Section 3.5.

3.2 Problem description

In this study the ankle/foot system is approximated by a roll-over shape, in order to simplify ankle/foot kinematics. The roll-over shape remains constant with reference to the ankle joint. This helps to reduce a degree of freedom from biped model while the kinematics of a walking motion is preserved. The roll-over shapes are

characterised by joining three quadratic polynomials, with first order continuity (continuity in slopes), in order to represent roll-over shapes created by the hindfoot, midfoot and forefoot parts of the foot. The dynamics of a biped model during single support phase as shown in Figure 3.2 is similar to a double pendulum. However, the pivot point of the biped model moves along the roll-over shape and therefore distances between the pivot points and body masses will be change and a single differential equation isn't able to present the entire single support phase. In order to consider the length changes during single support phase, the roll-over shape is descritised in the computational model into e number of pivot points. The black dashed lines in Figure 3.2 present distances between the pivot point and the body masses which are changed for the next time step as shown with blue dashed lines.

The overall assumptions of the biped motion are described below:

($A1$) The scuffing problem of the swing leg, which is inevitable for straight-legged walkers, is neglected during the single support phase (Garcia et al., 1998, McGeer, 1990).

($A2$) All impacts are inelastic and there is no sliding at the pivot points. As a result of this assumption, the pivot point remains in contact with the ground after the impact.

($A3$) There is no actuator or controller.

($A4$) The model configuration remains unchanged during instantaneous transitions.

($A5$) Angular momentum of the whole body at the impacting point is conserved (Goswami et al., 1996). Also, the angular momentum of the former stance leg during double support phase and the swing leg during single support phase about the hip is conserved.

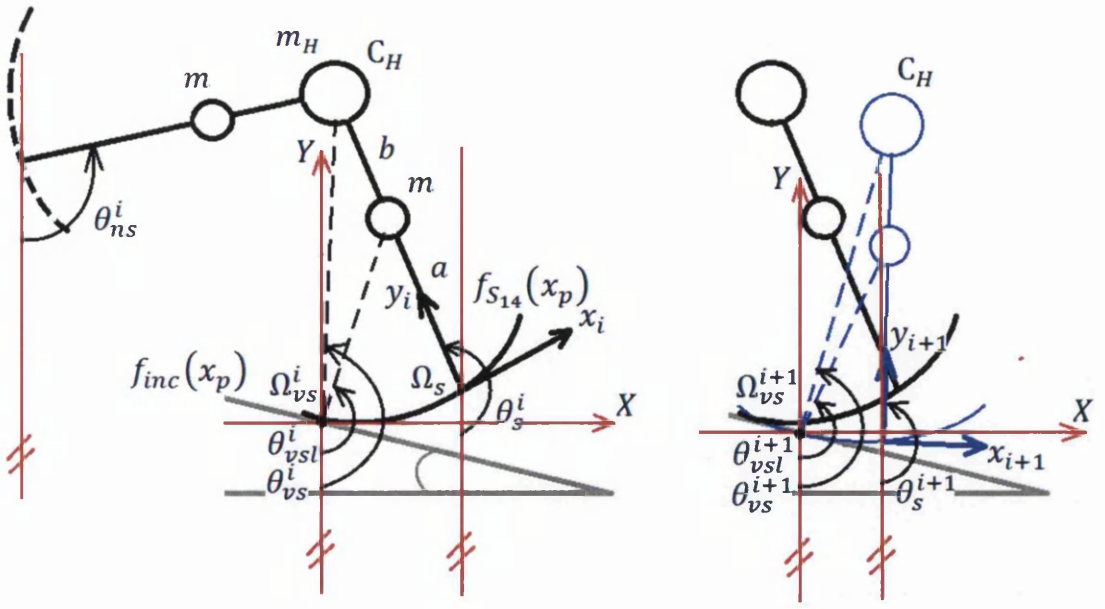

Figure 3.2. The angular positions and lengths of the actual stance leg (solid line), the virtual stance leg (dashed line connected to the hip mass) and the virtual stance lower leg (dashed line connected to the leg mass). The roll-over shape of the swing leg when it was acting as a stance leg during previous walking step is shown by dashed line. The virtual roll-over shape of the swing leg is used to find the position of impact between the swing leg and the inclined surface. Figure on the right shows the roll-over of the stance leg between two pivot points. Rotation of the local co-ordinate system $x_i - y_i$ to $x_{i+1} - y_{i+1}$ is shown.

3.2.1 Approximation of the stance leg rolling motion with a roll-over shape

As discussed earlier, a roll-over shape is a path followed by the centre of pressure described in a coordinate frame attached to the ankle joint (or prosthetic shank). The roll-over shape does not change during the walking process and hence can be described by a polynomial function with variable curvature. The objective of this Chapter is to study the influence of roll-over shapes on gait parameters for a stable walking process. This requires an ability to input complex geometry of roll-over shapes. As shown in Figure 3.3, the roll over shape has three distinct regions, hindfoot, midfoot and forefoot. Hence it is necessary to be able to control the length and curvature of the roll over shape in each region independently by maintaining a C^1 continuity at points S_2 and S_3.

The simplistic assumptions of circular roll-over shapes are not realistic and the proposed discrete point model allows a roll-over shape to be modelled and potentially optimised using the proposed mathematical formulation. The main impact occurs at heel strike. However, as a result of discretising roll-over shapes, the effects of smaller subsequent impacts need to be modelled in the mathematical formulation. The sensitivity of the accuracy of the simulation to the number of pivot points is described in Section 3.4.5.

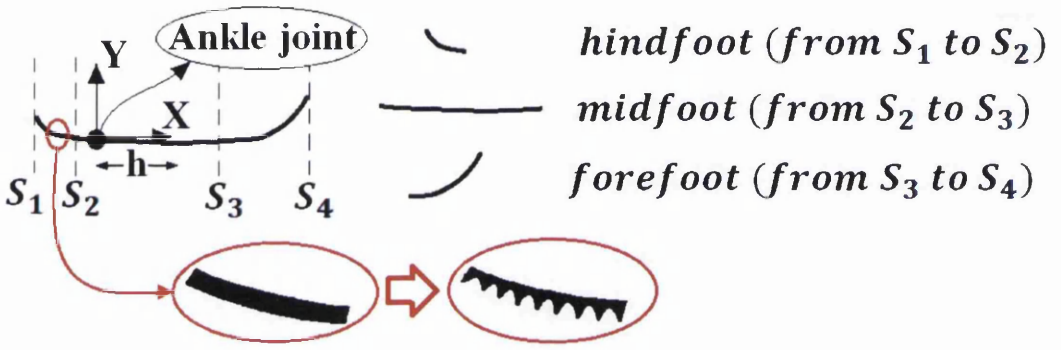

Figure 3.3. The roll-over shape characterised by four control points $\boldsymbol{S_1}$ to $\boldsymbol{S_4}$. The local co-ordinate system (x-y) rotates as the stance leg rolls-over.

In order to satisfy these conditions, a set of polynomial functions $f_{S_{14}}(x)$ is proposed by combining three different polynomial functions $f_{S_{12}}(x)$, $f_{S_{23}}(x)$ and $f_{S_{34}}(x)$ (Equation (3.1)) representing the hindfoot (rear part of the foot, including heel, from S_1 to S_2), the midfoot (from S_2 to S_3) and the forefoot (front part of the foot, including toes, from S_3 to S_4) respectively. The length of the roll-over shape is characterised by four control points S_1, S_2, S_3 and S_4. The curvature of the roll-over shape is characterised by three positive coefficients r_h, r_m and r_f referred to as the hindfoot gain, the midfoot gain and the forefoot gain, respectively. These functions are derived from a family of parabolic functions whose origins are defined at a zero slope point, and given by

$$f_{S_{14}}(x)=\begin{cases} f_{S_{12}}(x)=\dfrac{1}{r_h}(x-x_h)^2+y_h & \text{if } S_1 \le x \le S_2 \\ f_{S_{23}}(x)=\dfrac{1}{r_m}(x-x_m)^2+y_m & \text{if } S_2 \le x \le S_3 \\ f_{S_{34}}(x)=\dfrac{1}{r_f}(x-x_f)^2+y_f & \text{if } S_3 \le x \le S_4 \end{cases} \qquad (3.1)$$

In order to construct a roll-over shape with continuity in slope at control points S_2 and S_3, the co-ordinates of the zero slope points of the three parabolic functions are translated to (x_h, y_h), (x_m, y_m) and (x_f, y_f) respectively. The roll-over shape requires that a local co-ordinate system is defined with origin at the ankle joint and y axis along the stance leg. The mid foot function $f_{S_{23}}(x)$ passes through the origin and the ankle joint, and is a polynomial function with a large radius of curvature. If h is defined as the horizontal distance between the origin and the zero slope point of $f_{S_{23}}(x)$ then

$$x_m = h \qquad \text{and} \qquad y_m = -\frac{1}{r_m}h^2 \qquad (3.2)$$

The values (x_h, y_h) and (x_f, y_f) are determined by ensuring the continuity of slope at S_2 and S_3.

$$x_h = s_2 - \frac{r_h}{r_m}(s_2 - x_m) \qquad (3.3)$$

$$y_h = f_{S_{23}}(s_2) - \frac{r_h}{r_m^2}(s_2 - x_m)^2 \qquad (3.4)$$

$$x_f = s_3 - \frac{r_f}{r_m}(s_3 - x_m) \qquad (3.5)$$

$$y_f = f_{S_{23}}(s_3) - \frac{r_f}{r_m^2}(s_3 - x_m)^2 \qquad (3.6)$$

3.2.2 Approximation of the roll-over shape with multiple pivot points

As illustrated in Figure 3.3, the roll-over shape is discretised by e pivot points during the analysis. As e tends to infinity the shape of the roll-over curve would approach the original smooth curve. This will correspond to $(e-1)$ stance leg transition phases $(1<i\leq e)$, a double support transition phase $(i=1)$ and e single support phases where i shows i^{th} pivot point. At the end of a single support phase, the body rotates about the last pivot point $(i=e)$ until the first contact of the swing leg and the ground occurs $(i=1)$. Transition phases are used to find new initial conditions due to impact between pivot points and the ground. As a result of using a discrete pivot point model, small impacts occur during the rolling contact. For a sufficiently large number of pivot points, as shown in Section 3.4.5, the results converge to a unique solution. However, the resulting impact when the next pivot point makes a contact with the ground needs to be modelled. The assumption A4 ensures that the leg angular velocity is same before and after the smaller impacts resulting from contacts during the single support phase.

A schematic diagram with nine pivot points is shown in Figure 3.4. As the stance leg pivots around pivot point 1 during the rolling contact, the single support phase dynamics occurs as per the double pendulum model until pivot point 2 comes into contact with the sloping surface. This defines the stance leg transition phase. The consequence of the single support phase and the stance leg transition phase during the single support phase will continue until the swing leg contacts the sloping surface which is described by the double support transition phase. The initial conditions for the double pendulum motion about each pivot point consist of virtual leg lengths (l_{vs} and a_{vsl} in Figure 3.4), initial angular velocities and initial angular displacements. The calculation procedure for virtual leg lengths and initial angular displacements about a given pivot point is described in Section 3.4.1. Initial angular velocities during the single support phase and the double support phase are presented in Sections 3.4.2 and 3.4.3 respectively. The dynamics of the single support phase with

the initial conditions achieved by transition analysis is described in Section 3.4.4. The accuracy of discrete pivot point roll-over model is studied in Section 3.4.5.

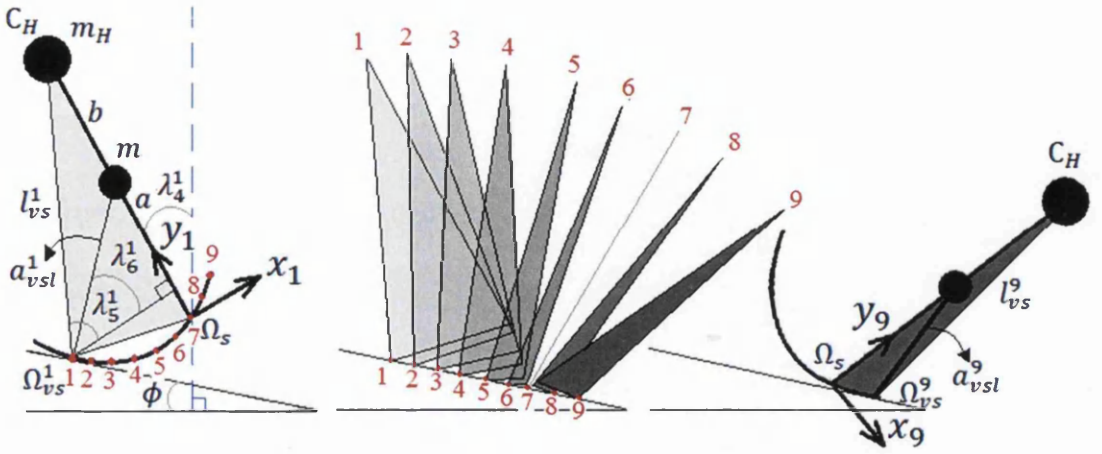

Figure 3.4. Discretising roll-overs shape to develop a multi-pivot point rolling contact model. Nine pivot points (e = 9) are used in this example so that they become in contact with the sloping surface alternatively as the roll-over shape rolls down the surface. Each triangle presents a geometry of the supported leg corresponding to a pivot point. The terms virtual stance leg l_{vs}^i and virtual stance lower leg a_{vs}^i show a distance between a pivot point and stance leg centre of mass and hip mass respectively.

3.3 Dynamics of passive walking with a discrete pivot point roll-over model

3.3.1 The contact point of the roll-over shape with the surface during single support phase

In Figure 3.4, the hip mass and leg mass are shown as point masses on the stance leg. The ankle joint is at the intersection of the stance leg and the roll-over shape. The origin of the local co-ordinate axis is defined at the ankle joint. In Figure 3.4 the ankle joint is shown at pivot point 7 (it should be noted that the ankle joint may not coincide with a pivot point). When the stance leg is rolling at pivot point 1, a virtual stance leg connecting pivot point 1 and the hip mass is introduced. Similarly, a virtual stance lower leg is defined that connects pivot point 1 with the centre of leg mass. The angular positions and lengths of the actual stance leg, virtual stance leg

and the virtual stance lower leg are represented by (θ_s, L), (θ_{vs}, l_{vs}^i) and $(\theta_{vsl}, a_{vsl}^i)$ respectively (see Figure 3.2). The virtual stance leg and virtual stance lower leg are used instead of the actual stance leg to analyse the biped motion. During the single support phase, angular velocities of virtual stance leg, the stance leg and the virtual stance lower leg are kept equal. This means that the grey triangle made by joining hip mass, pivot point and ankle joint $(C_H\hat{\Omega}_{vs}^i\Omega_s)$ remains constant (Figure 3.2) during the single support phase that occurs between two consecutive stance leg transition phases. The angular position and velocity of the swing leg is denoted by θ_{ns} and $\dot{\theta}_{ns}$ respectively (Figure 3.2) and the superscript i denotes the i^{th} time step. In the subsequent single support phase, the foot will roll-over around pivot point 2. The shape and the angular position of the triangle will change due to the position of Ω_{vs}^{i+1} and the angular position of the stance leg θ_s, as shown in Figure 3.4. The virtual stance leg and actual stance leg become identical as the pivot point approaches the ankle joint (see point 7 in Figure 3.4). Note that the local co-ordinate system defined at the ankle joint also changes during the rolling contact.

The distance between two consecutive pivot points is a function of the roll-over shape, the time-step and the initial conditions for each time-step. The length, angular position and angular velocity of the virtual stance leg and the virtual stance lower leg change in every time-step and depend on the position of the pivot point.

In this work a planar biped model is used to study the stability of bipedal walking motion in a direction of forward progression (sagittal plane). Restriction attention to the sagittal plane is logical as the dynamics of biped in the sagittal plane are almost decoupled from those in the frontal plane (Z direction) whereas stability in the Z direction can be achieved independently (Kuo, 1999, Westervelt, 2003). Therefore, a stable three-dimensional walking can be achieved by coupling the algorithm which are used to stabilise walking in the sagittal and the frontal plane. The global coordinate system (X_i, Y_i) and the local coordinate system (x_i, y_i) (as shown in Figure 3.2) are used to track the position of the pivot point on the roll-over shape of the stance leg. The gradient of the inclined surface about the local coordinate system is $-\tan(\phi + \theta_s - \pi)$. Just after the double support transition phase, the first pivot

point for the foot of the stance leg foot in contact with the ground during the single support phase, $\Omega_{vs}^1 = (x_p^1, y_p^1)$, can be derived from

$$f'_{S_{12}}(x_p^1) + \tan(\phi + \theta_s^1 - \pi) = 0 \quad \textbf{and} \quad y_p^1 = f_{S_{12}}(x_p^1) \qquad (3.7)$$

The point Ω_{vs}^1 is not necessarily located on the control point S_1 (as shown in Figure 3.4) and it can be somewhere inside the roll-over curve. If the Ω_{vs}^1 is outside the roll-over curve then its co-ordinates are given by:

$$x_p^1 = x_{S_1} \quad \text{and} \quad y_p^1 = f_{S_{12}}(x_p^1) \qquad (3.8)$$

The following condition is checked at each time step as the stance leg begins to rotate about the control point S_1

$$f'_{S_{12}}(x_c^1) + \tan(\phi + \theta_s^i - \pi) \geq 0 \qquad (3.9)$$

At a particular time step, the Equation (3.9) will not be satisfied. This leads to two intersection points between the roll-over function and the inclined surface. The first point is S_1 and the second intersection point becomes the next pivot point. The pivot point of i^{th} time step in the local coordinate system $(x_i - y_i)$ is given by:

$$f_{S_{14}}(x_p^i) - f_{inc}(x_p^i) = 0 \quad \text{and} \quad y_p^i = f_{S_{14}}(x_p^i) \qquad (3.10)$$

where $f_{inc}(x_p^i) = -(x_p^i - x_p^{i-1})\tan(\phi + \theta_s^i - \pi) + y_p^{i-1}$ is the equation of the inclined surface in the local coordinate system of the i^{th} time step.

At every pivot point the initial conditions, i.e. angular positions θ_{vs}^i, θ_{vsl}^i, and virtual lengths l_{vs}^i, a_{vs}^i and λ_4^i, λ_5^i, λ_6^i (as shown in Figure 3.4) required for the subsequent equation of motion are updated. Using the constant triangle assumption and trigonometry, the initial conditions of the biped motion for the pivot point of the i^{th} time step are given by:

$$\lambda_4^i = \theta_s^i - \pi \tag{3.11}$$

$$\lambda_5^i = \tan^{-1}\left(\frac{b + a - y_p^i}{-x_p^i}\right) \tag{3.12}$$

$$\theta_{vs}^i = \begin{cases} \lambda_4^i + \lambda_5^i + \dfrac{\pi}{2} & if \;\; x_p^i < 0 \\ \lambda_4^i + \lambda_5^i + \dfrac{3\pi}{2} & if \;\; x_p^i > 0 \end{cases} \tag{3.13}$$

$$\lambda_6^i = \tan^{-1}\left(\frac{a - y_c^i}{-x_c^i}\right) \tag{3.14}$$

$$\theta_{vsl}^i = \begin{cases} \lambda_6^i + \lambda_5^i + \dfrac{\pi}{2} & if \;\; x_p^i < 0 \\ \lambda_6^i + \lambda_5^i + \dfrac{3\pi}{2} & if \;\; x_p^i > 0 \end{cases} \tag{3.15}$$

$$a_{vs}^i = \sqrt{(a - y_p^i)^2 + x_p^{i\,2}} \tag{3.16}$$

$$l_{vs}^i = \sqrt{(a + b - y_p^i)^2 + x_p^{i\,2}} \tag{3.17}$$

3.3.2 The stance leg transition phase

All the pivot points are located on the roll-over shape and as the stance leg rotates about a pivot point a small impact occurs when the next pivot point makes contact with the sloping surface. During this stance transition phase, θ_{vs}^{i+} and θ_{vsl}^{i+} for the i^{th} time step are derived by using Equations (3.13) and (3.15). It is assumed that both the swing leg and the stance leg angles remain constant during the impact giving the conditions

$$\theta_{ns}^+ = \theta_{ns}^- \quad \textbf{and} \quad \theta_s^+ = \theta_s^- \tag{3.18}$$

Where "-" and "+" present parameter values before and after impact respectively. The conservation of angular momentum (Assumption A5) and the assumption of constant angular velocity of the swing leg (Assumption A4) during the stance leg transition phase lead to the condition

$$\dot{\theta}^{i+} = H^{i}(\theta)\dot{\theta}^{i-} \qquad (3.19)$$

where

$$H_{11}^{i} = \frac{ma_{vs}^{i}a_{vs}^{i-1}\cos(\theta_{vsl}^{i+} - \theta_{vsl}^{i-}) + (m_H + m)l_{vs}^{i}l_{vs}^{i-1}\cos(\theta_{vs}^{i+} - \theta_{vs}^{i-}) - mcl_{vs}^{i-1}\cos(\theta_{vs}^{i-} - \theta_{ns}^{i-})}{m_H l_{vs}^{i\,2} + ma_{vs}^{i\,2} + ml_{vs}^{i\,2} - mcl_{vs}^{i}\cos(\theta_{vs}^{i+} - \theta_{ns}^{i+})} \qquad (3.20)$$

$$H_{12}^{i} = H_{21}^{i} = 0 \quad \text{and} \quad H_{22}^{i} = 1 \qquad (3.21)$$

and $\theta = [\theta_{vs} \;\; \theta_{ns}]^T$ and θ_{vs} and θ_{ns} are measured from the negative *y*-axis as shown in Figure 3.2.

The - and + superscripts denote the pre and post- pivot point impact variables for the i^{th} time step respectively.

3.3.3 The double support transition phase

The impact resulting from the swing leg's contact with the sloping surface (heel-strike) is modelled via the double support transition phase. During this phase the angular position of virtual stance leg and the swing leg are related by

$$\theta_{vs}^{1} + \theta_{ns}^{1} = -2\phi + 2\pi \qquad (3.22)$$

where ϕ is the slope of the walking surface and 2π is the correction added because of the definition of angular positions (Figure 3.2).

It is assumed that both the swing leg and the virtual stance leg angles remain constant during the impact giving the condition

$$\theta^{1+} = J\theta^{e-} \tag{3.23}$$

where

$$J = \begin{bmatrix} 0 & 1 \\ 1 & 0 \end{bmatrix} \tag{3.24}$$

The matrix J exchanges the support and the swing leg angles for the upcoming single support phase.

The conservation of angular momentum (Assumption A5) leads to the condition

$$\dot{\theta}^{1+} = \frac{H^1(\theta)}{H_d^1}\dot{\theta}^{e-} \tag{3.25}$$

where the elements of $H^1(\theta)$ are

$$\begin{aligned} H_{11}^1 = {} & m_H m b^2 l_{vs}^e l_{vs}^1 \cos(\theta_{vs}^{e-} - \theta_{vs}^{1+}) + m^2 b^2 l_{vs}^1 a_{vs}^e \cos m(\theta_{vs}^{e-} - \theta_{vs}^{1+} + \lambda_6^e - \lambda_5^e) \\ & + m^2 b^2 a_{vs}^1 l_{vs}^e \cos(\theta_{vs}^{e-} - \theta_{vs}^{1+} + \lambda_5^{1+} - \lambda_6^1) + m^2 b^2 l_{vs}^1 a_{vs}^e \sin(\lambda_6^e)\cos(\theta_{vs}^{1+} - \theta_{ns}^{1+}) \end{aligned} \tag{3.26}$$

$$H_{12}^1 = -m^2 b^3 a_{vs}^1 \cos(\theta_{vs}^{1+} - \theta_2^{e-} + \lambda_6^1 - \lambda_5^1) \tag{3.27}$$

$$
\begin{aligned}
H_{21}^{1} &= mm_H bl_{vs}^{e} l_{vs}^{1\,2} \cos(\theta_{vs}^{1+} - \theta_{ns}^{1+}) \cos(\theta_{vs}^{e-} - \theta_{vs}^{1+}) \\
H_{2}^{1} &\quad + m^2 ba_{vs}^{e} l_{vs}^{1\,2} \cos(\theta_{vs}^{1+} - \theta_{ns}^{1+}) \cos(\theta_{vs}^{e-} - \theta_{vs}^{1+} + \lambda_6^e - \lambda_5^e) \\
&\quad + m^2 bl_{vs}^{e} l_{vs}^{1} a_{vs}^{1} \cos(\theta_{vs}^{1+} - \theta_{ns}^{1+}) \cos(\theta_{vs}^{e-} - \theta_{vs}^{1+} + \lambda_5^1 - \lambda_6^1) \\
&\quad + mm_H ba_{vs}^{e} l_{vs}^{1\,2} \sin(\lambda_6^e) + m^2 ba_{vs}^{e} l_{vs}^{1\,2} \sin(\lambda_6^e) + m^2 ba_{vs}^{e} l_{vs}^{1\,2} \sin(\lambda_6^e) \\
&\quad + mm_H ba_{vs}^{e} l_{vs}^{1\,2} \sin(\lambda_6^e) + m^2 ba_{vs}^{e} l_{vs}^{1\,2} \sin(\lambda_6^e) + m^2 ba_{vs}^{e} l_{vs}^{1\,2} \sin(\lambda_6^e)
\end{aligned}
\qquad (3.28)
$$

$$
H_{22}^{1} = -m^2 b^2 l_{vs}^{1} a_{vs}^{1} \sin(\lambda_6^1) \cos(\theta_{vs}^{1+} - \theta_{ns}^{1+}) \qquad (3.29)
$$

And

$$
H_{d}^{1} = mb^2 \left[m_H l_{vs}^{1\,2} + m l_{vs}^{1\,2} + m a_{vs}^{1\,2} - m l_{vs}^{1\,2} \cos^2(\theta_{vs}^{1+} - \theta_{ns}^{1+}) \right] \qquad (3.30)
$$

Again, the - and + superscripts denote the pre and post- pivot point impact variables for the i^{th} time step respectively. The e and 1 superscripts denote the biped parameters during the single support phase before and after impact.

3.3.4 Dynamics of the single support phase

The dynamic equations of the single support phase model are the standard double pendulum equations given by Goswami et al. (1996). In their work, the single support phase covered the entire step period and the equations were solved only once for each step period. In this implementation, the influence of transition phase is accounted by solving the following equations. The equations are initialised when the stance leg begins to rotate about every pivot point.

$$
M^i(\theta)\ddot{\theta} + C^i(\theta, \dot{\theta})\dot{\theta} + K^i(\theta) = 0 \qquad (3.31)
$$

The inertia matrix, $M(\theta)$, centrifugal terms, $C(\theta, \dot{\theta})$, gravitational stiffness matrix, $K(\theta)$, and initial conditions for the pivot point of the i^{th} time step, are

$$
M^i(\theta) = \begin{bmatrix} m a_{vs}^{i\,2} + m_H l_{vs}^{i\,2} + m l_{vs}^{i\,2} & -m l_{vs}^{i} c \cos(\theta_{vs} - \theta_{ns}) \\ -m l_{vs}^{i} c \cos(\theta_{vs} - \theta_{ns}) & mc^2 \end{bmatrix} \qquad (3.32)
$$

$$C^i(\theta)=\begin{bmatrix} 0 & -ml^i_{vs}c\dot{\theta}_{ns}\sin(\theta_{vs}-\theta_{ns}) \\ ml^i_{vs}c\dot{\theta}_{vs}\sin(\theta_{vs}-\theta_{ns}) & 0 \end{bmatrix} \quad (3.33)$$

$$K^i(\theta)=\begin{bmatrix} mga^i_{vs}\sin(\theta_{vs}+\lambda^i_6-\lambda^i_5)+(m_H gl^i_{vs}+mgl^i_{vs})\sin(\theta_{vs}) \\ -mgc\sin(\theta_{ns}) \end{bmatrix} \quad (3.34)$$

$$\theta^{initial}_{vs}=\theta^i_{vs},\ \theta^{initial}_{ns}=\theta^i_{ns},\ \dot{\theta}^{initial}_{vs}=\dot{\theta}^i_{vs} \quad \text{and} \quad \dot{\theta}^{initial}_{ns}=\dot{\theta}^i_{ns} \quad (3.35)$$

For a given time step, the angular position of the actual stance leg θ^{i+1}_s, the angular position of the swing leg θ^{i+1}_{ns} and the local coordinate system (x_{i+1}, y_{i+1}) for the next time-step is determined using numerical integration in MATLAB using ode45.

3.3.5 Sensitivity study modelling roll over shape using discrete pivot points

In order to investigate the accuracy of the proposed discrete pivot point model two examples are presented. The first example (Section 3.3.5.1) demonstrates the ability of the discrete pivot point model to simulate the dynamics of the rolling motion of a disk on an inclined surface with a point mass located at its centre. The convergence to the analytical solution is demonstrated in Figure 3.5. The second example illustrates that as the number of pivot points that define the roll over shape are increased the oscillation in step period and inter-leg angle in subsequent gait cycles is reduced and converge to a unique value. This provides an indication of number of pivot points required for a given analysis (e.g. 3000 pivot points).

3.3.5.1 Rolling motion of a disk on an inclined surface

The displacement time profile of the centre of a rolling disk on an inclined surface is calculated using an exact analytical solution. The acceleration of the stationary disk as it rolls down the slope with angle ϕ is given by $a = g\sin(\phi)$. For this example the angle ϕ is taken as 4^0. The first four seconds of the motion are simulated in order to study the accuracy of the discrete pivot point model. In the discrete model the contact point of the disk and the inclined surface is modelled as a pivot point of the inverted pendulum with the mass located at the centre of the disk. The mass rotates about the pivot point with a constant time step and the post pivot point is given by

the second intersection point of the disk and the inclined surface (similar to the discussion in Section 3.3.1). The virtual link which connects the post pivot point and the mass is the post inverted pendulum with initial conditions obtained by conserving angular momentum about the contact point. Figure 3.5 illustrates that by increasing the number of pivot points (NP) the trajectory of the discrete model motion converges to the analytical solution and for sufficiently large number of pivot points the discrete pivot point model is able to accurately model the rolling motion of a disk on an inclined surface.

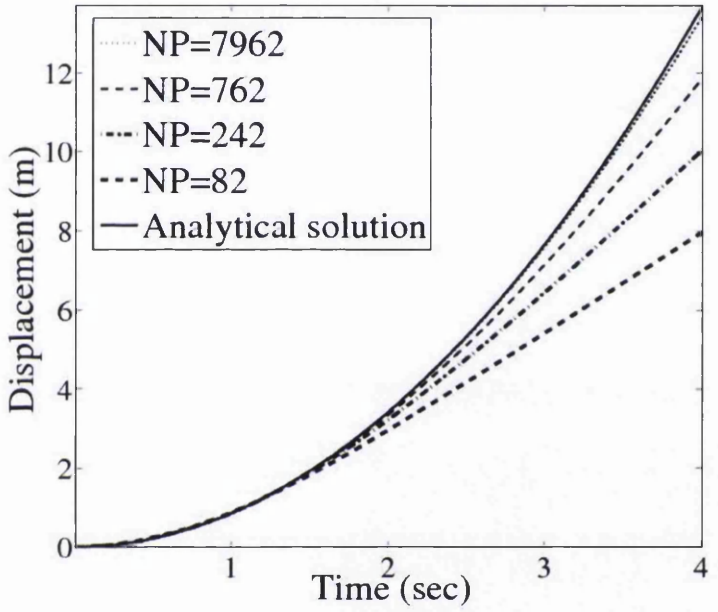

Figure 3.5. The results for the discrete pivot point model compared to the analytical solution for a rolling disk on an inclined surface.

3.3.5.2 Rolling motion of the biped model for a fixed roll-over shape

The roll over shape determines the location of the contact point with reference to the stance leg position as the stance leg rolls over during the single support phase. As described in Section 3.3 this causes a change in the initial conditions of the double pendulum governing equations. It is difficult to determine the optimal number of pivot points required to accurately model a complex roll over shape since an equivalent analytical solution is not available. As the numbers of pivot points to model a biped walking on an inclined surface were increased, the resulting step

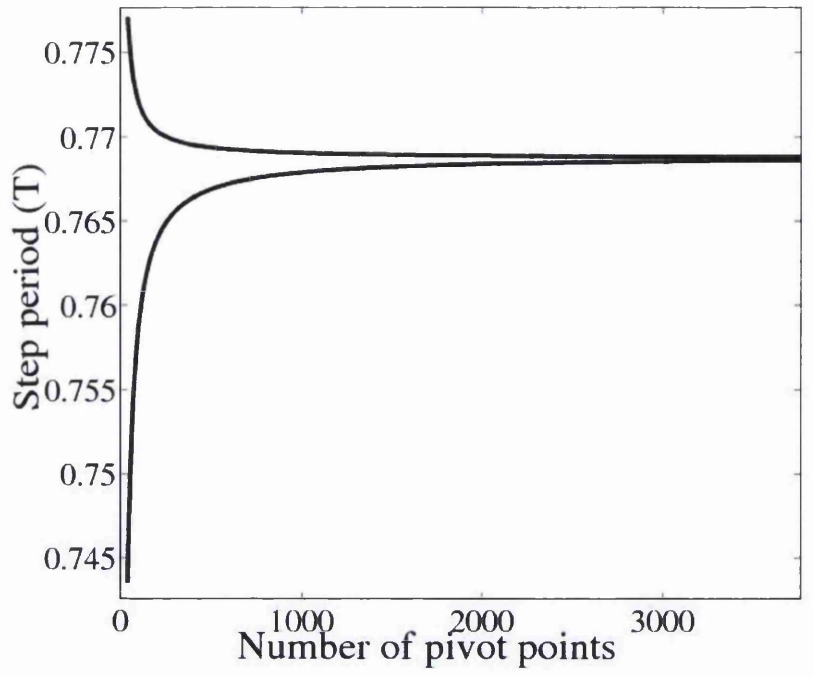

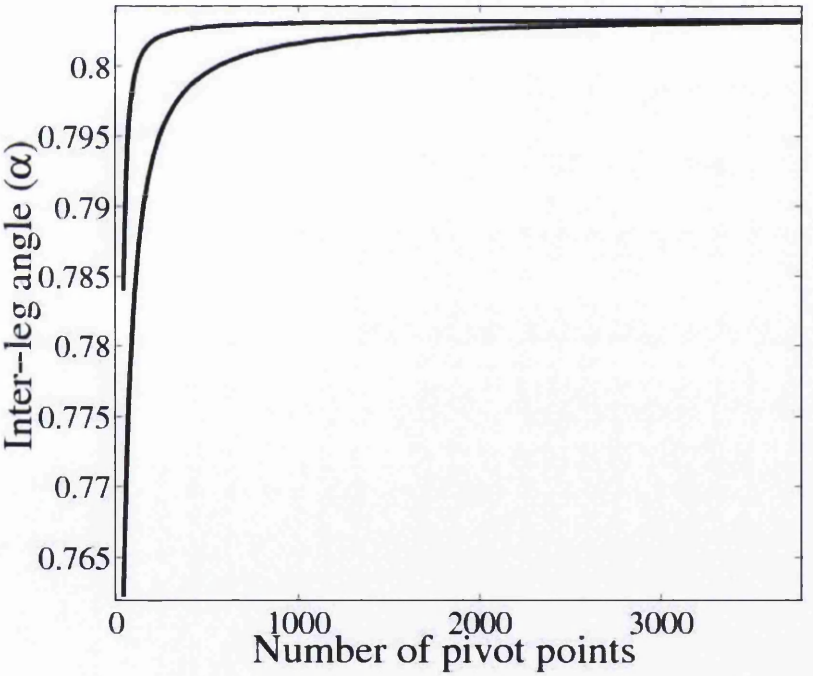

Figure 3.6. Sensitivity study to determine the minimum number of pivot points required. Under stable and periodic walking conditions and with a sufficient number of pivot points, the step period and the inter-leg angle value for consecutive walking steps converges to a unique value.

period and inter-leg angles for stable and periodic walking converged. The convergence rate in this example is $\frac{1}{N}$ where N is the number of pivot points. The corresponding values for mass ratio, length ratio, slope angle, hindfoot length, forefoot length and roll-over gain are 2, 1, 2^0, 16(cm), 16(cm) and 0.8. Figure 3.6 illustrates that the step periods and inter-leg angles for stable and periodic walking converge to a unique value. The minimum number of pivot points used need to be more than the corresponding value, i.e. 3000 in this example.

3.4 Results and Discussion

3.4.1 Modelling rollover shapes with polynomials

The biped model parameters of interest in this chapter are the forefoot and the hindfoot curvature values, defined by the corresponding gain values (r_f and r_h), along with the corresponding length values (L_f and L_h). The midfoot gain and the midfoot length are described by variables r_m and L_m respectively. As shown in Figure 3.3, the length of the roll-over shape is characterised by four control points S_1, S_2, S_3 and S_4. The distance between S_1 and S_2 is the hindfoot length, L_h, whereas the forefoot length, L_f, is the distance between S_3 and S_4.

Figures 3.7 and 3.8 illustrate the sample roll-over shapes corresponding to values of the gains and lengths given in Tables 3.1 and 3.2 respectively. Note that a gain value equal to zero corresponds to a point foot and the roll-over shape tends to become flat as the gain value increases. In both Figures the single solid point in the centre represents the ankle joint. It can be seen that the roll-over shape arc length increases as the r_f and r_h values increase. In prosthetic foot design, flexibility of the foot has a significant influence on lengths and gains of a roll-over shape. A flexible foot has lower roll-over shape length and gain value. For example eleventh roll-over shape in Figure 3.7 presents a stiffer prosthetic foot as compared to the first roll-over shape. The projection of the roll-over shape on the horizontal axis is referred to as horizontal roll-over shape length. The dashed lines in Figures 3.7 and 3.8 represent the extended roll-over shapes and the solid lines are the actual roll over shapes used

by the passive biped model and are referred to as effective roll over shapes. This is discussed further in Section 3.4.2.7.

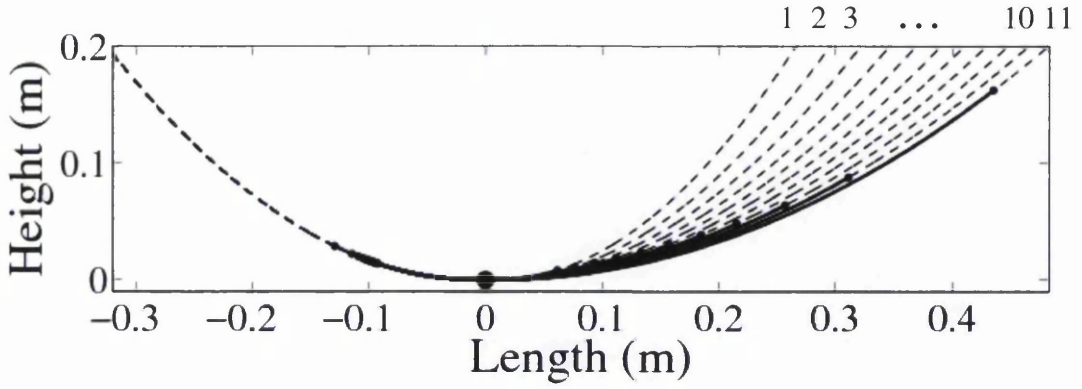

Figure 3.7. Roll-over shapes for different forefoot gain values (refer to Table 3.1 for all input values).

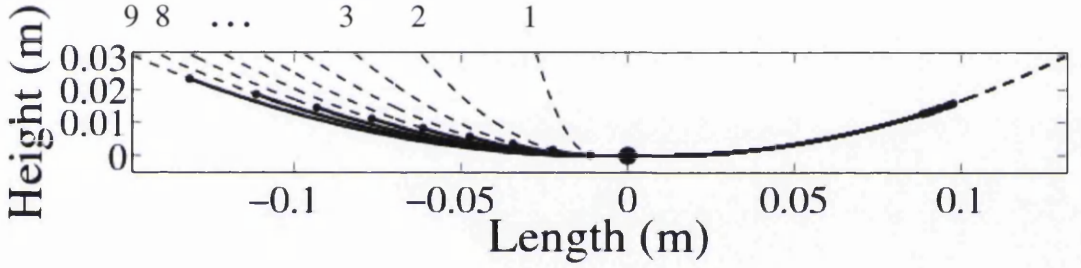

Figure 3.8. Roll-over shapes for different hindfoot gain values (refer to Table 3.2 for all input values).

Table 3.1. Various length and gain values used to describe roll-over shapes. Note that the hindfoot gain value is constant and all length values are in measured in cm. The corresponding roll-over shapes are shown in Figure 3.7.

No	1	2	3	4	5	6	7	8	9	10	11
r_h	0.5	0.5	0.5	0.5	0.5	0.5	0.5	0.5	0.5	0.5	0.5
r_f	0.33	0.41	0.49	0.57	0.65	0.73	0.81	0.89	0.97	1.05	1.13
L_f	5.13	6.67	8.37	10.22	12.3	14.7	17.47	20.51	24.68	30.12	42.55
L_h	8.27	8.41	8.57	8.7	8.9	9.07	9.29	9.58	9.92	10.46	11.93
L_m	2	2	2	2	2	2	2	2	2	2	2

Table 3.2. Various length and gain values used to describe roll-over shapes. Note that the forefoot gain value is constant and all length values are in measured in cm. The corresponding roll-over shapes are shown in Figure 3.8.

No	1	2	3	4	5	6	7	8	9
r_h	0.01	0.09	0.17	0.25	0.33	0.41	0.49	0.57	0.65
r_f	0.5	0.5	0.5	0.5	0.5	0.5	0.5	0.5	0.5
L_f	7.86	7.98	8.08	8.18	8.33	8.39	8.57	8.67	8.78
L_h	0.13	1.25	2.45	3.75	5.15	6.69	8.34	10.16	12.15
L_m	2	2	2	2	2	2	2	2	2

3.4.2 Phase plane limit cycles

The dependence of the actual stance leg angular velocity ($\dot{\theta}_s$) and angular displacement (θ_s) on the horizontal roll over shape lengths, and the hindfoot and forefoot gains, is plotted using phase plane limit cycle diagrams (Figure 3.10). A periodic stable system can be presented by a phase plane limit cycle. Any point near to the phase plane will be observed to the stable limit cycle as shown in Figure 3.9. Table 3.3 gives the legend used for Figure 3.10. The mass ratio $\left(\frac{m_H}{m}\right)$, length ratio $\left(\frac{b}{a}\right)$ and slope angle values used the analysis are 2, 1 and 2^o respectively.

The phase plane limit cycle diagrams show that the maximum value of the actual stance leg angular velocity and displacement increases with larger values of horizontal roll over shape lengths and forefoot gains. The jump in the actual stance leg angular velocity during the double support phase when the swing leg becomes the stance leg (the bottom right hand corner of the phase plane limit cycle diagram) is different as the horizontal roll over shape lengths and forefoot gains are changed. The reversal of this trend is observed at the critical values of horizontal roll over shape length (10cm) and hindfoot gain (0.7). It is also seen that for a forefoot gain of 0.4 the angular velocity before and after the double support contact remains the same.

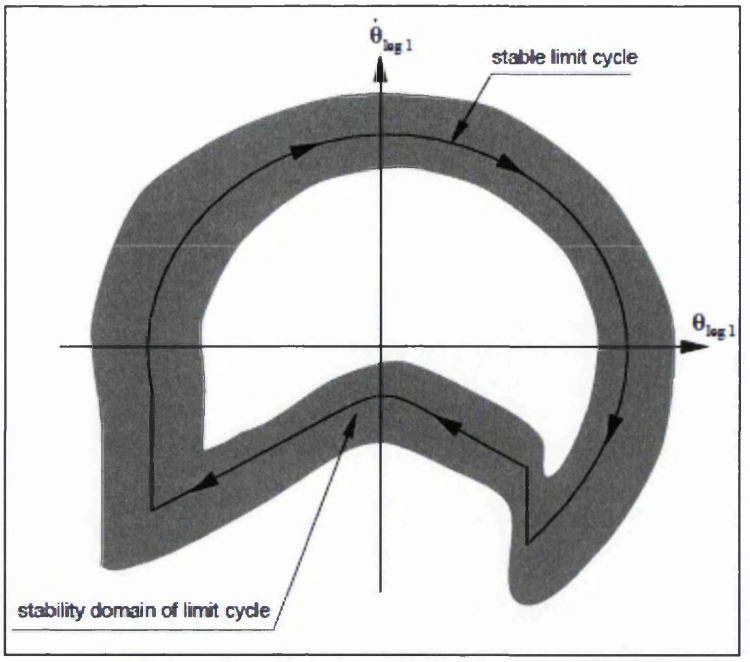

Figure 3.9. A phase plane limit cycle. The solid black curve shows a stable periodic walking and the shaded area is the schematic representation of initial conditions that will be converge to the stable limit cycle (Goswami et al., 1996).

Table 3.3. Legend and the corresponding values used for the phase plane limit cycle diagrams.

Phase plane limit cycle	Thin Solid line	Dashed line	Thick Solid line	Gain values
Horizontal Roll-over shape length	Point feet	10 (cm)	20 (cm)	r_f and r_h =0.8 r_m and L_m = 0
Hindfoot gain (r_h)	0.5	0.7	0.9	r_f =0.8 r_m and L_m = 0
Forefoot gain (r_f)	0.4	0.8	1	r_h =0.5 r_m and L_m = 0

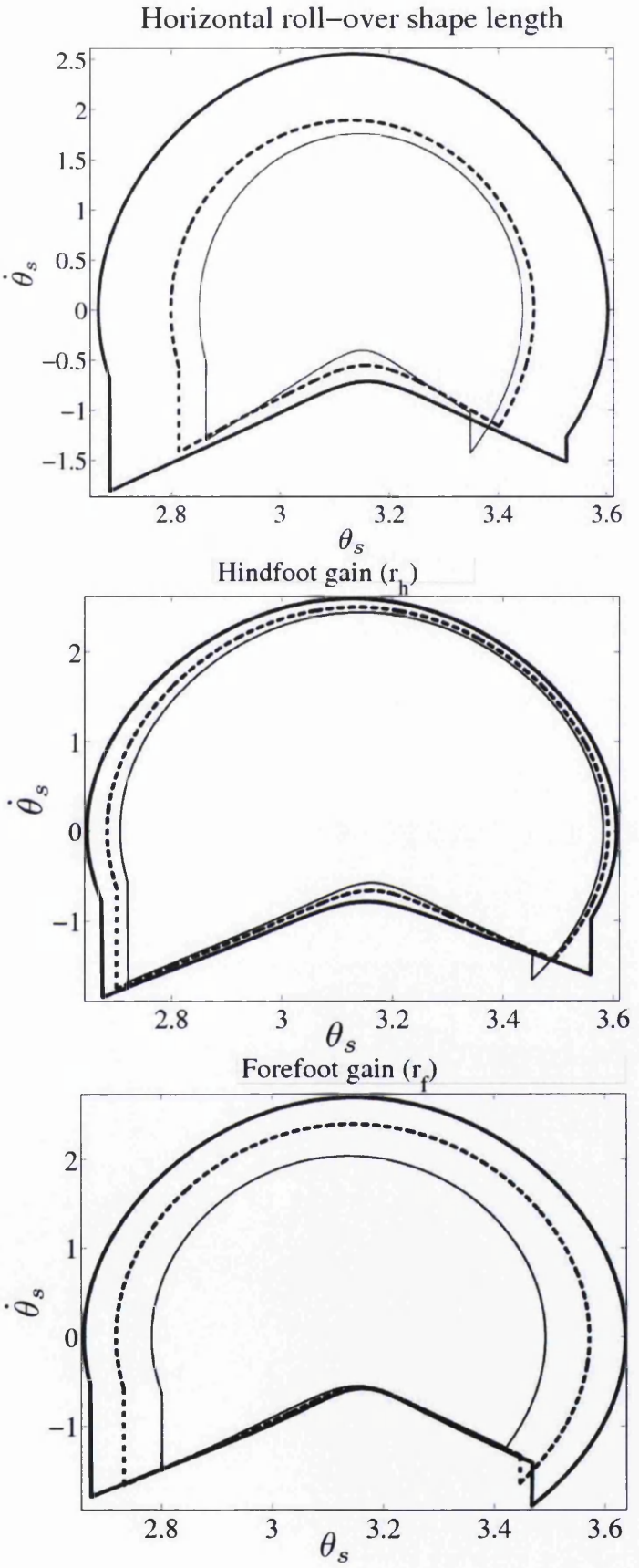

Figure 3.10. Phase plane limit cycles for different horizontal roll over shape lengths, hindfoot gains and forefoot gains.

3.4.3 Bifurcation diagrams

Bifurcation diagrams are commonly used to describe the evolution of gait descriptors (e.g. average velocity, step period, mechanical energy or inter-leg angle) as a function of biped model parameters (e.g. ground slope angle, mass ratio, length ratio). Each point on the bifurcation diagram has a unique phase plane limit cycle. An asymmetry in the walking cycle is noted with a corresponding bifurcation in the bifurcation diagram. In order to compare the bifurcation diagrams with the ones published by Goswami et al. (1996), identical values for the mass ratio, length ratio and slope values are chosen, i.e. 2, 1 and 2^{o} respectively. The values used for various bifurcation diagrams are given in Table 3.4. The first column denotes the biped model parameters used on the x-axis of the bifurcation diagram and the corresponding values used for r_f and r_h are shown in the subsequent columns. The midfoot length and midfoot gain values used are shown in the last column.

Table 3.4. Legend and the corresponding values used for the bifurcation diagrams.

Biped model parameter (x-axis)	Solid line	Dashed line	Dotted line	Midfoot length L_m (cm) & midfoot gain value r_m
Mass ratio $\frac{m_H}{m}$	r_f and r_h =0.8	r_f and r_h=0.5	Point feet	0 & 0
Length ratio $\frac{b}{a}$	r_f and r_h =0.8	r_f and r_h=0.5	Point feet	0 & 0
Slope angle	r_f and r_h =0.8	r_f and r_h=0.5	Point feet	0 & 0
Forefoot gain	r_h=0.5	r_h=0.2	r_h=0.01	2 & 1
Hindfoot gain	r_f=1	r_f=0.8	r_f=0.5	2 & 1
Horizontal Roll-over shape length	r_f and r_h=1	r_f and r_h=0.8	r_f and r_h=0.5	0 & 0

The evolution of the following six gait descriptors due to changes in the five biped model parameters (mass ratio, length ratio, slope angle, forefoot gain value and hindfoot gain value) are analysed, followed by the sixth biped model parameter, namely the horizontal roll-over shape length.

1. Average velocity
2. Mechanical energy
3. Step period
4. Inter leg angle (as defined in Figure 3.14)
5. Forefoot and hindfoot length
6. Roll-over shape arc length and inter-leg length

The bifurcation diagrams (Figures 3.11-13) are similar to the corresponding diagrams given by Goswami et al. (1996) for point feet, but in addition show the influence of various roll-over shapes defined by different forefoot, midfoot, hindfoot gain and length values. The bifurcation diagrams are plotted either until the passive walking has a period two response or becomes unstable.

Prosthetic foot designers have the ability to influence various gain and length values by changing the stiffness at various points in the prosthetic foot. There are other adjustments that are also undertaken to make the prosthetic foot specific to individual needs. The knowledge of inter-dependence of step period, inter-leg angle, average velocity and mechanical energy with various gain and length values and length and mass ratios directly relate to the human comfort, and hence are of interest to prosthetic foot designers. This inter-dependence is described below (Sections 3.4.3.1-3.4.3.7).

3.4.3.1 Average Velocity (Figure 3.11)

The average velocity increases significantly with increase in the foot gain value for a given mass ratio. However, for a given foot gain value, the increase in average velocity with respect to mass ratio is moderate.

The range of single periodic stability (i.e. the value of length ratio at which the gait motion switches over to double periodic) increases as the foot gain value increases. Figure 3.11 also illustrates that there is an exponential drop in the average velocity value as the length ratio increases. However, it is seen that the difference between the average velocity for different roll-over shapes, for a given mass or length ratio for a range of gain values and point feet, remains constant.

As the slope angle increases, the increase in the average velocity becomes significantly higher when the gain values are increased. It is also observed that the average velocity increases as the forefoot and hindfoot gain values increase. The influence of forefoot and hindfoot gain values on the stability of the passive walking can be observed in the last two figures. The forefoot gain bifurcation diagram illustrates that the passive walking becomes unstable for lower forefoot gains and higher hindfoot gains (solid line). The hindfoot gain bifurcation diagram also confirms this pattern (dotted line).

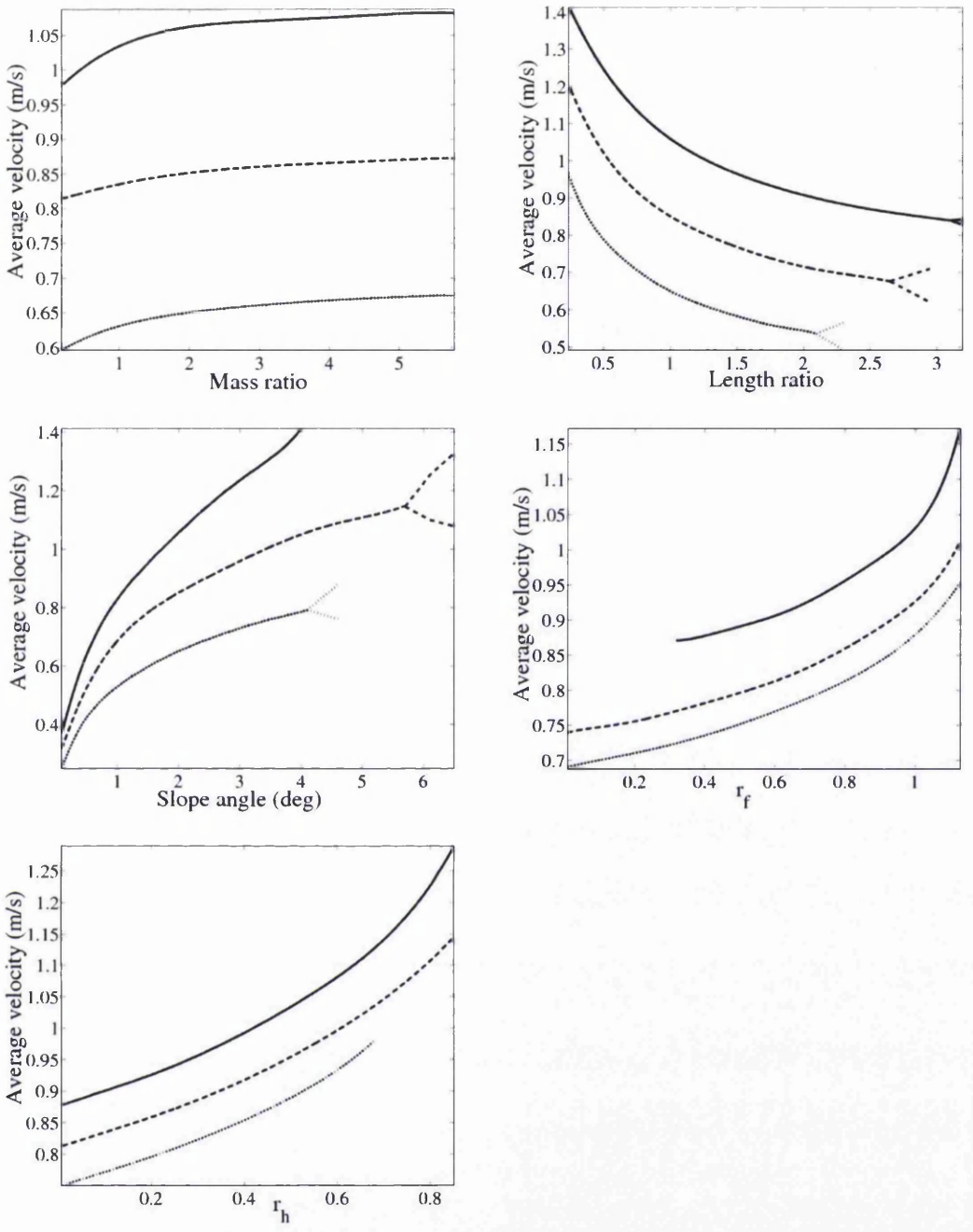

Figure 3.11. Bifurcation diagrams for average velocity. Refer to Table 3.4 for the legend.

3.4.3.2 Mechanical Energy (Figure 3.12)

The mechanical energy is the summation of the total kinetic and potential energies of the three point masses (hip mass and mass for each leg). An increase in the average velocity will result in an increase in the kinetic energy and hence the trends for various biped model parameters are similar to the average velocity bifurcation diagrams.

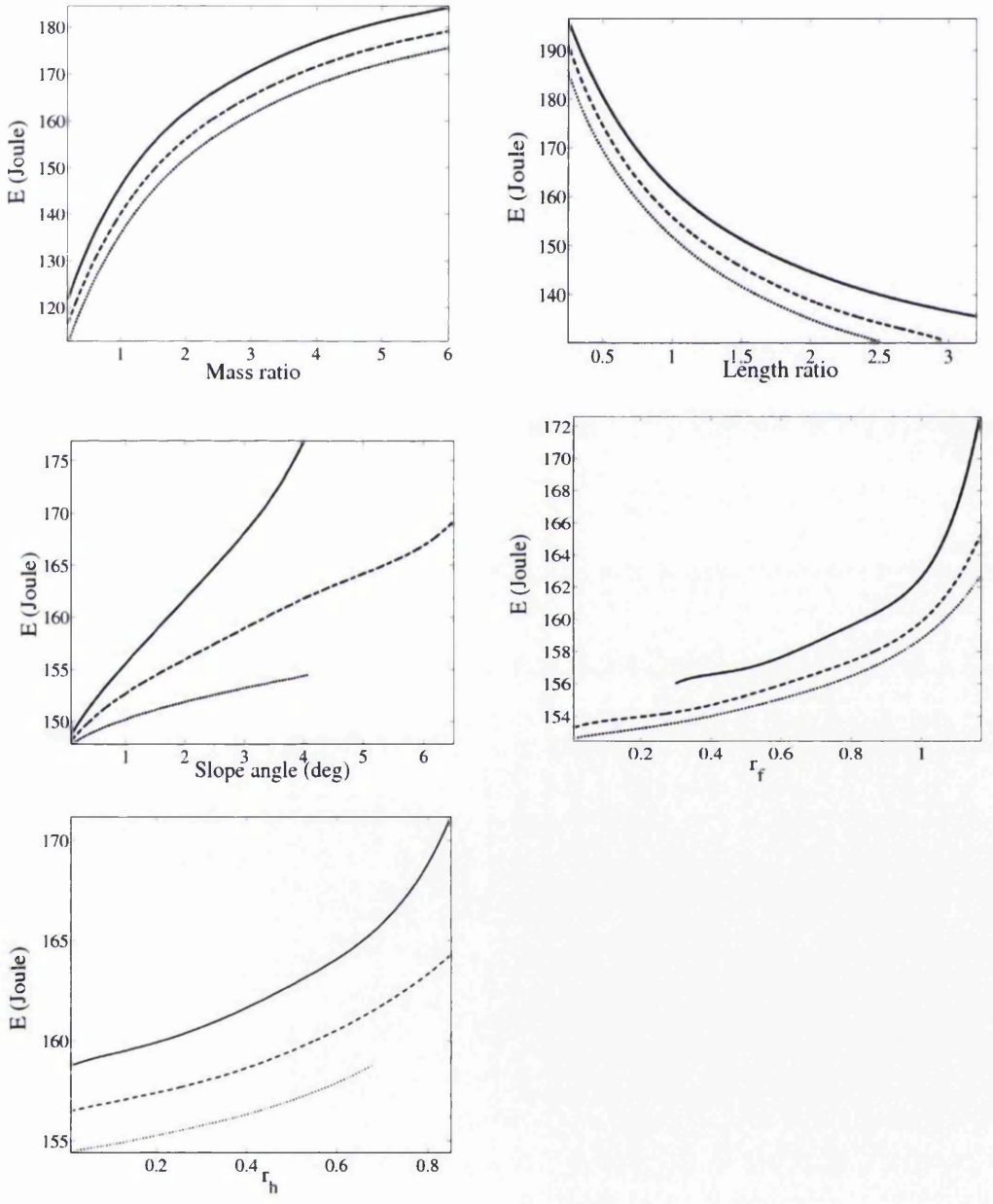

Figure 3.12. Bifurcation diagrams for mechanical energy. Refer to Table 3.4 for the legend.

3.4.3.3 Step Period (Figure 3.13)

For a given mass ratio, the effect of foot gain on the step period is moderate. However, there is an initial steep increase in step period followed by a moderate increase as the mass ratio increases. For a given length ratio, the effect of foot gain on the step period is also moderate, with a similar pattern to the mass ratio. The stability range of single period motion also increases with increased foot gain values (refer to the length ratio bifurcation diagram). The single periodic stability range initially increases with the slope angle (dotted and dashed lines). However, as the foot gain values increase, passive walking becomes unstable even at lower slope values as the gain value is further increased (solid line).

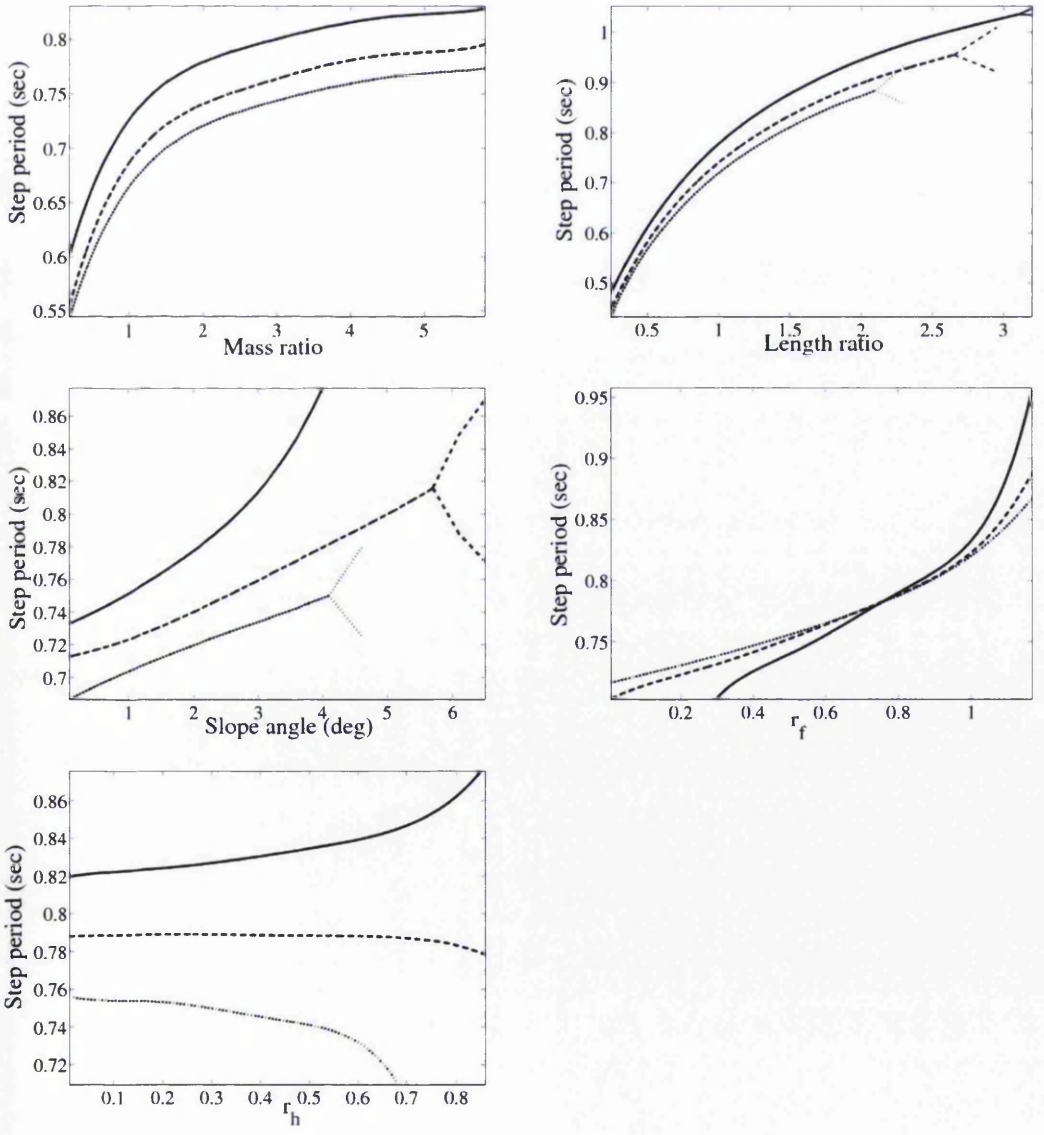

Figure 3.13. Bifurcation diagrams for the step period. Refer to Table 3.4 for the legend.

The rate of increase in the step period value with respect to forefoot gain becomes higher as the hindfoot gain value increases. In the last two bifurcation diagrams, it can be seen that the behaviour of the step period's curve changes at r_f and r_h values around 0.8. For a forefoot gain value of around 0.8, the three bifurcation graphs cross over. This value is referred to as the 'critical forefoot gain value' since the step period would remain constant for every acceptable value of hindfoot gain. This is an interesting observation with potential benefit in the design of control systems. However, it also illustrates the need to further understand the non-linear dependence of various biped model parameters on gait descriptors and also highlights the limitations of existing experimental approaches where one biped model parameter is changed at a time.

3.4.3.4 Inter-leg Angle (Figure 3.14)

The inter-leg angle is defined in Figure 3.14. The corresponding distance between the contact points of two legs is defined as the inter-leg length. The analysis of the inter-leg angle is important as it effectively controls the step length. In the case of a rolling contact the calculation of the step length is complex. The step length is equal to the distance of the contact points at the double support phase plus the arc length of the roll-over shape.

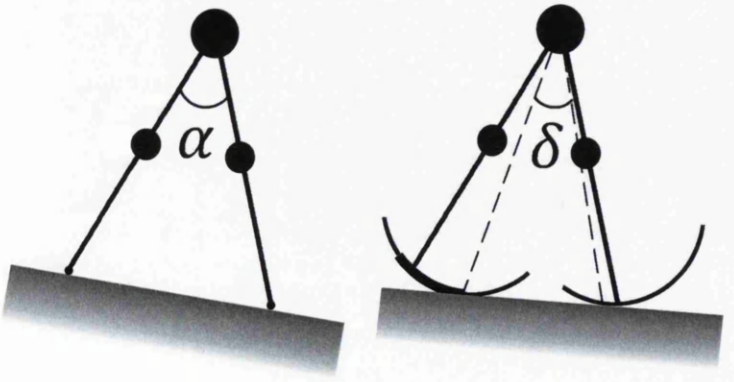

Figure 3.14. Inter-leg angles α and δ.

For different forefoot and hindfoot gains (described by solid, dashed and dotted lines) and point feet (dotted line) the variation in δ is much smaller than the variation in α (see Figure 3.15). However, the existence of a critical mass ratio (at about 1.8) is seen, where the inter-leg angle δ remains constant for any acceptable foot gain. As the mass ratio increases beyond the critical mass ratio, any increase in the foot gain decreases the inter-leg angle δ. The behaviour is opposite for mass ratio values lower than the critical mass ratio value.

The length ratio variation is similar to the mass ratio variation and demonstrates an initial increase in the inter leg angle for smaller length ratios. A critical length ratio (~1.1) occurs when all of the lines intersect and the inter-leg angle δ is constant for all acceptable values of forefoot and hindfoot gain. The Figure 3.15 also shows that the range of single period stability (i.e. the value of length ratio at which the gait motion switches over to period two motion) increases as the foot gain increases. In the last two bifurcation diagrams, where the variation in r_f and r_h are considered, the mass ratio and length ratio is 2 and 1. These values are very close to the critical values of ~1.8 and ~1.1 respectively. Hence, the value of δ remains approximately constant for a range of forefoot and hindfoot gains.

3.4.3.5 Forefoot and hindfoot lengths (L_f and L_h) (Figure 3.16)

The biped uses more horizontal hind foot length L_h to remain stable as the foot gain increases for a given mass or length ratio or slope angle. It also tends to use higher hind foot length as the mass or length ratio or slope angle increases for a given value of foot gain. Similar observations are seen for horizontal fore foot length L_f. The observations in the last two bifurcation diagrams are trivial. As the forefoot gain increases, i.e. as the roll-over shape becomes wider or tends to become flat, the horizontal forefoot length, L_f, increases. In contrast the horizontal hindfoot length, L_h, remains relatively constant. Similar observations are seen for the hindfoot gain variation.

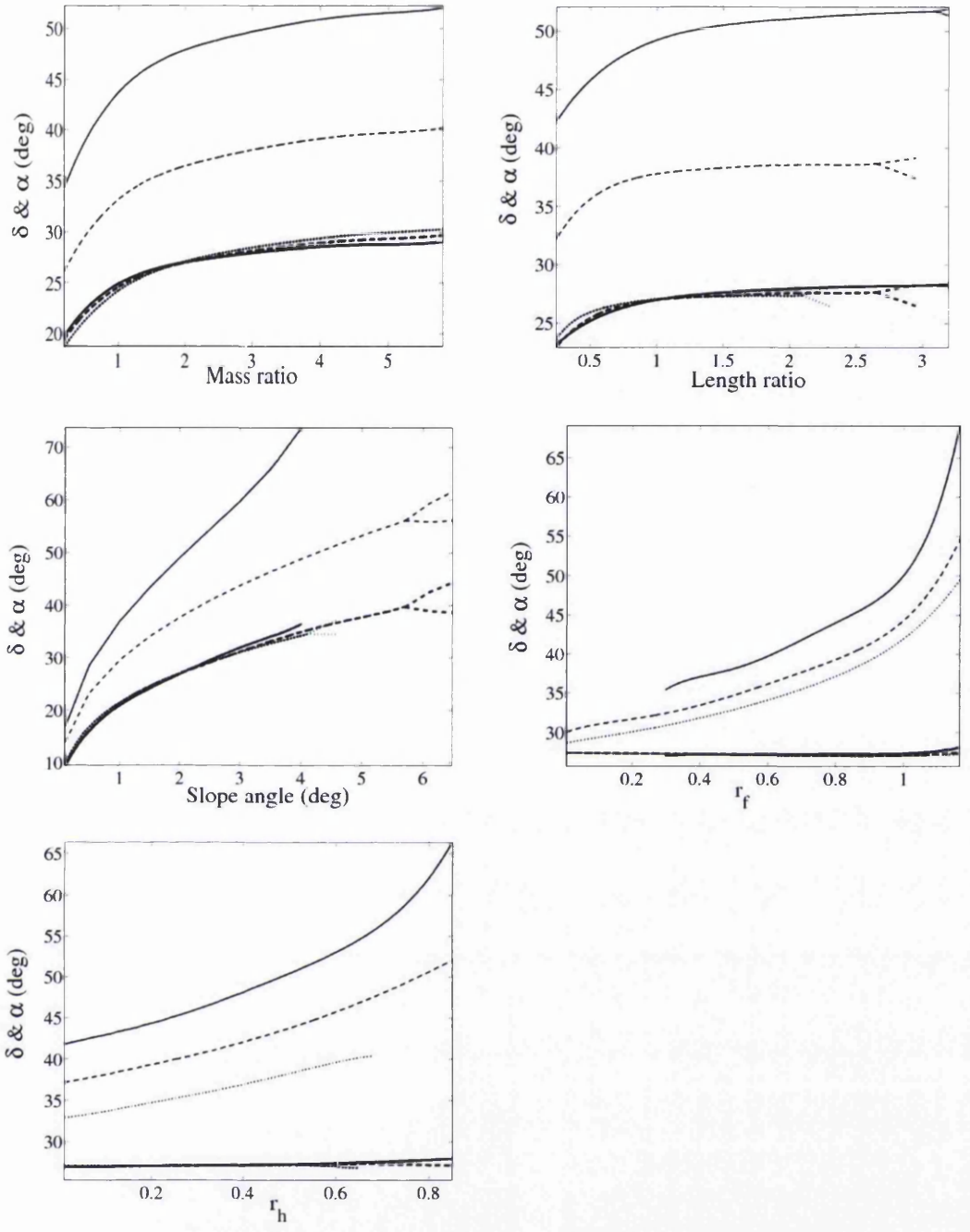

Figure 3.15. Bifurcation diagrams for the inter-leg angles. Refer to Table 3.4 for the legend.

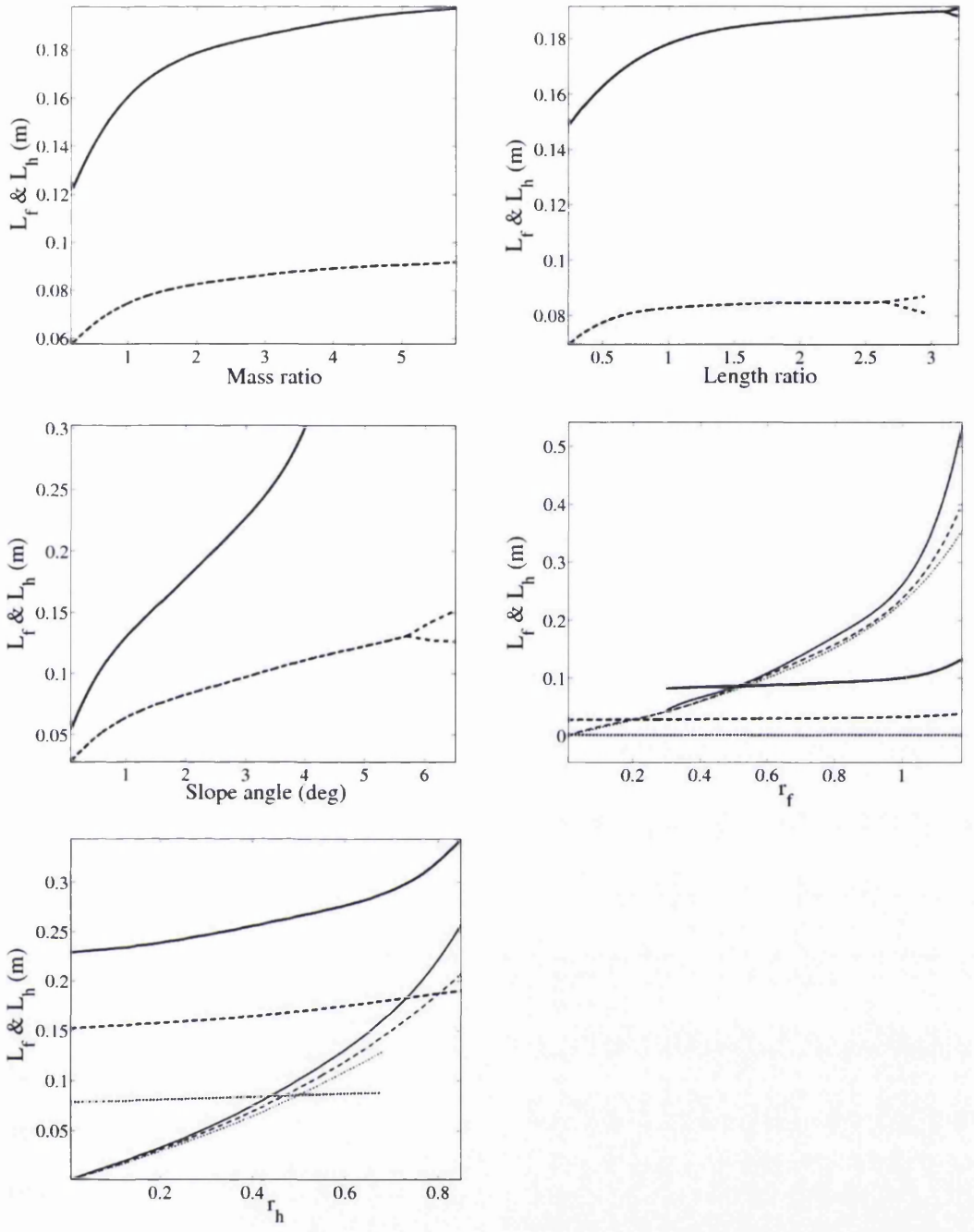

Figure 3.16. Bifurcation diagrams for the forefoot and hindfoot lengths. Refer to Table 3.4 for the legend.

3.4.3.6 Roll-over shape arc length and inter-leg length (L_e and L_i) (Figure 3.17)

The inter leg length is directly influenced by the inter-leg angle δ. A similar pattern of variation with the existence of critical mass and length ratio values is observed. The bifurcation diagrams for variation in r_f and r_h also show that the inter leg length remains almost constant for various values of forefoot and hindfoot gains. The pattern of variation for the effective roll-over shape arc length, L_e, is similar to that for the hind foot and fore foot lengths.

3.4.3.7 Effect of the horizontal roll-over shape length on gait descriptors (Figure 3.18)

The roll-over shape arc length is expected to be determined experimentally and input into the computational model proposed in this chapter. If the arc length is too long the biped model will choose a shorter roll-over shape arc length, referred to as the effective roll-over arc length, based on the governing equations. Hence the resulting horizontal roll-over shape length will be reduced. It can be seen that the average velocity increases linearly with the horizontal roll-over shape length until it is less than or equal to the maximum roll-over shape arc length for which the biped kinematics allows stable walking. The excess arc length is effectively ignored and hence the velocity value remains same. For large gain values, the passive walking becomes period two (solid line), however, the forefoot and hindfoot lengths remain single period (L_f and L_h bifurcation diagrams). This is because the input roll-over shape is smaller or equal to the effective roll-over shape chosen by the biped.

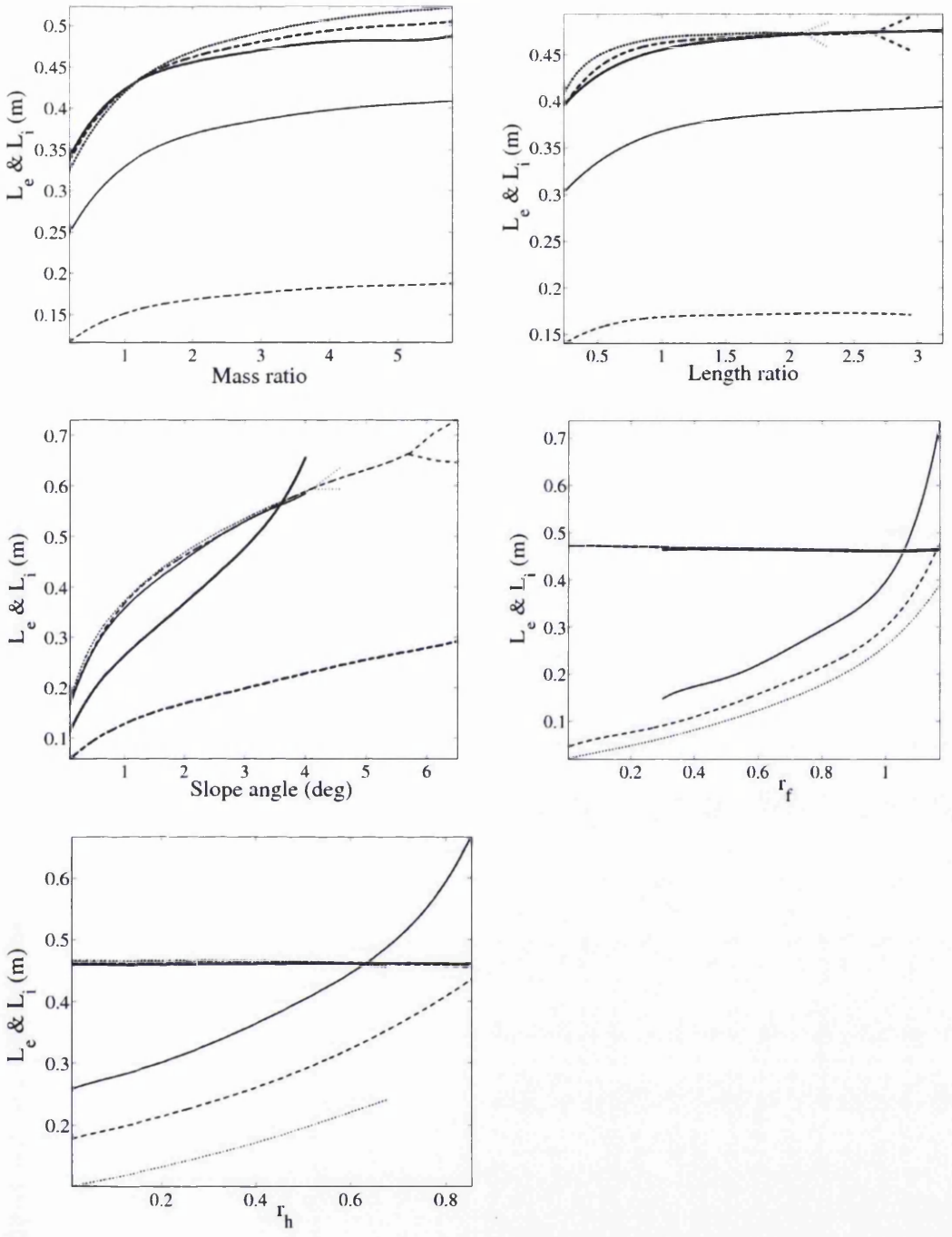

Figure 3.17. Bifurcation diagrams for the roll-over shape arc length and the inter-leg length. Refer to Table 3.4 for the legend.

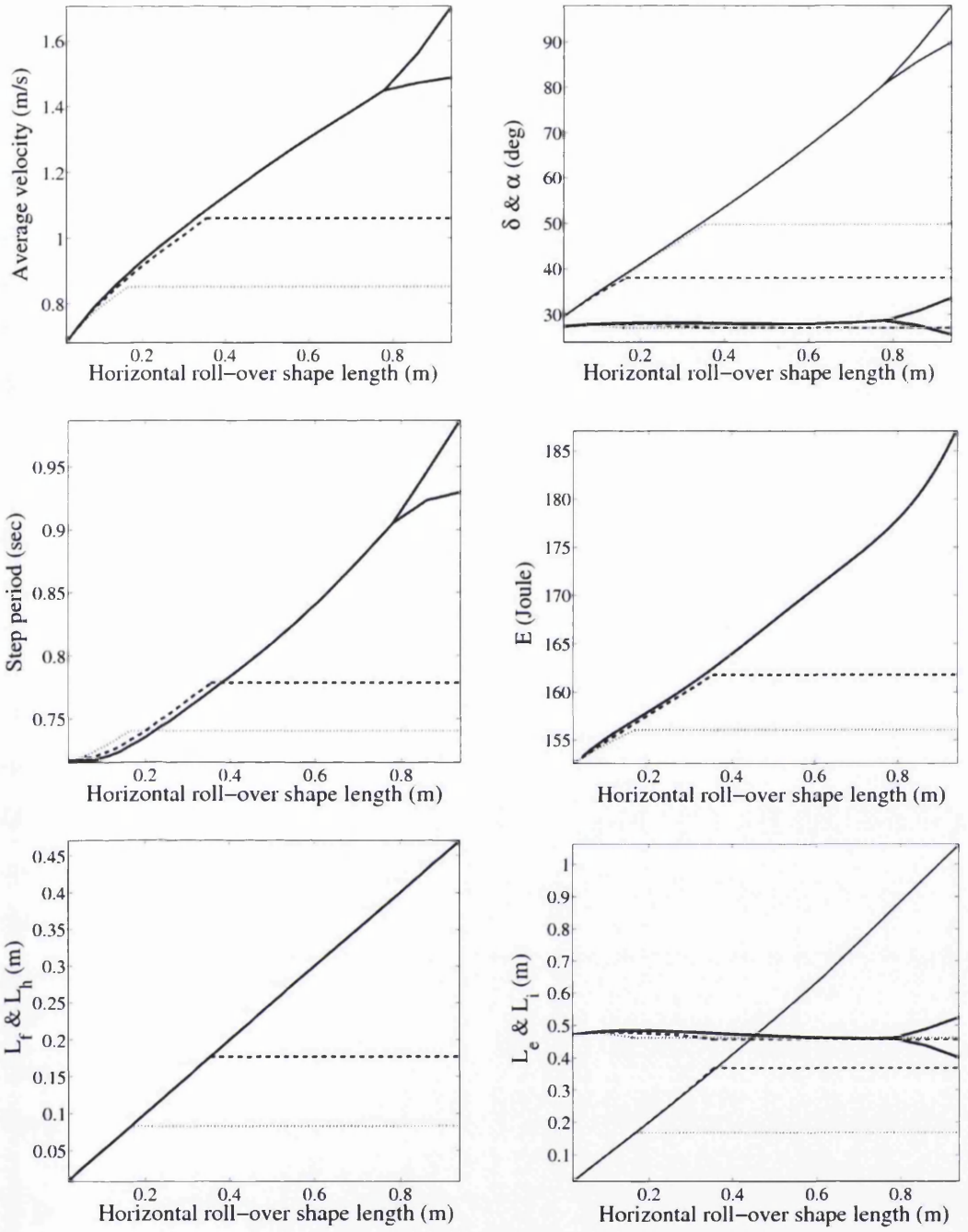

Figure 3.18. Bifurcation diagrams to illustrate the effect of horizontal roll-over shape length. Refer to Table 3.4 for the legend.

3.5 Conclusions:

Modelling the rolling contact of a foot is a challenging task, and previous research has mostly relied on point, flat or curved/circular feet. For a human foot, the centre of pressure moves forward as it rolls from the heel strike position to the toe off position. Over the last decade, experimental research on prosthetic foot design has introduced a new concept referred to as 'roll-over shape'. The roll-over shape is a locus of centre of pressure defined in a co-ordinate frame such that y-axis is always aligned with the straight line joining the ankle and knee or the line joining the ankle and hip (Hansen et al., 2004b). Roll-over shapes, although independent of walking speed, depend on various conditions such as age, medical conditions, shoe type, shoe heel height, shoe flexibility, slope of the walking surface, and can be determined experimentally.

A discrete pivot point roll-over model has been developed that takes the roll-over shape as an input parameter and computes its effect on the stability and kinematics of passive biped model. The fundamental double pendulum equations proposed by Goswami et al. (1998) have been revisited to model the influence of variable curvature of roll-over shapes and the continuous angular velocity of the swing leg during the roll-over phase. The traditional single support phase is replaced with two phases: the stance leg transition phase and the single support phase. The corresponding governing equations have been re-developed. The initial conditions for the double pendulum model are updated at each stance leg transition phase and the procedure has been described.

A parametric study was undertaken for various gains (r_f and r_h), lengths (L_f and L_h), and mass and length ratios, on various slopes, to study the effect on the average velocity, step period, inter-leg angle and mechanical energy of the system. This is important as the experimental research reported in Section 2.3 has shown evidence that the analysis of roll over shapes for the optimal design of prosthetic feet has become an increasingly important area of research. The stiffness and other adjustments used in an optimal prosthesis design influence the shape and size of the corresponding roll-over shape. The results of the parametric study provide a first step in discovering trends in order to gain further insights in the complex inter-

dependency among various gait parameters. The effect of unbalance masses on the kinematics of the walking resulting from replacing one leg of the biped with a prosthetic leg is discussed in the next chapter.

Chapter 4 Optimising the 'heel to toe' roll-over shape for symmetric passive bipedal walking motion with unbalanced masses

4.1 Introduction

A prosthetic foot is an artificial limb and effectively is a dead weight that is not supported by human muscles and its nervous system. As a result, transtibial amputees tend to feel that the prosthetic foot is heavy even if it weighs only quarter of the corresponding weight of the human leg. This Chapter proposes a mathematical formulation, derived from first principles, to investigate whether the mass imbalance has an influence on the kinematics of the gait. This is important as the human desire to maintain symmetric walking gait irrespective of imbalances may result in sub-optimal energy consumption levels.

The recent work (Srinivasan et al., 2009) has proposed a forward dynamic model that is essentially a multi-link model with point mass assumption for each link and the forward motion corresponds to the dynamics of an inverted pendulum. The model was coupled with inverse dynamics where an experimentally determined trajectory of the walking gait was used to compute moments at various joints as a function of the forward progression. The model assumed a roll-over shape for the physiological leg and discovered an optimal roll-over shape for the prosthetic foot that minimised the energy consumption. The roll-over shape has been widely used to understand the knee-ankle-foot kinematics as it is invariant to many gait parameters such as added weight, speed and shoe heel height (Hansen and Childress, 2010, Ren et al., 2010, Wang and Hansen, 2010). Hansen et al. (2003) developed an alignment algorithm and computational alignment system to match the roll-over shape of prosthetic feet with an ideal shape. However, the ideal roll-over shape was considered same as the roll-over shape of the able-bodied foot/ankle system during walking.

It can be argued that the Srinivasan et al. (2009) model can potentially become amputee specific if its anthropometric data (e.g. location and magnitude of point masses, lengths of corresponding links, moments of inertia etc) is input to the model. However, the applicability of this approach is constrained as a result of the following assumptions:

- It is very unlikely that the amputee will have access to his/her motion analysis describing the required trajectory of their natural walking gait for the computation of joint torques.
- The prosthetic foot stiffness design may not be optimal if the model uses any other standard walking gait to calculate the joint moments.
- It is likely that the amputee will adapt to a non-optimal stiffness of the prosthetic foot and without realising force themselves to achieve symmetric walking by expending higher levels of energy.

Many gait descriptors have been presented to study the asymmetry of walking with a prosthetic foot (Sagawa Jr et al., 2011, Van der Linde et al., 2004). In this Chapter walking asymmetry is evaluated using the Inter-leg angle and the step period. An example of the asymmetric walking is shown in the schematic diagram in Figure 4.1. If both physiological and prosthetic feet have the same roll-over shape as input then, based on the kinematic considerations alone, the walking is asymmetric, as shown by the shadowed triangle describing the asymmetry in terms of the inter-leg angle as well as the step length. The proposed mathematical formulation exploits the benefits of passive walking and develops an amputee specific optimal roll-over shape for the prosthetic foot by changing the roll-over gain and the forefoot arc length so that (Figure 4.1b) the walking is stable and symmetric with respect to the step period and the inter-leg angle. The mathematical formulation discussed in Chapter 3 produces an optimal region defined by boundaries that minimise limping with reference to the inter-leg angle (solid curve in Figure 4.1c) and step period (dotted curve in Figure 4.1c). Thus for a given forefoot arc length, an optimal range for the gain (or the curvature of the roll-over shape) can be determined. Details of obtaining optimal range are discussed more in section 4.4.1.

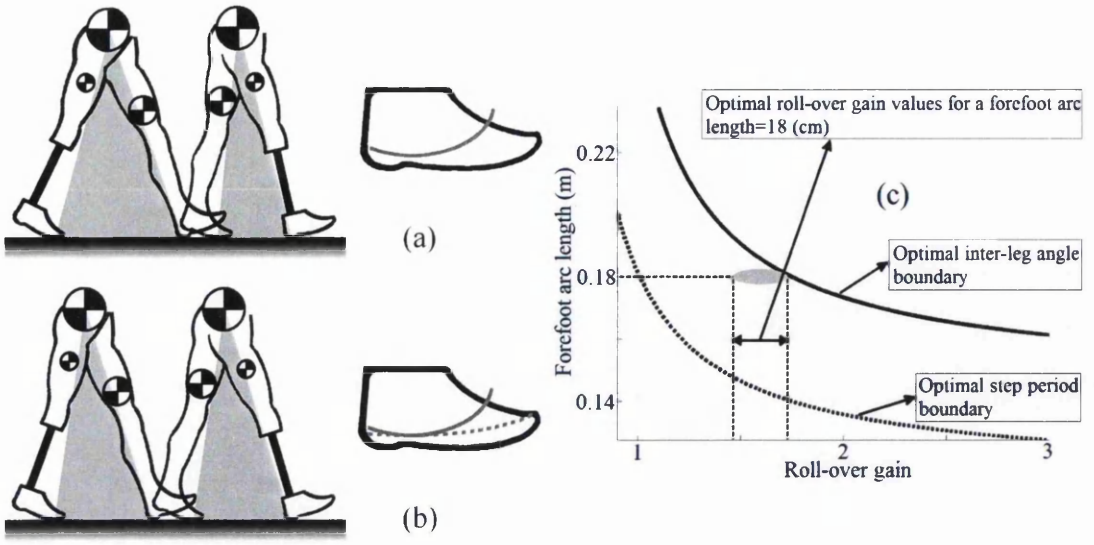

Figure 4.1. Walking with identical roll-over shapes (a) and with an optimal roll-over shape (b). The grey region represents the inter-leg angle and the dotted curve shows an optimal roll-over shape. The gait is symmetric while the prosthetic leg roll-over shape is within the optimal roll-over shape range (c). Solid and dotted lines describe symmetric gait with respect to the inter-leg angle and step period respectively. The ellipsoid shows the range of optimal roll-over gain for a forefoot arc length of 18cm.

Gard and Childress (2001) studied the kinematics of the walking motion and measured the trajectory of a mass as it rolls on a circular arc. It was demonstrated that the trajectory can be modelled by a simple inverted pendulum but with a longer virtual leg length extending to a virtual floor beneath the actual floor. However, to study the dynamics of the biped walking motion, it is not possible to accurately model the entire rolling motion in the single support phase even using a simple double pendulum dynamics as the distance between the rolling contact point and hip and leg masses changes during the rolling motion.

A detailed review of the applicability of the roll-over shape for a biped walking process and of various computational approaches for modelling biped walking motion are described in Chapter 3 along with a mathematical formulation to input an arbitrary shaped roll-over shape in a passive walking biped model with identical masses for both legs. This computational model is extended in this Chapter in order to study the effect of the mass imbalance on walking symmetry resulting from the

lighter prosthetic foot and is presented in Section 4.2. It has been shown in Section 4.2.2 that the proposed model is able to reproduce the circular trajectory of the hip mass as it rolls on a circular arc. It also demonstrates that the actual roll-over shapes are not symmetric around the ankle joint as the forefoot length is longer than the hindfoot length. The predicted trajectories are shown. The section also describes the assumptions used in the analysis and discusses the minimum number of pivot points required to ensure convergence in predicted values of inter-leg angles. Section 4.3 describes the creation of a passive walking biped model with anthropometric and prosthetic foot data. For the physiological foot a roll-over shape is chosen that is consistent with experimentally observed shapes. The multiple pivot point model that describes the roll-over shape is briefly described. Results are discussed in Section 4.4 and the Chapter is concluded in Section 4.5.

4.2 Dynamics of passive walking

The dynamics of the biped walking motion with unbalanced mass has been modelled using the schematic as shown in Figure 4.2. The effect of a roll-over shape for each leg is modelled as rolling contacts discretised by multiple pivot points where each pivot point is assumed to be a point contact (Figure 4.2).

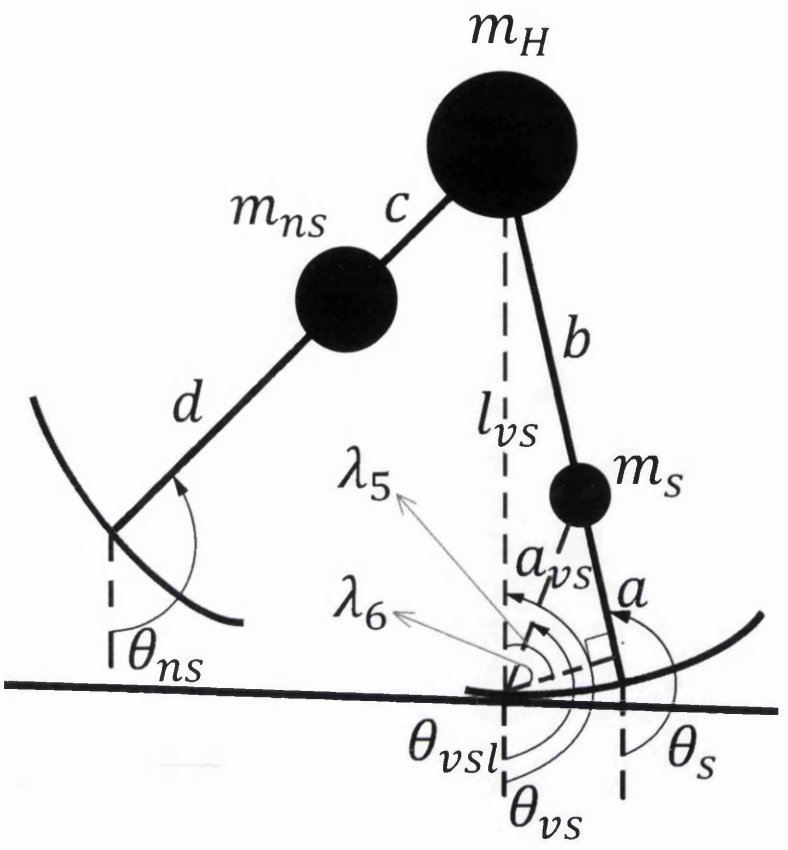

Figure 4.2. A schematic representation of a two linked model with different masses and different positions of the corresponding centre of masses rolling down a shallow slope. The dashed lines represent the virtual stance leg (l_{vs}) and the virtual stance lower leg (a_{vs}).

In a multiple pivot point model the dynamics of the walking process during the single support phase and the rolling of the stance leg between every two consecutive pivot points is assumed to be similar to the double pendulum dynamics proposed in Chapter 3. The initial conditions for each pivot point are changed for every contact point. The supported leg is defined as a link which connects the current pivot point to the hip mass. This virtual leg is different from the actual stance leg (Figure 4.2). In this work, the supported leg is called as virtual stance leg (l_{vs}) and its length, initial angular displacement and initial angular velocity is changed from one pivot point to another. The kinematical model also defines another parameter, referred to as a virtual stance lower leg (a_{vs}), which connects the pivot point to the centre of mass of the stance leg. Its initial conditions are assumed to be identical to those used for the

virtual stance leg and hence, change at every time-step. The equations of motion for every pivot point are similar to the dynamics of the point feet biped (Goswami et al., 1998) but have different positions for the centre of leg masses and values of leg masses for both prosthetic and physiological feet. Thus

$$M^i(\theta)\ddot{\theta} + C^i(\theta,\dot{\theta})\dot{\theta} + K^i(\theta) = 0 \tag{4.1}$$

where $\theta = [\theta_{vs} \quad \theta_{ns}]^T$ and θ_{vs} and θ_{ns} are measured from the negative y-axis, as shown in Figure 4.2.

The inertia matrix, $M(\theta)$, centrifugal terms, $C(\theta,\dot{\theta})$, gravitational stiffness matrix, $K(\theta)$, and initial conditions for the i^{th} pivot point, are

$$M^i(\theta) = \begin{bmatrix} m_s a_{vs}^{i^2} + m_H l_{vs}^{i^2} + m_{ns} l_{vs}^{i^2} & -m_{ns} l_{vs}^i c\cos(\theta_{vs} - \theta_{ns}) \\ -m_{ns} l_{vs}^i c\cos(\theta_{vs} - \theta_{ns}) & m_{ns} c^2 \end{bmatrix} \tag{4.2}$$

$$C^i(\theta,\dot{\theta}) = \begin{bmatrix} 0 & -m_{ns} l_{vs}^i c\dot{\theta}_{ns} \sin(\theta_{vs} - \theta_{ns}) \\ m_{ns} l_{vs}^i c\dot{\theta}_{ns} \sin(\theta_{vs} - \theta_{ns}) & 0 \end{bmatrix} \tag{4.3}$$

$$K^i(\theta) = \begin{bmatrix} m_s g a_{vs}^i \sin(\theta_{vs} + \lambda_6^i - \lambda_5^i) + (m_H g l_{vs}^i + m_{ns} g l_{vs}^i)\sin(\theta_{vs}) \\ -mgc\sin(\theta_{ns}) \end{bmatrix} \tag{4.4}$$

$$\theta_{vs}^{initial} = \theta_{vs}^i, \quad \theta_{ns}^{initial} = \theta_{ns}^i, \quad \dot{\theta}_{vs}^{initial} = \dot{\theta}_{vs}^i \text{ and } \dot{\theta}_{ns}^{initial} = \dot{\theta}_{ns}^i \tag{4.5}$$

4.2.1 Transition phases

In addition to a double support transition phase, the multiple pivot point model also defines a stance leg transition phase to occur during every walking step. The double support transition phase occurs once in each walking step when the body rotates about the last pivot point of the stance leg and the swing leg has just made contact with the ground at its first pivot point. After the first pivot point contacts the ground, the body begins to swing about this contact while the second pivot point contact occurs, which is called as stance leg transition phase. This process continues until the swing leg contacts the ground. The impacts during transition phases are assumed to be inelastic and sliding at the pivot points is not allowed.

4.2.1.1 The double support transition phase

During both transition phases the body configuration remains unchanged and the angular momentum of the whole body is conserved about the impacting pivot points. The angular momentum of the former stance leg about the hip is also conserved during the double support transition phase. The geometry of the body at the first pivot point impact (double support transition phase) leads to the following relationship between the angular position of the virtual stance leg and the swing leg:

$$\theta_{vs}^{1} + \theta_{ns}^{1} = -2\phi + 2\pi \tag{4.6}$$

The assumption that the body configuration remains unchanged during impact leads to the following equation:

$$\theta^{1+} = J\theta^{1-} \tag{4.7}$$

where

$$J = \begin{bmatrix} 0 & 1 \\ 1 & 0 \end{bmatrix} \tag{4.8}$$

The conservation of angular momentum about the impacting pivot points and the hip leads to the condition:

$$\dot{\theta}^{1+} = \frac{H^1(\theta)}{H_d^1}\dot{\theta}^{1-} \tag{4.9}$$

where the elements of $H^1(\theta)$ are

$$\begin{aligned} H_{11}^1 = {} & m_H m_s b^2 l_{vs}^{e-} l_{vs}^{1+} \cos(\theta_{vs}^- - \theta_{vs}^+) + m_s^2 b^2 l_{vs}^{1+} a_{vs}^{e-} \cos(\theta_{vs}^- - \theta_{vs}^+ + \lambda_6^{e-} - \lambda_5^{e-}) \\ & + m_s m_{ns} b^2 l_{vs}^{e-} a_{vs}^{1+} \cos(\theta_{vs}^- - \theta_{vs}^+ + \lambda_5^{1+} - \lambda_6^{1+}) \\ & + m_s^2 b^2 l_{vs}^{1+} a_{vs}^{e-} \sin(\lambda_6^{e-}) \cos(\theta_{vs}^+ - \theta_{ns}^+) \end{aligned} \tag{4.10}$$

$$H_{12}^1 = -m_s m_{ns} b^2 c a_{vs}^{1+} \sin(\lambda_6^{1+}) \tag{4.11}$$

$$\begin{aligned} H_{21}^1 = {} & m_s m_H b l_{vs}^{e-} l_{vs}^{1+2} \cos(\theta_{vs}^+ - \theta_{ns}^+) \cos(\theta_{vs}^- - \theta_{vs}^+) \\ & + m_s^2 b a_{vs}^{e-} l_{vs}^{1+2} \cos(\theta_{vs}^+ - \theta_{ns}^+) \cos(\theta_{vs}^- - \theta_{vs}^+ + \lambda_6^{e-} - \lambda_5^{e-}) \\ & + m_s m_{ns} b l_{vs}^{e-} l_{vs}^{1+} a_{vs}^{1+} \cos(\theta_{vs}^+ - \theta_{ns}^+) \cos(\theta_{vs}^- - \theta_{vs}^+ + \lambda_5^{1+} - \lambda_6^{1+}) + m_s m_H b a_{vs}^{e-} l_{vs}^{1+2} \sin(\lambda_6^{e-}) \\ & + m_s m_{ns} b a_{vs}^{e-} l_{vs}^{1+2} \sin(\lambda_6^{e-}) + m_s^2 b a_{vs}^{e-} a_{vs}^{1+2} \sin(\lambda_6^{e-}) \end{aligned} \tag{4.12}$$

$$H_{22}^{1} = -m_s m_{ns} b c l_{vs}^{1+} a_{vs}^{1+} \sin(\lambda_6^{1+}) \cos(\theta_{vs}^{+} - \theta_{ns}^{+}) \tag{4.13}$$

and

$$H_d^1 = m_s b^2 (m_H l_{vs}^{1+2} + m_s l_{vs}^{1+2} + m_{ns} a_{vs}^{1+2} - m_s l_{vs}^{1+2} \cos^2(\theta_{vs}^{+} - \theta_{ns}^{+})) \tag{4.14}$$

The superscripts "+" and "-" denote post and pre-pivot point impact variables respectively and the value beside represents the number of pivot points, which for the double support phase is equal to 1.

4.2.1.2 The stance leg transition phase

During a walking step the stance leg transition phase occurs *(e-1)* times from the second pivot point impact up to the eth pivot point. The assumption that the swing leg and the stance leg angle remains unchanged during the impact gives the following condition for the i^{th} pivot point impact $(2 \le i \le e)$:

$$\theta_{ns}^{+} = \theta_{ns}^{-} \text{ and } \theta_s^{+} = \theta_s^{-} \tag{4.15}$$

The value of the time-step t^* between each pivot point is assumed to be sufficiently small so that the consecutive pivot points accurately define the given roll-over shape. The sensitivity and convergence properties of using different number of pivot points for links with equal masses are discussed in Chapter 3. During the stance leg transition phase the roles of the supported leg and the swing leg remain unchanged and the conservation of angular momentum about the hip during the double support transition phase is replaced with the conservation of angular momentum of the swing leg with respect to hip. The conservation of angular momentum leads to the following condition

$$\dot{\theta}^{i+} = \frac{H^i(\theta)}{H_d^i}\dot{\theta}^{i-} \tag{4.16}$$

where

$$\begin{aligned} H_{11}^i &= m_H l_{vs}^i l_{vs}^{i-1}\cos(\theta_{vs}^{i+} - \theta_{vs}^{i-}) + m_s a_{vs}^i a_{vs}^{i-1}\cos(\theta_{mvs}^{i+} - \theta_{mvs}^{i-}) \\ H_{11}^i &= m_H l_{vs}^i l_{vs}^{i-1}\cos(\theta_{vs}^{i+} - \theta_{vs}^{i-}) + m_s a_{vs}^i a_{vs}^{i-1}\cos(\theta_{mvs}^{i+} - \theta_{mvs}^{i-}) \\ &\quad + m_{ns} l_{vs}^i l_{vs}^{i-1}\cos(\theta_{vs}^{i+} - \theta_{vs}^{i-}) - m_{ns} cl_{vs}^{i-1}\cos(\theta_{vs}^{i-} - \theta_{ns}^{i-}) \end{aligned} \tag{4.17}$$

$$H_{12}^i = H_{21}^i = 0 \tag{4.18}$$

$$H_{22}^i = H_d^i = m_H {l_{vs}^i}^2 + m_s {a_{vs}^i}^2 + m_{ns} {l_{vs}^i}^2 - m_{ns} cl_{vs}^i \cos(\theta_{vs}^{i+} - \theta_{ns}^{i+}) \tag{4.19}$$

In addition to a double support transition phase, the multiple pivot point model also defines a stance leg transition phase to occur during every walking step. The double support transition phase occurs once in each walking step when the body rotates about the last pivot point of the stance leg and the swing leg has just made contact with the ground at its first pivot point. After the first pivot point contacts the ground, the body begins to swing about this contact while the second pivot point contact occurs, which is called as stance leg transition phase. This process continues until the swing leg contacts the ground. The impacts during transition phases are assumed to be inelastic and sliding at the pivot points is not allowed.

4.2.2 Verification of the model with a trajectory of hip mass rolling on a circular arc

The roll-over shape model proposed in Section 4.2 was used to model the simple inverted pendulum experiment undertaken by Gard and Childress (2001) as described in the introduction section. The hip mass of 52.3 kg, with gain value (r) 0.77 and an equal value of 11 cm was used for both the hindfoot (Arc_h) and forefoot arc length (Arc_f). The trajectory of the hip mass is plotted in Figure 4.3a. Clearly the shape is circular, as observed by Gard and Childress (2001). However, a motion trajectory of the two link model with three masses corresponding to a mid person

(see Table 4.1) is shown in Figure 4.3b. A realistic roll over shape is used where the hindfoot and forefoot lengths and the gain are $Arc_h = 3\text{cm}, Arc_f = 14\text{cm}$ and $r = 1.5$. The trajectory is not circular in shape.

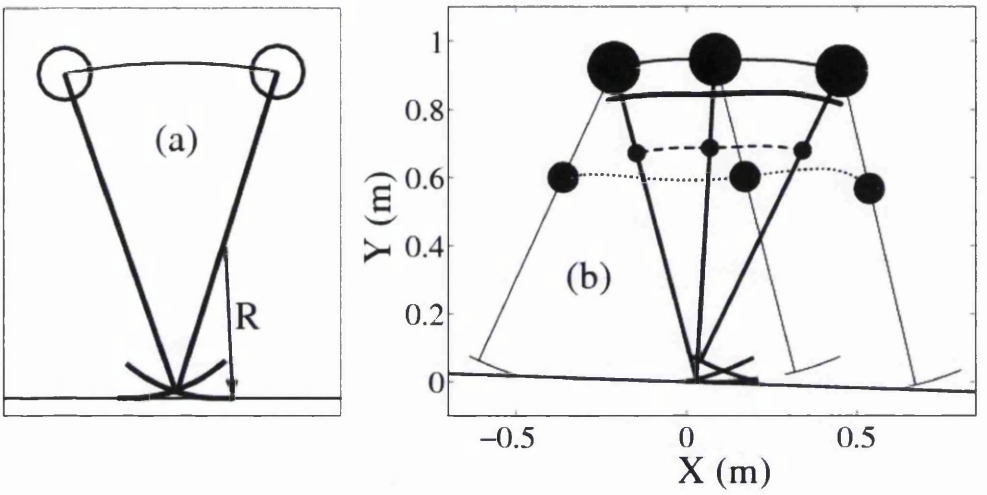

Figure 4.3. (a) shows the motion trajectory of a mass rolling on a surface with identical hindfoot and forefoot using computational model which is similar to the schematic figure presented by Gard and Childress (2001) (b) describes the motion trajectory of the studied model with two masses located on the stance leg and the swing leg mass. It can be seen that roll-over shape used in Figure 3b is asymmetric as compared to the one shown in Figure 3a. Dotted, dashed and solid lines represent swing leg, stance leg and hip mass respectively. The trajectory of the overall centre of mass is shown with a bold curve.

4.2.3 Sensitivity of the roll over shape model using discrete pivot points

A comparison of the multiple pivot point model with the analytical solution for the rolling motion of a disk on an inclined surface is shown in Chapter 3. It is found that if the number of pivot points is sufficiently large then the solution given by the multiple pivot point model converges to the analytical displacement profile. For a two linked model an analytical solution does not exist. However, the oscillations in inter-leg angle and step period were shown to converge to a unique value.

For an unbalanced mass, as proposed in this Chapter, the walking is asymmetric or unstable. Figure 4.4 illustrates the convergence of inter-leg angle and step period values for a passive biped walking motion with increasing number of pivot points on the optimal roll-over shape corresponding to the right corner of ellipsoid shown in Figure 4.1c $\left(Arc_h = 3\text{cm},\ Arc_f = 18cm \text{ and } r = 1.725\right)$. Figures 4.4a and b show that the oscillations in the inter-leg angle and the step period converge to one and two values respectively. The values for hip mass, intact leg mass and residual leg mass correspond to the mid person masses presented in Table 4.1. The minimum number of pivot points used should be more than 3000 in this example to ensure convergence. This value was also used in all examples presented in this Chapter.

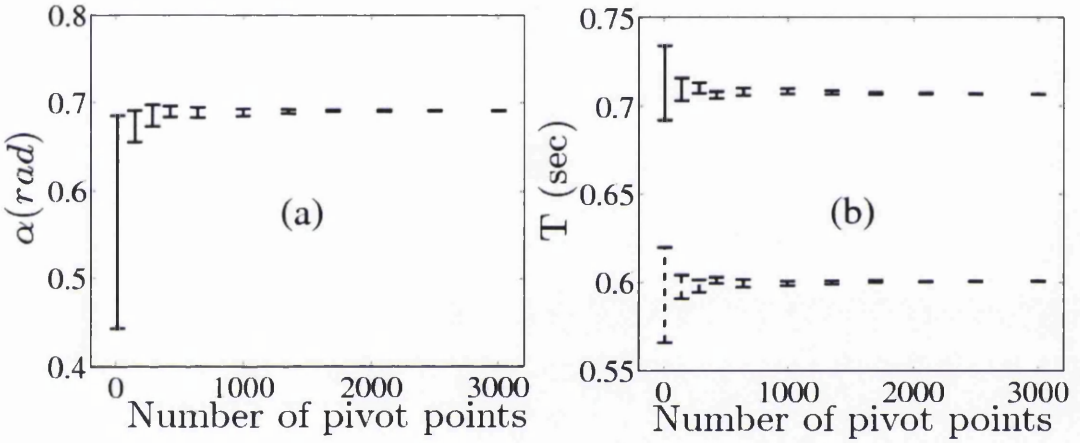

Figure 4.4. The discretised roll-over shape is optimised for producing a symmetric inter-leg angle value. Figure 4a shows that the inter-leg angle converges to a unique value as the number of pivot points increase. However the corresponding values for step period are two periodic and as seen in Figure 4b both values converge to two unique values.

4.3 Amputee specific anthropometric data and input roll-over shape

Sample anthropometric data (weights, centre of mass (COM) positions and lengths) for small, medium and large individuals were given by Armstrong (1988) and are tabulated in Table 4.1. This data can also be generated for any individual. The weight of the prosthetic foot is estimated from the information available on the website of a commercial prosthetic foot manufacturer, (Chas-A-Blatchford-and-

Sons-Ltd, 2013). The upper body mass and the leg masses are modelled as point masses on the hip joint and at centre of mass of the leg respectively. The values used for the case study presented in this Chapter are detailed in Table 4.1.

Table 4.1. Anthropometric data (mass distribution and the segment lengths) for small, medium and large persons. (*) and (**) present the data were taken from (Armstrong 1988) and (Chas-A-Blatchford-and-Sons-Ltd, 2013) respectively.

	Small person	Mid person	Large person
Foot length*	88.4 cm	94.6 cm	100.8 cm
Total mass (m_{tm})*	63.3 kg	81.5 kg	97.7 kg
Thigh COM*	70.2 cm	75 cm	79.8 cm
Calf COM *	30.7 cm	33 cm	35.3 cm
Foot COM *	2.6 cm	2.8 cm	3 cm
Thigh mass (m_{tc})*	7.7 kg	9.8 kg	11.8 kg
Calf mass (m_{cc})*	3.1 kg	3.8 kg	4.5 kg
Foot mass (m_{fc})*	0.8 kg	1 kg	1.1 kg
Physiological lower leg length*	54.9819 cm	59.1233 cm	63.4362 cm
Physiological upper leg length*	33.4181 cm	35.4767 cm	37.3638 cm
Mass ratio $\left(\mu = \frac{m_H}{m_{physiological\ leg}} = \frac{m_{tm} - 2\times(m_{tc} + m_{cc} + m_{fc})}{(m_{tc} + m_{cc} + m_{fc})}\right)$	3.4569	3.5822	3.6149
Length ratio $\left(\beta = \frac{\text{Physiological upper leg length}}{\text{Physiological lower leg length}}\right)$	0.6078	0.6000	0.5890
Prosthetic lower leg length	62.89 cm	68.67 cm	74.10 cm
Prosthetic upper leg length	25.51 cm	25.93 cm	26.70 cm
Prosthetic lower leg mass (m_{pll})**	1.4 kg	1.4 kg	1.4 kg
Leg's mass ratio	0.7845	0.7671	0.7586

$\left(\upsilon = \frac{m_{prosthetic\ leg}}{m_{physiological\ leg}} = \frac{(m_{tc} + m_{plt})}{(m_{tc} + m_{cc} + m_{fc})}\right)$			
Leg's length ratio $\left(\gamma = \frac{\text{Prosthetic upper leg length}}{\text{Physiological upper leg length}}\right)$	0.7634	0.7309	0.7146

In this case study, the roll-over shape for both legs is assumed to remain unchanged during the walking process. Three parameters, namely the hindfoot arc length (Arc_h), forefoot arc length (Arc_f) and the roll-over gain value, are used to uniquely describe a roll-over shape. The hindfoot arc length and forefoot arc length values present the rear part and the front part of roll-over shape respectively and are measured from the position of the ankle in relation to the roll-over shape. The ankle position on the roll-over shape is where the x value is assumed to be zero (Figure 4.5). A roll-over gain value describes the curvature of the roll-over shape. A higher gain value corresponds to a wider roll-over shape and vice a versa. The polynomial function that describes the roll-over shape is given by:

$$f_R(x) = \frac{1}{r}(x-h)^2 - \frac{1}{r}h^2 \tag{4.20}$$

where h is defined as the horizontal distance between the origin and the optimum point of the roll-over shape function.

To analyse the motion, the continuous roll-over shape is modelled as discrete pivot points using the model described in Section 4.2. Two roll-over shape curves used for the physiological leg are shown in Figure 4.5 and have the hindfoot arc length (Arc_h) and the forefoot arc length (Arc_f) set as 3cm and 14cm respectively. The corresponding gain values are 1.5 (solid line) and 2.5 (dashed line). Also shown in Figure 4.5 are sample roll-over shapes determined from experiments (Sam et al., 2004).

The biped is assumed to walk down a shallow slope (2^o) without using any controllers or actuators. The scuffing problem of the kneeless swing leg with the

ground is neglected during the single support phase (Garcia et al., 1998, McGeer, 1990).

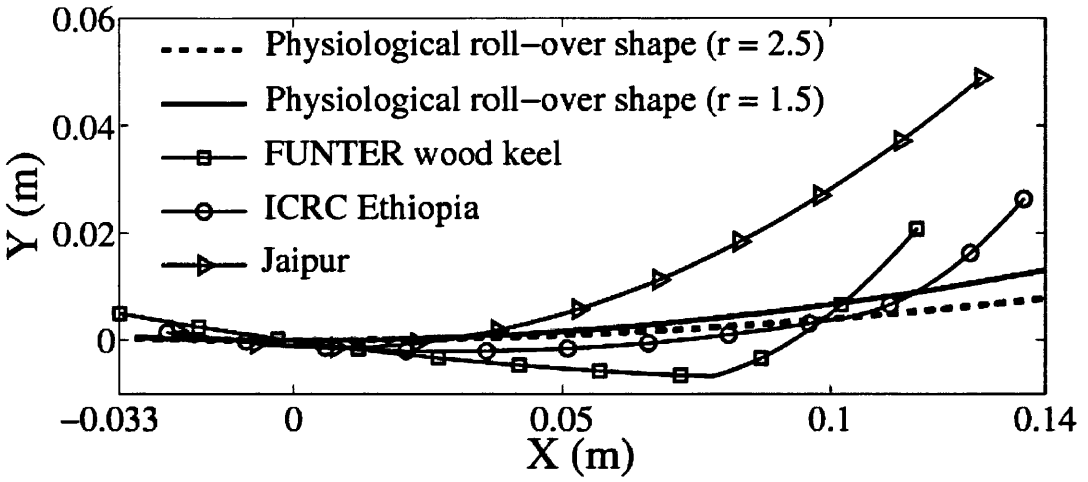

Figure 4.5. Three individual roll-over shapes measured by Sam et al. (2004). Curves represented by the solid and dashed lines are used as the physiological roll-over shapes in this Chapter.

4.4 The effect of the prosthetic foot roll-over shape on asymmetric walking

The effect of changing roll-over shape on asymmetric walking is investigated using bifurcation diagrams in Section 4.4.1 and using phase plane limit cycles in Section 4.4.2. The bifurcation diagram is used to determine the step period difference and inter-leg angle difference between consecutive walking steps and the phase plane limit cycle is used to investigate the angular velocity and displacement for every time-step during walking steps. Both techniques are used to evaluate the effect of the prosthetic foot's forefoot arc length and gain values with respect to the inter-leg angle and the step period. The relationship between the forefoot arc length and roll-over gain within an optimum area is also described in Section 4.4.1.

The anthropometric data used to generate the results in Sections 4.4.1 and 4.4.2 is for the mid person (Table 4.1) and the physiological foot has a roll-over shape described by a hindfoot arc length value of $Arc_h = 3\text{cm}$, a forefoot arc length value of $Arc_f = 14\text{cm}$ and a gain value of $r = 1.5$ (Figure 4.5). In Figures 4.6 and 4.8, the

solid and dotted curves correspond to gait parameters when the physiological leg and the prosthetic leg act as the supported leg respectively (refer to Figure 4.2 and Section 4.2 for the definition of the supported leg).

4.4.1 Bifurcation diagrams

The mass of a modern prosthetic foot is significantly smaller than the physiological foot, and the centre of mass positions are different for both legs. Bifurcation diagrams have been widely used in literatures to study the passive walking of biped models (Garcia et al., 1998, Goswami et al., 1998, Kurz et al., 2008). In this chapter bifurcation diagrams are used to study the walking asymmetry of a passive model with unbalanced leg masses.

The detailed anthropometric data, as shown in Table 4.1, was not published by the researchers. However, with the assumption that passive walking is more effective at capturing the natural trends in asymmetric walking resulting from unbalanced mass properties, the proposed formulation, for the first time, can attempt to provide an insight into the different observations. The results are shown in Figures 4.6a and d.

For a mid person (Table 4.1), the leg mass ratio (ν) is 0.77 and length ratio (γ) is 0.73 (shown by Section A-A in Figure 4.6). For the same roll-over shape for both prosthetic and physiological feet $(Arc_h = 3\text{cm},\ Arc_f = 14\text{cm}$ and $r = 1.5)$, and leg mass ratio $(\nu = 0.77)$ it is possible to adjust the mass distribution to vary the leg length ratio. Figures 4.6a and d show the range of inter-leg angles and step periods for the physiological leg (solid curve) and the prosthetic leg (dotted curve). The curves intersect at $\gamma = 0.87$ (Figure 4.6a) for the inter-leg angle bifurcation diagram and at $\gamma = 0.82$ (Figure 4.6d) for the step period bifurcation diagram.

Asymmetric walking means that the inter-leg angle and step period values are unequal when the prosthetic and physiological feet act as the supported leg. The literature, however, disagrees whether the inter-leg and step period values are larger or smaller when the prosthetic foot acts as the supported leg. Skinner and Barrack (1990), Smith and Martin (2007) and Hekmatfard et al. (2013) observed that the step length value is smaller and the step period value is larger for the prosthetic single support phase as compared to the physiological single support phase. Exactly

opposite effects have been reported by Robinson et al. (1977), Mizuno et al. (1992) and Isakov et al. (2000) i.e. the step length for the prosthetic stance is larger than for the physiological stance and the prosthetic leg stance period is slightly shorter than for the physiological leg. Note that mathematically, the step length is directly proportional to the inter-leg angle value. The proposed mathematical formulation may allow one possible explanation. It is shown in Figure 4.6a that for $\gamma > 0.87$ the inter-leg angle for physiological foot is greater than the prosthetic foot and the trend reverses for values less than 0.87. The observations reported in the literature, however, are function of actual roll-over shapes used and the corresponding anthropometric data of the amputee.

For a given leg mass ratio $(\nu = 0.77)$ and leg length ratio $(\gamma = 0.73)$, the symmetry in inter-leg angle and/or step period can be improved by adjusting the independent roll-over shape parameters Arc_f and r for the prosthetic foot. Figures 4.6b, e, c, and f correspond to optimal roll-over shapes obtained by varying Arc_f values. The forefoot arc length $\left(Arc_f^{\alpha} = Arc_f^{T}\right)$ was arbitrarily chosen to be 17cm for this study to determine corresponding optimal gain values. The gain values were found to be $r^{\alpha} = 2.27$ (Figures 4.6b and e) and $r^{T} = 1.1$ (Figures 6c and f), where the superscript α or T denotes optimal prosthetic roll-over parameters with respect to the inter-leg angle or the step period respectively. In summary, Figures 4.6b and e show the bifurcation diagrams for the optimal prosthetic roll-over shape values, $Arc_h^{\alpha} = 3\text{cm}$, $Arc_f^{\alpha} = 17\text{cm}$, and $r^{\alpha} = 2.27$, that were optimised for symmetric walking with reference to the inter-leg angle. Figure 4.6b shows that the bifurcation curves for the prosthetic and physiological legs intersect at $\gamma = 0.73$ (Section A-A). However, Figure 4.6e illustrates that the walking is not symmetric with reference to the step period.

Similarly, Figures 4.6c and f show the bifurcation diagrams for roll-over shape values that were optimised for the step period: $Arc_h^{T} = 3\text{cm}, Arc_f^{T} = 17\text{cm}$ and $r^{T} = 1.1$. Figure 4.6f shows that the corresponding bifurcation curves intersect at $\gamma = 0.73$ (Section A-A). However, for these prosthetic foot roll-over shapes the walking is not symmetric with reference to the inter-leg

angle (Figure 4.6d). It should be noted that for the same shoe size or the foot length, the roll-over shape arc lengths for both feet do not have to be same. Hence, the forefoot arc length values for prosthetic foot can differ from the physiological leg value and both values will be less than the corresponding shoe size of the amputee (Curtze et al., 2009, Sam et al., 2004).

It was discovered that for given amputee specific anthropometric data, it is not possible to achieve symmetric walking with reference to both inter-leg angle and step period by adjusting the forefoot arc length and the gain value of the prosthetic foot roll-over shape. The locus of intersection points as defined in Figures 4.6b and f is plotted in Figure 4.7c for various forefoot arc length and gain values. The solid curves in Figure 4.7 correspond to symmetry with respect to inter-leg angle and the dotted curves represent symmetry with respect to step period. For Figures 4.7a, c and e, the input roll-over shape for the physiological leg has values $Arc_h = 3\text{cm}, Arc_f = 14\text{cm}$ and $r = 1.5$, whereas the gain value r is changed to 2.5 for Figures 4.7b, d and f. Figure 4.7 shows that the higher prosthetic foot roll-over gain values (i.e. increasing the stiffness of the prosthetic foot) are associated with smaller prosthetic forefoot arc lengths for symmetric walking. Comparison of Figures 4.7a, c and e with Figures 4.7b, d and f highlights that a higher physiological foot roll-over gain also requires a higher prosthetic forefoot arc length. Also, for a given physiological roll-over shape, the anthropometric data with reference to the small (Figures 4.7a, b), mid (Figures 4.7c, d) or large (Figures 4.7e, f) person does not influence the prosthetic foot roll-over shape parameters for symmetric walking with reference to the step period (dotted curves in Figure 4.7 are same for Figures 4.7a, c and e, as well as Figures 4.7b, d, and f) whereas the optimum curve with respect to inter-leg angle is significantly different. The shorter curves shown in Figures 4.7 b, d, and f arise because of the non-existence of symmetric walking solutions for the assumed anthropometric and roll-over shape data.

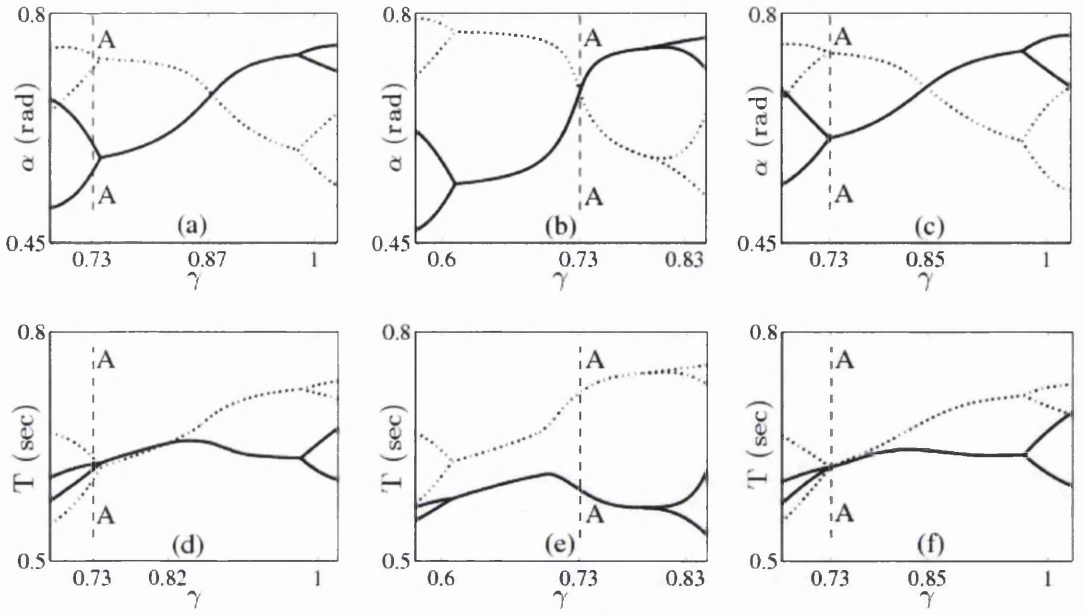

Figure 4.6. Bifurcation diagrams for inter-leg angle (a, b, c) and step period (d, e, f). The solid and dotted curves correspond to gait parameters when the physiological leg and the prosthetic leg act as the supported leg respectively (refer to Figure 4.2 and section 4.2 for the definition of supported leg). The dashed line A-A represents the leg length ratio of a mid person as described in Table 4.1. The plots (a,d) correspond identical roll-over gain value (r=1.5) for both legs. The optimal roll-over gain value (r=2.27 and r=1.1) with respect to the inter-leg angle and step period value respectively in plots (b,e) and (c,f). Optimal gain value means the inter-leg angle value is same for both legs (Section A-A) in plot b whereas the step period value (Section A-A) is identical for plot f.

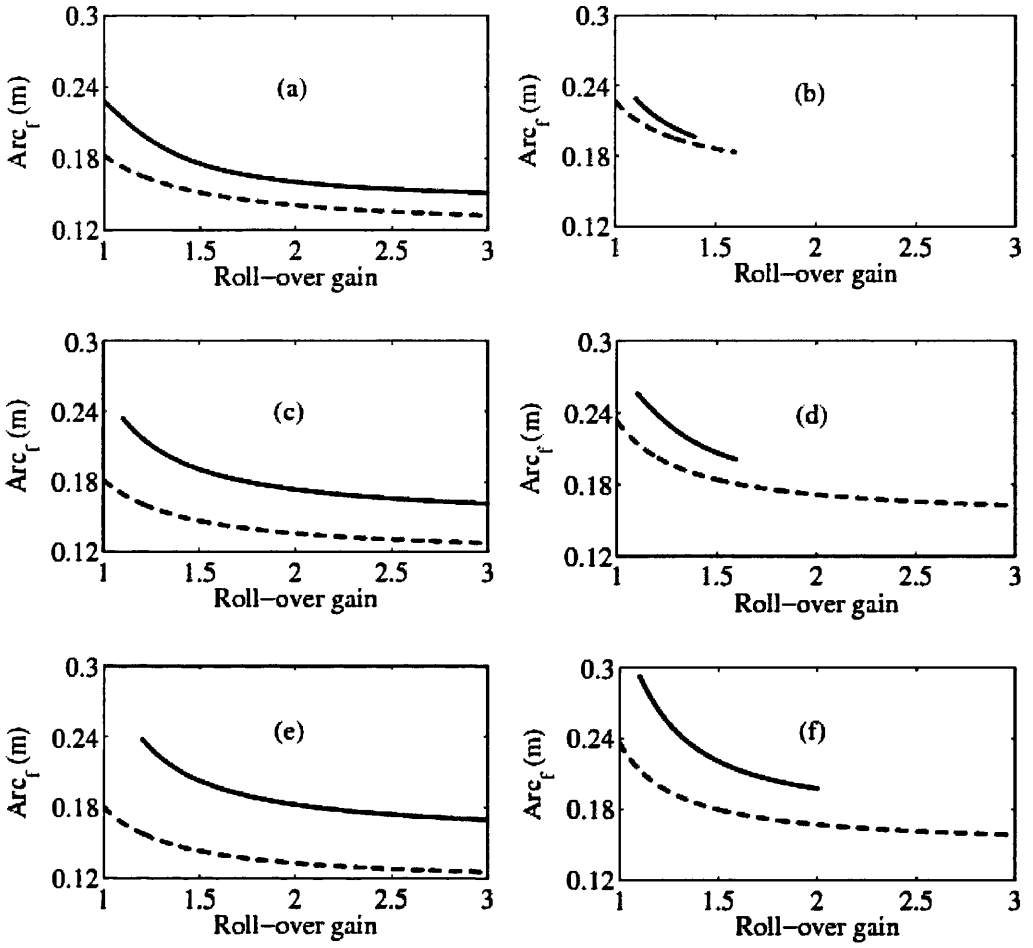

Figure 4.7. The locus of points of intersection on the physiological and prosthetic foot bifurcation diagrams (as shown in Figures 4.6b and f) for small (a, b), medium (c, d) and large (e, f) persons. The corresponding schematic diagram is shown in Figure 4.1c. The solid and dashed curves represent the optimal roll-over parameters with respect to the inter-leg angle and the step period respectively. The first and second columns show the optimal relationship for small, mid and large body while the physiological roll-over gain is 1.5 and 2.5 respectively.

4.4.2 Phase plane limit cycles

The effect of optimising roll-over shape with respect to the inter-leg angle and the step period on the angular velocity and angular displacement variation with respect to time is studied using phase plane limit cycles. The physiological roll-over shape gain, hindfoot arc length and forefoot arc length values are 1.5, 3cm and 14cm respectively and the leg mass ratio and leg length ratio correspond to the mid person with prosthetic leg ($\nu = 0.77$ and $\gamma = 0.73$). Figures 4.8a, b and c correspond to walking with identical roll-over shapes for both physiological and prosthetic feet. Figure 4.8c shows that the unbalance leg mass and COM leads to 4-period walking and the prosthetic leg part of the limit cycle is larger than the physiological part. During the double support phase, the effect of the prosthetic leg impact on its post-impact angular velocity is higher than for the physiological leg. The initial angles of the legs are corresponding to the inter-leg angle is such that $\alpha = \theta_s^1 - \theta_{ns}^1$.

For a prosthetic foot gain value of 1.2 (Figure 4.6c), the optimal forefoot arc length values with reference to inter-leg angle and step period are $Arc_f^{\alpha} = 21.5\text{cm}$ and $Arc_f^T = 16\text{cm}$ respectively. The corresponding phase plane limit cycles are shown in Figures 4.8g, h, i and d, e, f, respectively. Figures 4.8g and i show that optimising the prosthetic roll-over shape with respect to inter-leg angle is a better criterion than optimising the step period (Figures 4.8d, f), as the phase plane limit cycles for physiological and prosthetic feet are closer to each other. As a result of this observation, the optimal range proposed in the schematic (Figure 4.1c) is towards the inter-leg angle curve (or boundary).

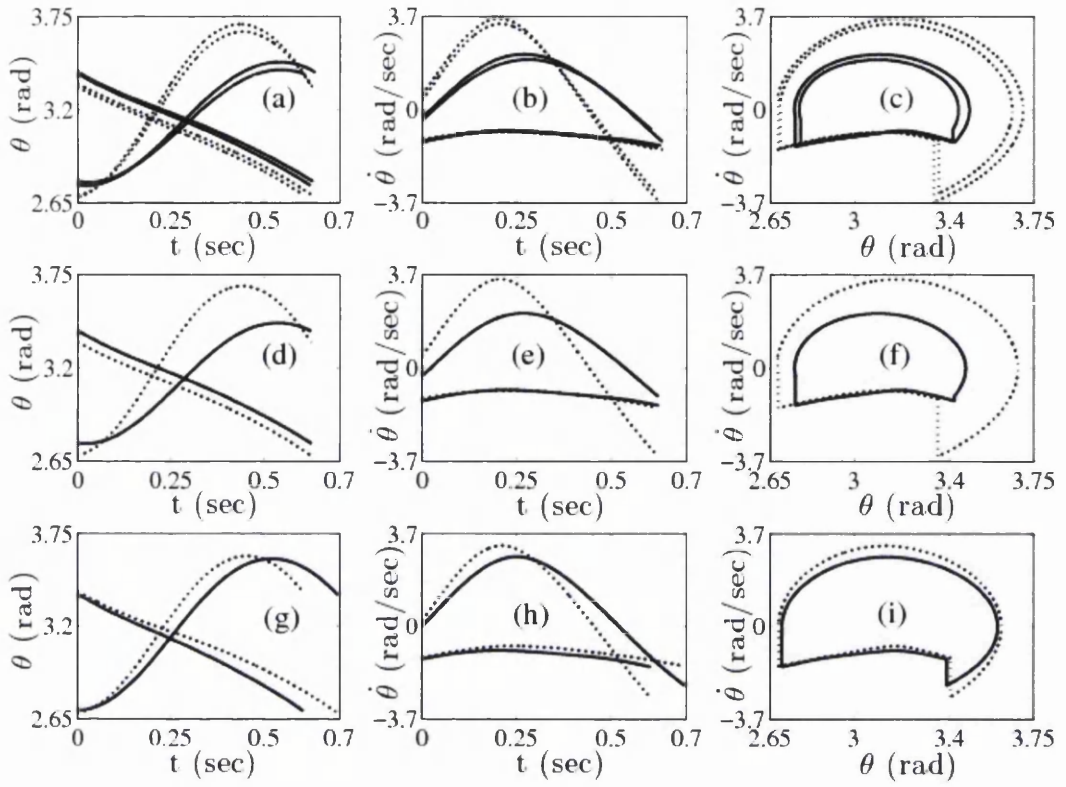

Figure 4.8. The first, second and third rows describe the gait parameters of a mid person walking with an unbalanced leg mass corresponding to identical roll-over shapes for both legs, prosthetic roll-over shape optimised with respect to step period and inter-leg angle.

4.5 Conclusion

Roll-over shapes have been used in the literature to characterise the direction of the ground reaction with reference to the position of the ankle-knee part of the leg. The roll-over shape of a prosthetic foot can be adjusted by varying the stiffness of the foot. The proposed passive walking kinematic model does not require information on joint torques, and hence does not need the motion or natural gait analysis of an amputee which is often unavailable. The model quantifies the natural tendency for asymmetry resulting from the mass unbalance, in terms of both the inter-leg angle and the step period, so that the necessary corrective action required at the prosthetic foot is measured by predicting an optimal prosthetic foot roll-over shape. The sensitivity of the roll-over shape with the stability and symmetry of the walking

process in terms of the inter-leg angle and step period is assessed using bifurcation diagrams and phase plane limit cycles.

Chapter 5 Prosthetic Foot Design Optimisation Based on Roll-Over Shape and Ground Reaction Force Characteristics

5.1 Introduction

The human ankle-foot system includes biological systems that can recognise various parameters (nerve sensing) such as walking speed, added weight, and heel heights, process those parameters (human brain) and make suitable adjustments to the foot in order to provide stability and optimum gait characteristics. It is obvious that biological foot systems are able to adapt to various walking terrains easily where as the artificial foot systems cannot achieve this due to the lack of adaptability (Markowitz et al., 2011).

According to DeLisa (1998), the normal gait cycle is defined as the "time interval or sequence of motion occurring from heelstrike to heelstrike of the same foot." The gait cycle is divided into two phases. These phases are the single support phase and the double support phase. The single support phase contributes to 80 percent of the overall cycle and the double support phase to 20 percent. During the start of the double support phase both feet are in contact and as the body moves forward the mass is concentrated on one foot. This is the foot that rolls over on the ground and is referred to as the stance leg. After the heel strike, the human ankle system stores the resulting elastic strain energy. During the toe off phase, the ankle system returns this energy along with additional energy as necessary to lift the foot from the ground and propel the human body upward and forwards. Once the foot is lifted from the ground (toe-off) the single support phase begins and continues until the foot makes an initial contact with ground (heel-strike).

The two most commonly used prosthetic foot designs, the Conventional Feet (CF) and the Energy-Storing-and-Returning (ESAR) feet, are discussed in this Chapter.

According to Versluys et al. (2008) the most common and probably economical conventional prosthetic foot is the SACH foot. It incorporates of a rigid wooden keel, a soft cushion heel and a metallic or composite belting component which is surrounded by a combination of foam and other materials. The cushion heel allows a

varying degree of compression during heel strike simulating plantar flexion where as the belting component of the foot allows a limited amount of dorsiflexion due to the rigid keel that resists deflection at late mid stance. Overall the SACH foot is a simple and a low cost design but is limited in imitating the biological foot characteristics.

Energy storing and returning foot designs are the next generations of prosthetic foot designs emerge due to the desire of amputees to participate in sports. According to Drongelen (2000) energy storing and returning feet incorporate a lightweight carbon fiber construction and vary in complexity and cost. Most ESAR feet utilise the entire distance up to the socket for their function and as a result of this are able to deflect/deform along their entire length and allow dorsiflexion. The rear ends of the design consist of a leaf spring component which provides a spring like response during the heel strike. The higher dorsiflexion moment allows the keel to be compressed and thus energy to be absorbed and then released in order to propel the amputee forward.

The idea of designing a prosthetic foot that replicates every detail of the way biological foot (the ankle system supported by muscles) works is a difficult challenge. Despite the fact that prosthetic foot designs are improved considerably with the development of energy storing and returning foot designs, it is found that the problems related with prosthetic foot designs are poor prosthetic durability and comfort. The former being primarily associated with the premature failure of prosthetic feet, while the latter being due to inadequate prosthetic socket fit, poor prosthetic alignment and poorly functioning components, including knee joints (Andrysek, 2010). According to Macfarlane et al. (1991), endangering instabilities are referred to asymmetrical gait which may lead to problems related to premature degenerative arthritis and loss of motor and sensory nervous control with amputation.

During the last decade, many investigations have been performed to optimise prosthetic foot designs but most of them were based on the structural behavior of the foot in terms of stress and strain characteristics. In this Chapter, it is investigated whether stiffness profile of a prosthetic foot can be optimised to restore amputees' normal gait pattern, which consequently can result in minimal energy consumption.

The finite element method is widely used for parametric analysis such as the study of shape and size design, material or alignment parameter effects. It has also been used

to investigate the interaction between prosthetic sockets and the residual limbs. Saunders et al. (2003) illustrated a finite element analysis test in order to investigate the heel response effects of a solid ankle design. In order to undertake this investigation, Saunders et al. (2003) had to measure the exerted forces and contact surface between the foot and the floor at heel strike, at middle stance and push off in the gait cycle of a below-knee amputee. The forces that were collected from the experiment were applied to a below-knee solid ankle cushion heel model in order to calculate the displacement and stress that was applied to the foot. Lee and Zhang (2005) used maximum loadings as described in the ISO10328 standard to design a prosthetic foot using finite element model.

Two of the recent publications, Bonnet et al. (2012) and Omasta et al. (2012), have used experimentally determined ground reaction forces to input the finite element models of prosthetic feet and the resulting deflections in the prosthetic feet were compared with experiments. Omasta et al. (2012) illustrated a finite element analysis method to investigate the stress distribution in load-bearing components of a specific prosthesis in detail. The ground reaction forces of an amputee were measured and input to the finite element model. The resulting deflections in the foot were compared with experiments. Bonnet et al. (2012) measured boundary conditions from a gait analysis for an amputee's self selected and fast walking speeds in order to calculate stress, stain, and stain energy for a prosthetic foot during a walking step. The finite element model was validated from a mechanical test from where heel and forefoot load displacement curves were obtained. The ground reaction forces were applied as the external forces for the finite element model.

The novelty in this Chapter is that the experimentally determined ground reaction forces are synchronised with a recently proposed gait descriptor, referred to as roll-over shapes, and used as a design parameter to optimise the stiffness profile of the prosthetic foot. Amputee weight and the weight transfer during gait are taken into consideration by the roll-over shape and ground reaction force combination enabling engineers to optimise the overall stiffness of the prosthetics so that amputee's normal gait pattern may be restored.

The roll-over shape is defined as a trajectory of the centre of pressure as the foot rolls over the surface and is defined in a local co-ordinate system with y-axis being aligned with the ankle-knee axis. The effective roll-over shape that the ankle foot

conforms to between heel strike and toe off (the 'roll-over' interval walking), is a simple way to represent the function of a prosthetic foot during the period of gait (Hansen et al., 2003). According to a number of investigations performed by Hansen and Childress (2010), it is found that the effective roll-over shape characteristics of able-bodied persons "do not change appreciably as persons walk faster or slower, as they walk carrying weight attached to their trunk, or as they wear shoes with different heel heights" (Hansen and Childress, 2010). Due to this observed invariance, it is proposed that the effective roll-over shape be used as a design parameter in order to optimise prosthetic foot designs in order to replicate the biological gait characteristics at the specified conditions.

5.2 Experimental determination of a synchronised roll-over shape and ground reaction force values

An able-bodied person, with subject body specifications as listed in Table 5.1, was asked to wear a normal pair of shoes and the resulting gait motion data were measured at Swansea University's sport science research laboratory. The subject practiced the gait on a preinstalled walking path so that after few walking steps the whole stance foot surface landed upon a force plate (FP) (type 92866AA, Kistler Instruments, Farnborough, UK) and the swing leg landed next to the force plate which is referred to as a "clean" hit. Data trials were collected for five "clean" hits and were used to determine the mean roll-over shape which is described further in the section 5.2.2. Taking a few steps before the foot contacted the force plate minimised the inherent initial variability of body motion. The kinematics of walking motion was captured using 2 retro-reflective spherical markers (diameter 1 cm) attached to the subject and located on the lateral malleolus (LM) and knee joint centre (KJC) of the leg being studied. Another marker was attached to the front corner of the FP (corresponding to the intersection of the transverse and sagittal planes) to determine a global coordinate system. The global coordinate system is defined as a coordinate system with its origin located on the force plate corner as specified by a marker with x-axis being parallel to the force plate and the origin of the local coordinate system aligned to the ankle joint motion which also rotates corresponding to the shank angle.

The global coordinate system together with joints trajectory and the force plate data allowed the motion analysis and force plate data to be linked together and a MATLAB script was written to calculate the roll-over shape synchronised with the corresponding values for ground reaction forces. The corresponding algorithm is explained in Section 5.2.2. The force plate signal was sampled at 1200 Hz at a resolution of 16 bits with a vertical force range of 10 kN (Kistle Bioware V5.1.1.0). All kinematic data were collected at 240 Hz using a high speed video camera Casio Exilim EX-F1 manufactured by the Casio Electronic Company, London, UK. Quintic software (Quintic Consultancy, Sutton Coldfield, UK) was used to analyse the marker coordinate data and calibrate subsequent performance area and the camera. A meter rule was placed in the plane of action and was used to calibrate the Quintic analysis software.

Table 5.1. Subject specifications

Gender	Weight (kg)	Height (cm)	Age (years)	Foot Length (cm)
Male	72	177	27	27

5.2.1 Force plate data and Ground Reaction Forces

During the single support phase, the Centre of Pressure (COP) moves as the leg and the body rolls from the hindfoot to the forefoot of the stance leg. A roll-over shape is measured by capturing the position of COP with respect to a local coordinate system located on ankle joint such that y-axis remains parallel to the shank. When the stance foot starts to roll on the walking surface, the force plate records the location of COP and the resulting data at each time step is saved with reference to the global coordinate system. The data were filtered afterwards using Bioware (Butterworth dual pass low pass filter, pass band 100 Hz, stopband 200 Hz) to eliminate noises of the force plate. Figure **5.1** describes the location of COP with respect to time which

also shows that the contact length between stance foot and the force plate is about 24 (cm). The corresponding vertical component of ground reaction force (GRFv) time history is shown in Figure **5.2**.

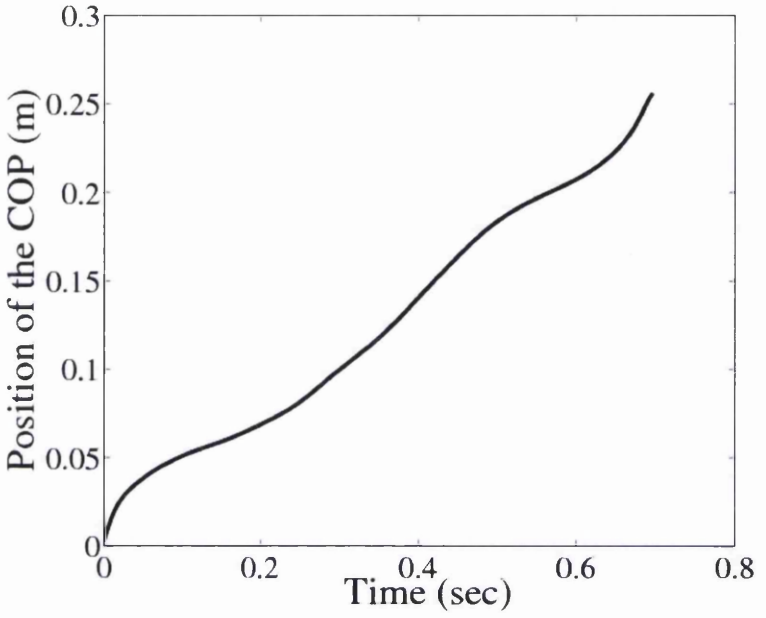

Figure 5.1. The temporal movement of the position of COP as the stance foot rolls from the heel contact to toe off is measured from the force plate data.

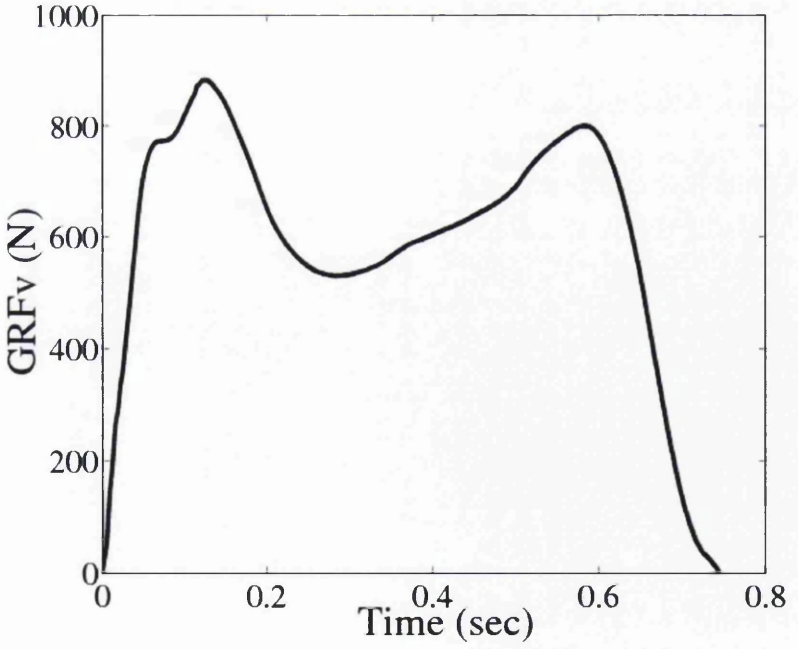

Figure 5.2. Experimentally determined ground reaction force values during a walking step.

5.2.2 Kinematic data and roll-over shape

The motion camera captured a walking step motion with retroreflective spherical markers attached to knee joint (KJC), ankle joint (LM) and the force plate (FP) corner. The angular displacements of the markers for a gait cycle are analysed with Quintic software. Figure 5.3 is plotted in Quintic software and describes the KJC and LM motion trajectory with green and yellow colours respectively and the marker in the left corner of the FP shows the origin of the global coordinate system. The time which the motion camera starts to record data is different from the force plate. The instance when the FP began to record the data was indicated by the illumination of a signal light emitting diode (red light in Figure 5.3) and was used to temporally synchronise the force plate and video camera. The following transformation is used to determine the position of COP in the local coordinate system. The relationship between the two co-ordinate systems is schematically shown in Figure 5.4.

$$\begin{bmatrix} x^i_{local} \\ y^i_{local} \end{bmatrix} = \begin{bmatrix} \cos(\theta^i_{ankle}) & \sin(\theta^i_{ankle}) \\ -\sin(\theta^i_{ankle}) & \cos(\theta^i_{ankle}) \end{bmatrix} \begin{bmatrix} X^i_{global} - X_{ankle} \\ Y^i_{global} - Y_{ankle} \end{bmatrix} \tag{5.1}$$

where (X,Y) and (x,y) present position of COP with respect to the global and local coordinate system and (i) denotes the i^{th} pivot point. The angle between the local and the global coordinate system is shown by θ_{ankle} and the position of the ankle joint in global coordinate system is presented by (X_{ankle}, Y_{ankle}).

Figure 5.5a shows position of COP, ankle joint and the knee joint at each time step with respect to the global coordinate system and Figure 5.5b describes position of COP or the roll-over shape with respect to the local coordinate system. Tick lines in Figure 5.5a connect the ankle joint to the knee joint during a walking step while in the local coordinate system a single line describes the connection between the knee and ankle joints for entire walking step as shown in Figure 5.5b.

In summary, the roll-over shape is measured in four steps as follow:

1- Location of body COPs during a walking step are determined using the FP and the Bioware in the global coordinate system (GCS) as described in Figure 5.1.

2- The positions of the knee and ankle joints are determined at each time step by markers and Quintic video analysis software (see Figure 5.3).
3- The red light in Figure 5.3 is used to identify the starting time of FP. The video camera starts records motion before the starting time of the FP. The time deference between FP and video camera is then calculated and the corresponding values are synchronised in the MATLAB script.
4- By importing data from steps 1-3 in MATLAB and using Equation 5.1, the position of COPs are determined with respect to the local coordinate system (roll-over shape) as shown in Figures 5.4 and 5.5.

It is observed that the roll-over shape retains all three stages of the gait cycle: heel-strike (or Controlled Plantarflexion), middle phase (or Controlled Dorsiflexion) and toe off (or Power Plantarflexion). For computational purpose, the roll-over shape shown in Figure 5.5b is redrawn in Figure 5.6a. The polynomial function described in Chapter 3 is used to model the experimental roll-over shape and is shown as a dashed curve in Figure 5.6b and the part of this curve shown by a thick solid line is used in the computational model. Parameters of the computational model roll-over shape are determined corresponding to the experimental roll-over shape as shown in Table 5.2. The calculation procedure of ground reaction force values at corresponding points on the roll-over shape is described in the next Section.

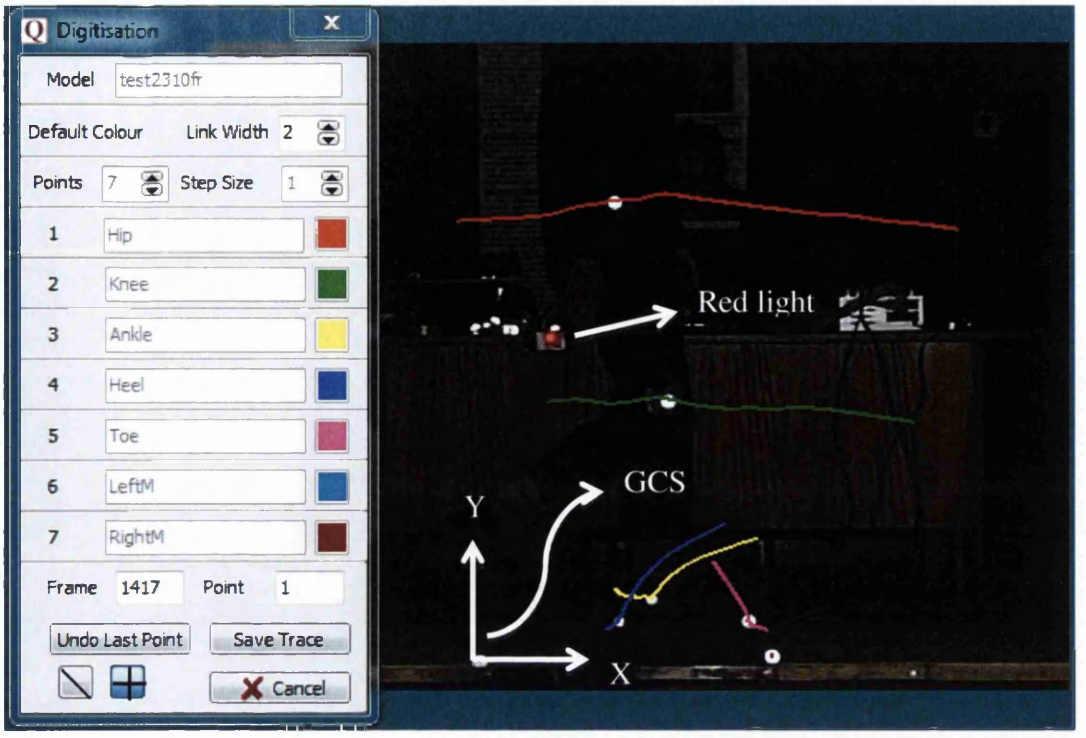

Figure 5.3. Trajectory of the knee (green line) and the ankle (yellow line) joint for a walking step. White circles show the location of markers. The marker which is located on the left corner of the force plate shows the origin of the global coordinate system. The red light is used to synchronise the force plate data and the motion camera data.

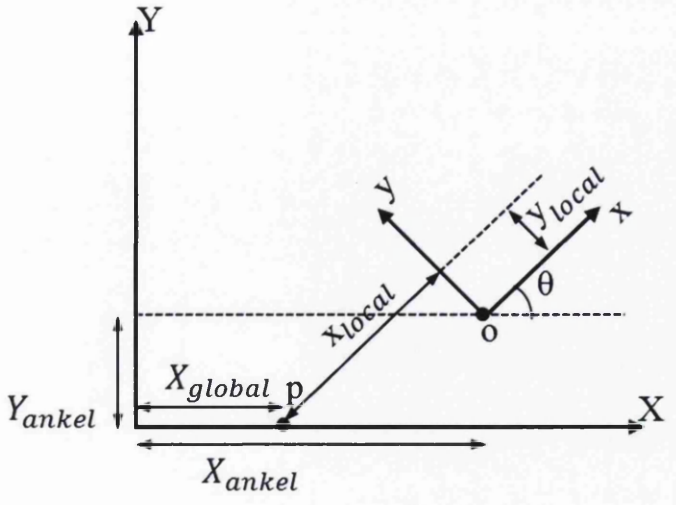

Figure 5.4. Global (X-Y) and local (x-y) coordinate systems.

.

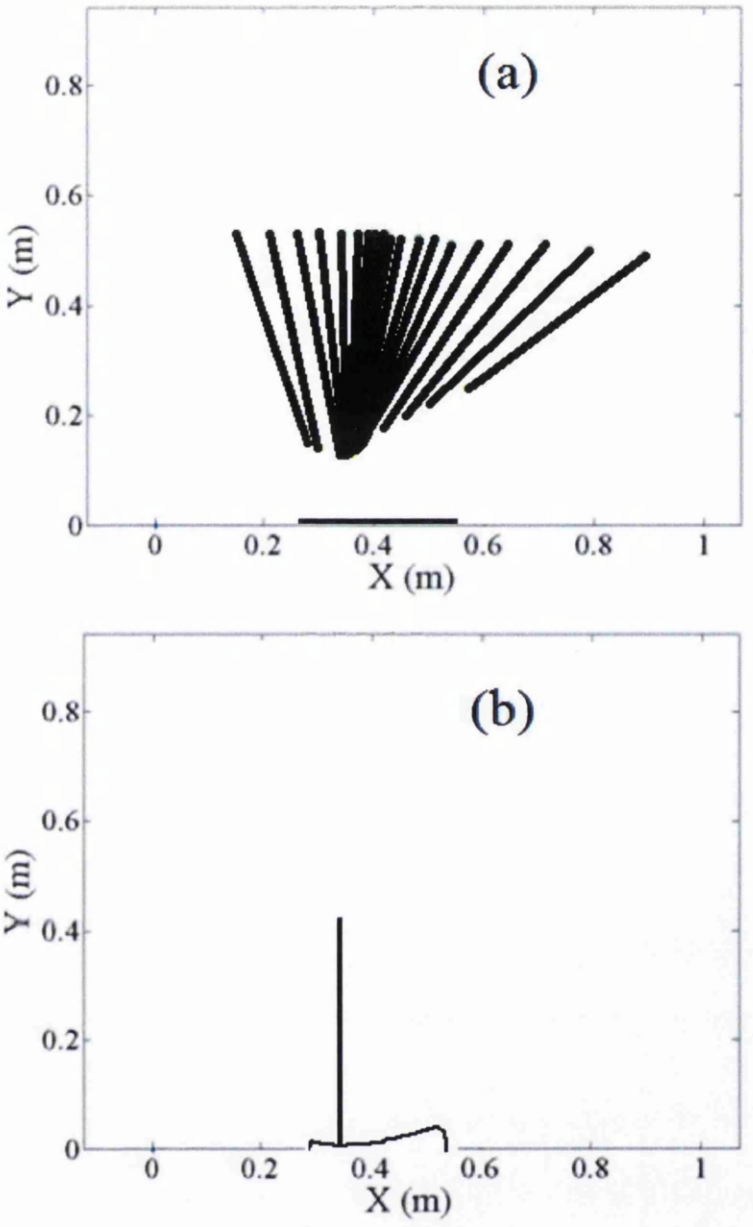

Figure 5.5. Straight and curved lines in (a) and (b) describe the position of COP with respect to the global and local coordinate systems respectively. Tick lines in (a) connect the ankle joint to the knee joint at different time steps.

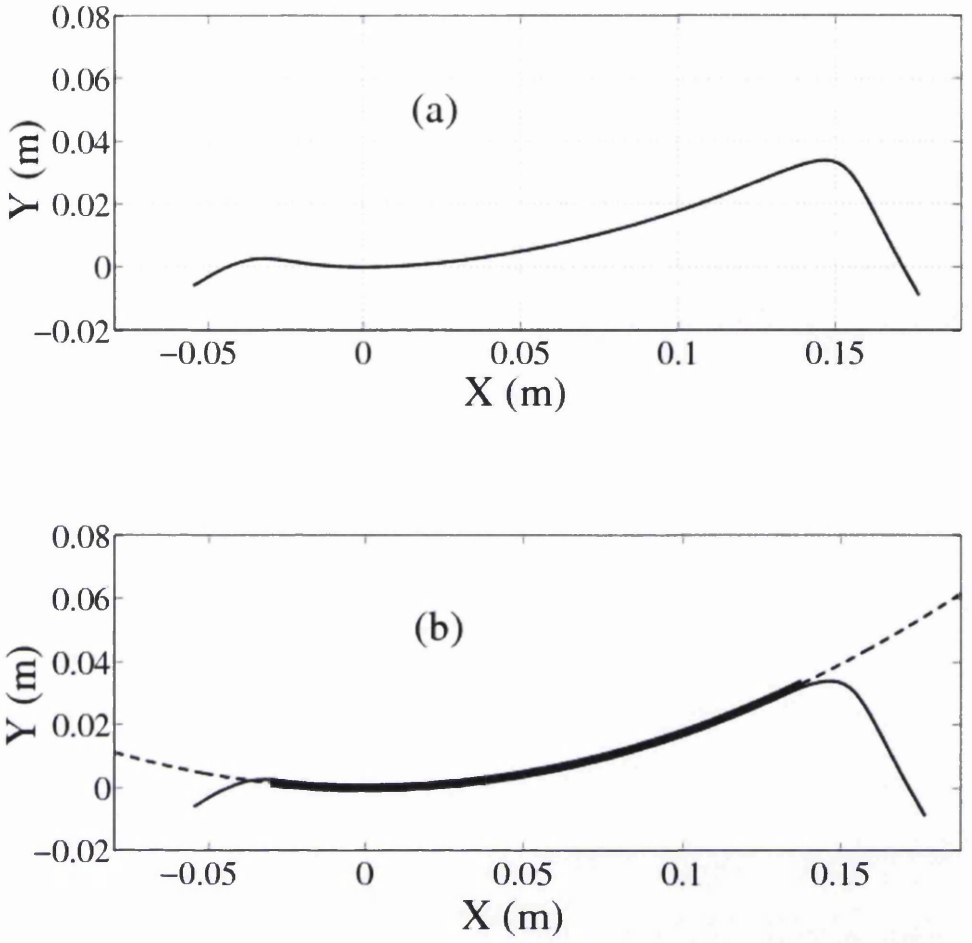

Figure 5.6. A polynomial equation (as shown by dashed curve) is used to represent the experimentally determined roll-over shape shown in Figure a. The curve shown by a thick solid line shown in Figure b is input to the computational model.

Table 5.2. Parameters of the experimental roll-over shape

r_f	L_h (m)	L_f (m)
0.572	0.03	0.14

5.2.3 Computational Modelling of ground reaction forces (GRF)

The kinematic computational model as described in Chapter 4 is extended to calculate ground reaction forces. The roll-over shape measured in Section 5.2.2 is input the computational model. The location of the body centre of mass is considered to calculate GRF at each contact point. The position (X_G^i, Y_G^i) of Centre of Mass (COM) at ith time step is a function of legs angular displacement, location of body masses and magnitude of body masses at each time step (see equations 5.2 and 5.3) where all the variables are determined using Equation 4.1. GRF in horizontal and vertical directions at each time step are described by following equations.

$$X_G^i = \frac{m_s a_{vs}^i \sin(\theta_{mvs}^i) + m_H l_{vs}^i \sin(\theta_{vs}^i) + m_{ns}(l_{vs}^i \sin(\theta_{vs}^i) - c\sin(\theta_{ns}^i))}{m_s + m_H + m_{ns}} \tag{5.2}$$

$$Y_G^i = \frac{-m_s a_{vs}^i \cos(\theta_{mvs}^i) - m_H l_{vs}^i \cos(\theta_{vs}^i) - m_{ns}(l_{vs}^i \cos(\theta_{vs}^i) - c\cos(\theta_{ns}^i))}{m_s + m_H + m_{ns}} \tag{5.3}$$

$$\dot{X}_G^i = \frac{m_s a_{vs}^i \dot{\theta}_{mvs}^i \cos(\theta_{mvs}^i) + m_H l_{vs}^i \dot{\theta}_{vs}^i \cos(\theta_{vs}^i) + m_{ns}(l_{vs}^i \dot{\theta}_{vs}^i \cos(\theta_{vs}^i) - c\dot{\theta}_{ns}^i \cos(\theta_{ns}^i))}{m_s + m_H + m_{ns}} \tag{5.4}$$

$$\dot{Y}_G^i = \frac{m_s a_{vs}^i \dot{\theta}_{mvs}^i \sin(\theta_{mvs}^i) + m_H l_{vs}^i \dot{\theta}_{vs}^i \sin(\theta_{vs}^i) + m_{ns}(l_{vs}^i \dot{\theta}_{vs}^i \sin(\theta_{vs}^i) - c\dot{\theta}_{ns}^i \sin(\theta_{ns}^i))}{m_s + m_H + m_{ns}} \tag{5.5}$$

$$F_x^i = m_s a_{vs}^i \ddot{\theta}_{mvs}^i \cos(\theta_{mvs}^i) - m_s a_{vs}^i \dot{\theta}_{mvs}^{i\,2} \sin(\theta_{mvs}^i) + m_H l_{vs}^i \ddot{\theta}_{vs}^i \cos(\theta_{vs}^i) - m_H l_{vs}^i \dot{\theta}_{vs}^{i\,2} \sin(\theta_{vs}^i)$$
$$+ m_{ns}\left(l_{vs}^i \ddot{\theta}_{vs}^i \cos(\theta_{vs}^i) - l_{vs}^i \dot{\theta}_{vs}^{i\,2} \sin(\theta_{vs}^i) - c\ddot{\theta}_{ns}^i \cos(\theta_{ns}^i) + c\dot{\theta}_{ns}^{i\,2} \sin(\theta_{ns}^i)\right) \quad (5.6)$$

$$F_y^i = m_s a_{vs}^i \ddot{\theta}_{mvs}^i \sin(\theta_{mvs}^i) + m_s a_{vs}^i \dot{\theta}_{mvs}^{i\,2} \cos(\theta_{mvs}^i) + m_H l_{vs}^i \ddot{\theta}_{vs}^i \sin(\theta_{vs}^i) + m_H l_{vs}^i \dot{\theta}_{vs}^{i\,2} \cos(\theta_{vs}^i)$$
$$+ m_{ns}\left(l_{vs}^i \ddot{\theta}_{vs}^i \sin(\theta_{vs}^i) + l_{vs}^i \dot{\theta}_{vs}^{i\,2} \cos(\theta_{vs}^i) - c\ddot{\theta}_{ns}^i \sin(\theta_{ns}^i) - c\dot{\theta}_{ns}^{i\,2} \cos(\theta_{ns}^i)\right)$$
$$+ (m_s + m_H + m_{ns})g \quad (5.7)$$

The ground reaction forces measured in Section 5.2.2 are compared with the forces calculated using the passive model described in Chapter 3 and equation 5.7. Experimental GRF are measured for an able subject (Table 5.3) with the total mass of 72 kg. This mass is between the small and mid body weight as used in Chapter 4. Hence, the mass ratio, the length ratio and the leg's length of the computational model is calculated by using interpolation between the small and mid body masses as shown in Table 5.3. As the subject used in the experiment is an able person, the masses of the legs are assumed to be identical for the computational model.

Table 5.3. Specifications of the able subject.

Total mass (kg) $m_H + 2m_{leg}$	**Mass ratio**	**Length ratio**	**Leg's length (m)**
72	3.5168	0.6041	0.9136

Figure 5.7 describes the experimental GRF (solid line) and the computational GRF (dashed line) in vertical direction. The experimental data shows the GRF between two GRF peaks when the pre-stance leg starts to swing. Experimental data of double support phase are ignored as the phase is instantaneous for computational model and the time is normalised for both with respect to their step period. The results show that both the computational and the experimental GRF follow the same trend so that in vertical direction first peak occurs at heel strike and then GRF starts to decrease

while it reaches to its minimum value and then increases until the opposite leg heel strike and in horizontal direction GRF starts from a negative to a positive value. However, in vertical direction, the difference between the two peaks GRF value and the minimum GRF value of the experimental results is higher than the one obtained from the computational model. This may be due to the fact that the computational model is passive while the human powers the joints using both the passive and the active elements such as tendons and muscles. Active walking affects on kinetics and kinematics of the motion and cause GRF to drop more than the passive model. For the finite element model described in the next section, experimentally determined GRF and the roll-over shape is used to optimise the stiffness profile of three different prosthetic feet.

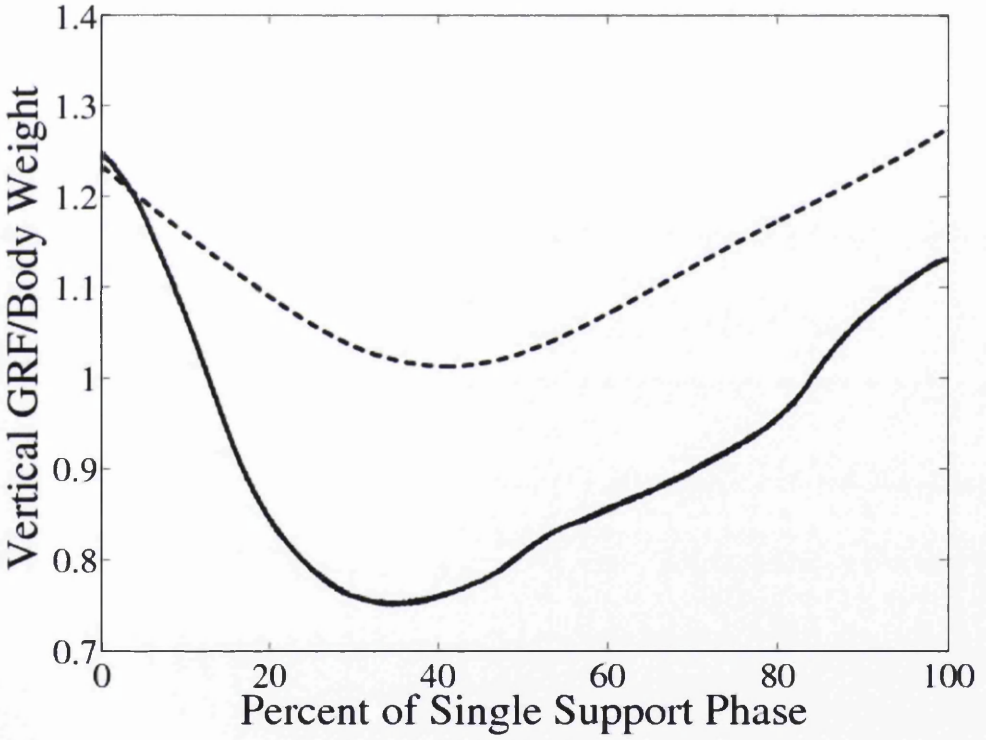

Figure 5.7. The experimental GRF (solid line) and the computational GRF (dashed line).

5.3 Methodology

The stiffness of the prosthetic foot is designed so that under the transient loading of ground reaction forces, it produces deflection that is compared with the corresponding roll-over shape curve (Figure 5.8). The following three design guidelines are proposed to input an experimentally determined roll-over shape and ground reaction force data in a finite element analysis model of prosthetic foot.

First Design Guideline: In order to apply the ground reaction forces to the finite element model, the foot profile is divided into small sections shown by the vertical ground reaction force vectors. The magnitudes for the ground reaction force vectors are selected at a predetermined rate (e.g. a value of 0.01 seconds is taken in this study) during the rolling single support phase and corresponding points on the roll-over shape (and foot) are determined using the method discussed in Section 5.2. Transient Structural analysis in ANSYS® was used in this experiment to simulate the deformation of prosthetic feet as each GRF was applied sequentially and linearly for 0.01 second time interval and released in a linear fashion as shown in Figure 5.8. Fixed boundary condition is applied at the top of the shank.

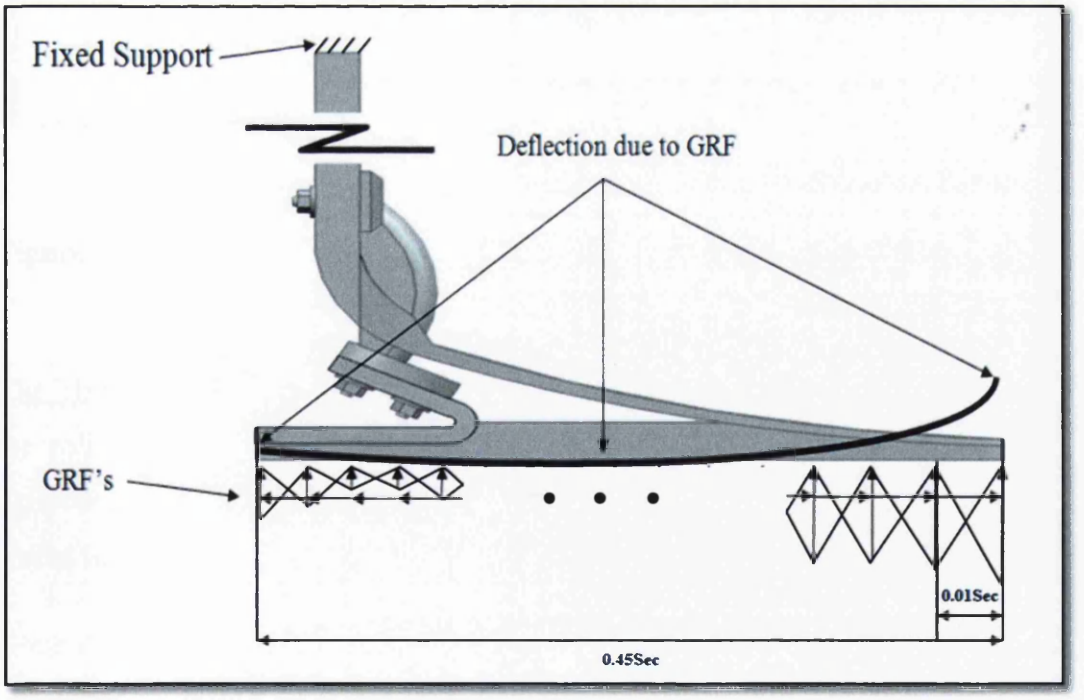

Figure 5.8. Application of transient ground reaction forces in a finite element model.

The Second Design Guideline: The pylon/blade (as identified in Figure 5.9) is positioned at the zero slope position of the roll-over shape or the zero position along the y component of the roll-over shape. If the pylon was placed anywhere except the zero position, then it would result to an early heel strike and toe off (if positioned forward to the zero position along the y component) or late heel strike and late toe off (if positioned backward to the zero position along the y component). The positioning of the pylon was essential for effectively mimicking the given roll-over shape as it is the point where deflection needs to be low due to the fixed support boundary condition.

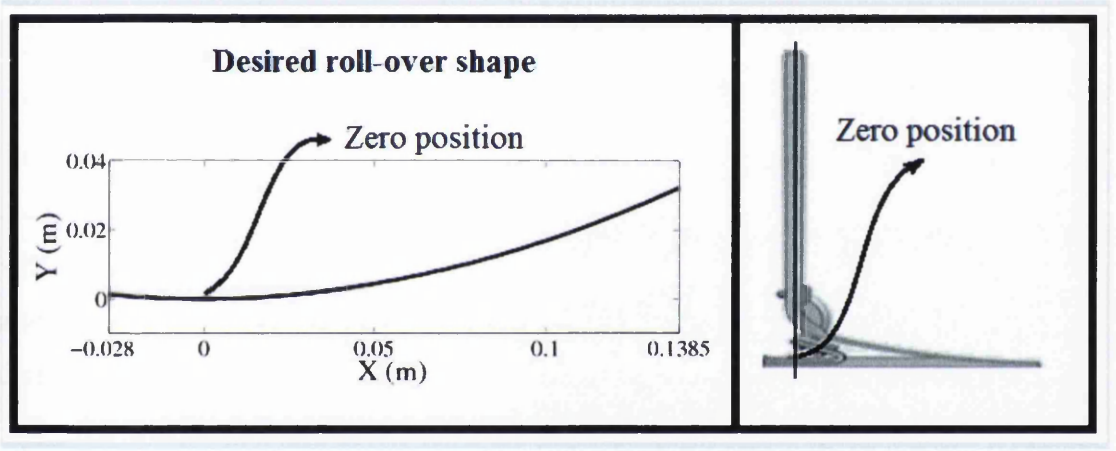

Figure 5.9. Pylon's zero position as suggested by a given roll-over shape.

The Third Design Guideline: The length of the prosthetic foot is considered equal to the roll-over shape arc length. This allows the finite element model to relate the deflection of the foot as measured by the roll-over shape to the ground reaction forces in order to optimise the stiffness profile of the foot.

Once the boundary conditions were applied, the next step was to assign material properties at different sections of the foot in order to influence the resulting stiffness behavior. During the optimisation process the geometry of the prosthetic foot can also be changed. The mesh and time interval sensitivity study performed in order to

identify the maximum allowable element and the time interval size that are required for efficient simulation analysis.

5.3.1 Design Case Studies:

Three commonly used prosthetic foot designs (two ESAR and one SACH) are optimised so that the deflection resulting from applying transient ground reaction forces matches the given roll-over shape.

The first ESAR foot (ESAR_1) consists of four assembled parts namely front leaf spring, rear leaf spring, foot shell and the connector. The front leaf spring and the rear foot spring influences front and rear prosthetic foot deflection and the stored and returned energy respectively. The front leaf spring works as a shank and forefoot. It has different thickness along the shape so that shank part is thicker and stiffer than the forefoot part. The rear foot spring has uniform thickness. In order to optimise the deflection of the foot to a given roll-over shape under the loading of a constant set of transient GRFs, the springs can be altered so that the forefoot and hindfoot become stiffer or softer. A foot shell sole is constructed by softer material and is located underneath of the prosthetic foot where it remains in contact with the ground. The connector attached the springs together.

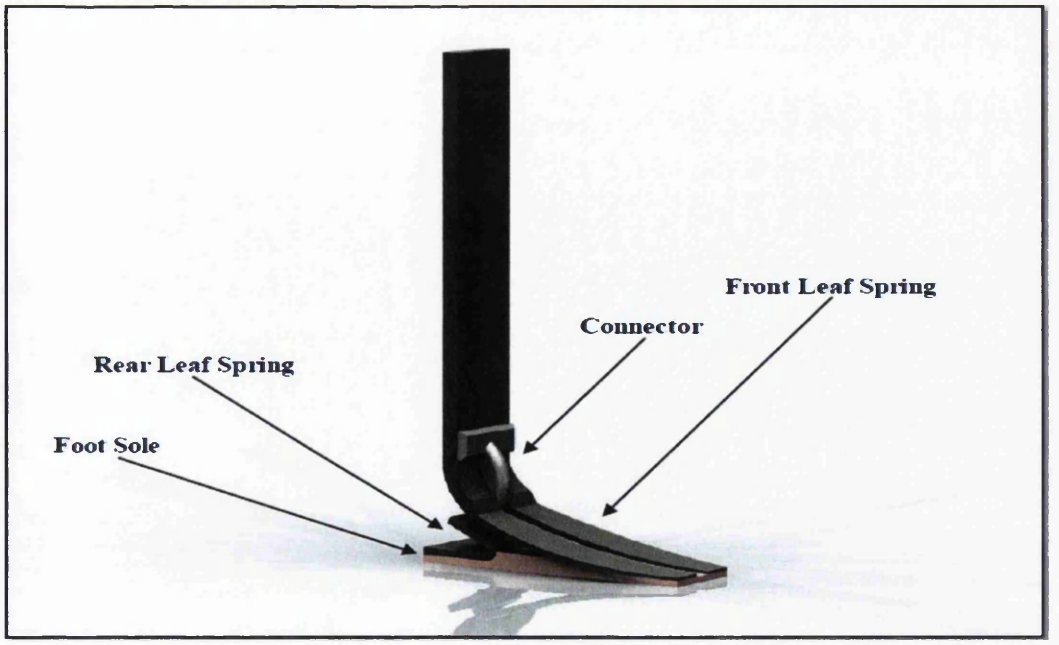

Figure 5.10. The ESAR_1 foot geometry.

The second ESAR foot (ESAR_2) consists of five parts, namely the rear leaf spring, front leaf spring, pylon, foot shell and the connector. The real leaf spring for both ESAR_1 and ESAR_2 foot models are designed similarly. The front leaf spring of the ESAR_2 foot consists of the forefoot area and the shank which is a different part and is constructed by different material. Each part of the geometry can be removed and replaced with an alternative material similarly to the ESAR_1 foot in order to vary stiffness so that the resulting deflection matches the given roll-over shape.

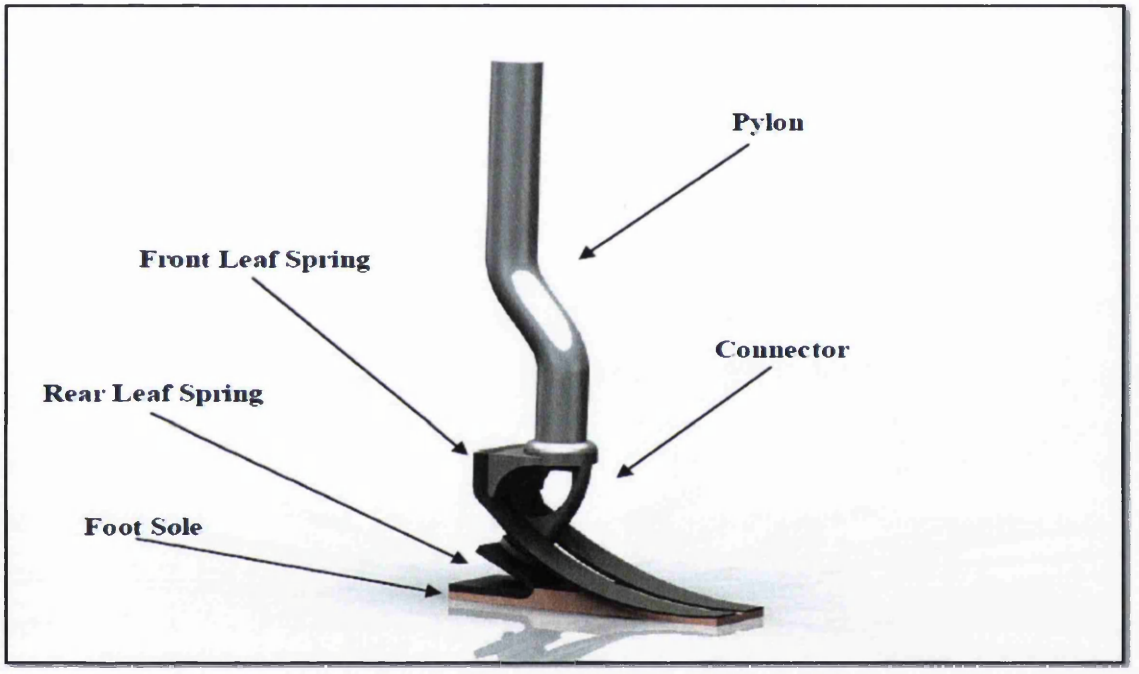

Figure 5.11. The ESAR_2 foot geometry.

The SACH foot is the third geometry produced for this investigation and consists of six parts; these are the pylon, pylon's reinforced ring, keel, belting, cushioned heel and the foot shell insert. The cushioned heel limits the amount of heel strike impact where as the belting of the foot allows the foot to deflect and dorsiflexed during push-off and return back to its initial position. The keel of the foot supports the pylon through a reinforce ring which holds the pylon firm in place. All components except the pylon and reinforced ring are surrounded by a soft foam material which makes up the foot shell insert.

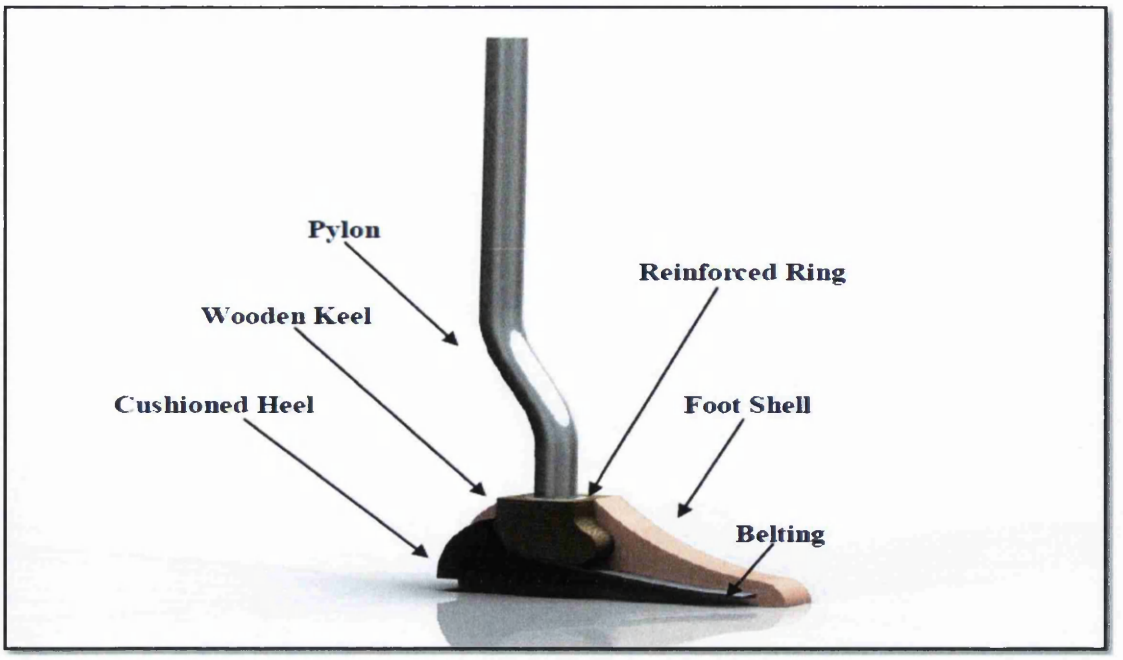

Figure 5.12. The SACH foot geometry.

5.3.2 Review of materials used for the prosthetic feet

All the three prosthetic feet (ESAR_1, ESAR_2 and SACH) have been constructed by using multiple materials. These materials are reviewed in this section as they will be used for modelling the behaviour of various components in the finite element analysis described later in this Chapter. The following materials are presented by Rihs and Polizzi (2001) to design prosthetic feet.

- **Carbon Fibre:** widely used in ESAR feet components and also as a keel and a socket Pylons
- **Kevlar, Aramid (polyp-phenyleneterphthalamide):** can be strengthening by adding extra materials to enhance fitness and durability of the foot.
- **Fibre Glass/Fibre Epoxy:** widely used in flexile keel of conventional feet such as SACH and Seattle foot and also in low impact ESAR feet.
- **Nylon 66:** widely used in prosthetic foot clamps. Nylon 66 is more effective than the other flexible and strong materials such as high density polyethylene, polypropylene, Delrin, copolymers and reinforced nylon (Valenti, 1990).
- **Polyurethane:** widely used in conventional foot such as SACH and Seattle foot as a filler to provide an aesthetically pleasing and durable cosmetics

Ranjan et al (2009). A low density Polyurethane can also be used as a foot heel to absorb energy.

- **Aluminium:** widely used in prosthetic feet pylons.

The advantage and disadvantage of the materials are described in Table 5.4 and are given by Rihs and Polizzi (2001).

Table 5.4. The advantage and disadvantage of the material proposed by Rihs and Polizzi (2001).

Materials	Advantage	Disadvantage
Carbon Fibre	• High stiffness • High Strength • Light weight • Creep resistance • Chemically inert • Superior bonding with resins	• Low shear modulus • Low impact strength • Brittle • Expensive
Kevlar, Aramid (polyp-phenyleneterphthalamide)	• High tensile strength • Light weight • Low density • Low cost fibers • Fatigue and stress resistance • Impact resistance • Creep resistance • Vibration damping resistance	• Poor adhesion to polymers • Low compressive strength • Moisture absorber
Fibre Glass/Fibre Epoxy	• Accept high filler levels • Wide curing latitude • Inexpensive Tooling • Thermosetting Material	• Poor bonding to resins • Poor resistance to solvents • Upper service temperature limited to 93^0C
Nylon 66	• Low coefficient of friction • Tough, strong and impact resistance • Abrasion resistance • Process able by thermoplastic methods	• High moisture absorption with related dimensional stability • High shrinkage in mould

	• Resistance to base • Good solvent resistance	• Mechanical and electrical properties influenced by moisture content • Subject to attack by strong acids and oxidizing agents
Polyurethane	• Very good chemical resistance • Easy processability • Low cost • Excellent insulator	• Low tensile strength • Environmental stress cracking • Lack of rigidity • Poor scratch resistance
Aluminium	• High corrosion resistance • Lightweight • Low Density • 100% recyclable • Easy prosesability	• Low elastic modulus • Expensive compared to alternative metals • Susceptible to fatigue more than alternative metals

5.3.3 Mesh and Force Sensitivity Studies:

As discussed in Section 5.2, the force plate measured data at 1200 Hz. This generated excessively large number of ground reaction forces that are not necessary for the subsequent finite element analysis. For a force sensitivity study, a number of ground reaction forces were applied to the foot profile at different time intervals. The larger the time interval, the lower is the number of ground reaction forces applied along the foot profile. To study the dependence of number of forces applied on the deflection profile of the prosthetic foot, the ground reaction forces measured at time periods 0.2Sec, 0.1Sec, 0.04Sec, 0.03Sec, 0.02Sec and 0.01Sec are applied and the resulting deflection curves are shown in Figure 5.13. Note that the total stance leg duration is 0.45 seconds. It is seen that the deflection profile converges after 0.04 seconds. A time period value of 0.01 seconds is chosen for sampling ground reaction forces and is used for all examples in this study.

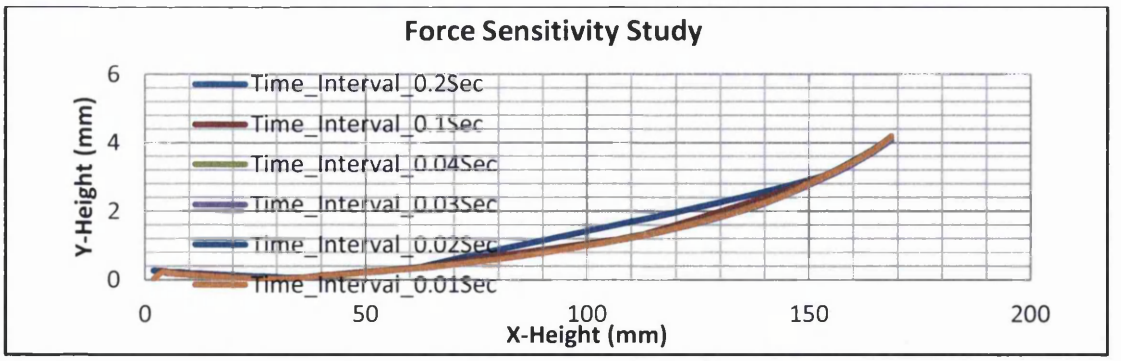

Figure 5.13. The graph represents the force sensitivity study performed using time intervals of 0.2Sec, 0.1Sec, 0.04Sec, 0.03Sec, 0.02Sec and 0.01Sec.

Once the time period independent results were obtained, the next step is to perform a mesh sensitivity study for each finite element analysis model. The results obtained during the mesh sensitivity study for each finite element model are shown in Figures 5.14, 5.15 and 5.16. The Figures 5.14 and 5.16 indicate that the ESAR_1 and SACH foot deflection for all specified element sizes is identical indicating that mesh independent results were achieved. The graph 5.15 on the other hand indicates that the element size course default is not accurate for effective simulation and thus the minimum element size allowable for a meaningful simulation is 6mm.

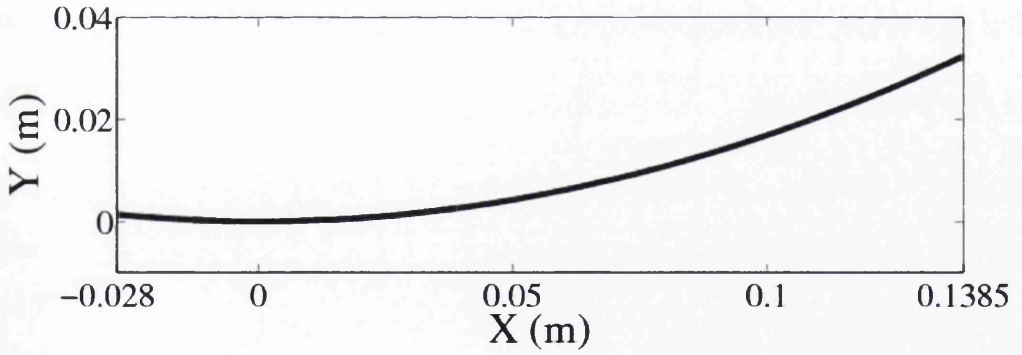

Figure 5.14. Mesh sensitivity study of the ESAR_1 foot. Solid curve shows the simulations with four different mesh sizes (coarse default, 6mm, 5mm, and fine default).

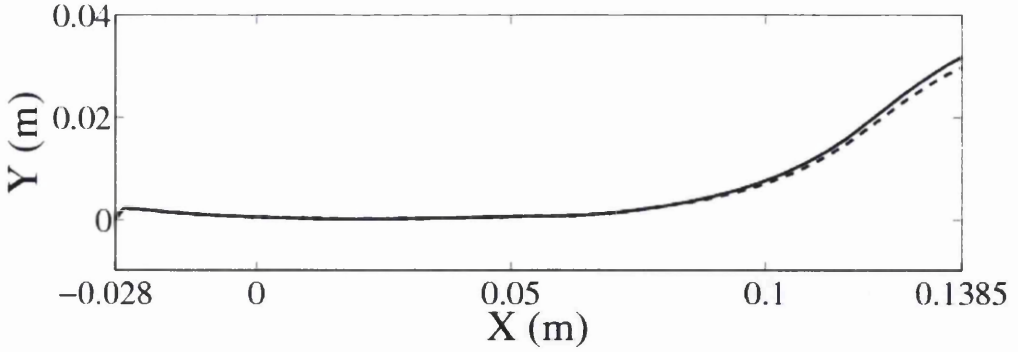

Figure 5.15. Mesh sensitivity study of the ESAR_2 foot. Solid curve shows the simulations with three different mesh sizes (6mm, 5mm, and fine default). The dashed curve shows the deflection curve for coarse default option.

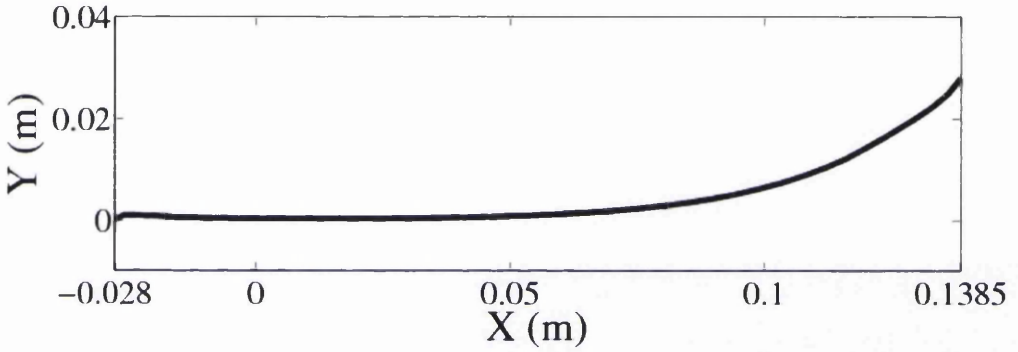

Figure 5.16. Mesh sensitivity study of the SACH foot. Solid curve shows the simulations with four different mesh sizes (coarse default, 6mm, 5mm, and fine default).

5.4 Discussion on Results

For each design case study (ESAR_1, ESAR_2 and SACH) three design iterations were undertaken to match the resulting deflection curve with the given roll-over shape. The material and geometry modifications performed for each simulation are as follows:

5.4.1 ESAR_1 design case study

In this case study, the material of front leaf spring (and hence its properties) of the ESAR_1 foot is changed in two design iterations from Ultra High Modulus Carbon Fiber to High strength Carbon Fiber and then to High strength carbon fiber epoxy. The corresponding material properties are tabulated in Table 5.5. The corresponding

deflection curves for original design and design iterations 1 and 2 are shown along with the given roll-over shape (ROS).

Table 5.5. Material properties assigned to the finite element model ESAR_1 for each simulation

Material Properties				
Initial Design				
Material	Ultra High Modulus Carbon Fiber	Ultra High Modulus Carbon Fiber	Structural Steel	Polypropylene
Properties	Front L. Spring	Rear L. Spring	Connector	Foot Sole
Density	2160kg/m3	2160kg/m3	7850kg/m3	905kg/m3
Young's Modulus	8.3E+05Mpa	8.3E+05Mpa	2E+11Pa	1000Mpa
Poisson Ratio	0.2	0.2	0.3	0.4103
Design iteration 1				
Material	***High Strength Carbon Fiber***	Ultra High Modulus Carbon Fiber	Structural Steel	Polypropylene
Properties	***Front L. Spring***	Rear L. Spring	Connector	Foot Sole
Density	***1540kg/m3***	2160kg/m3	7850kg/m3	905kg/m3
Young's Modulus	***65000Mpa***	8.3E+05Mpa	2E+11Pa	1000Mpa
Poisson Ratio	***0.058***	0.2	0.3	0.4103
Design iteration 2				
Material	***High Strength Carbon Fiber Epoxy***	Ultra High Modulus Carbon Fiber	Structural Steel	Polypropylene
Properties	***Front L. Spring***	Rear L. Spring	Connector	Foot Sole
Density	***1580kg/m3***	2160kg/m3	7850kg/m3	905kg/m3
Young's Modulus	***56000***	8.3E+05Mpa	2E+11Pa	1000Mpa
Poisson Ratio	***0.307***	0.2	0.3	0.4103

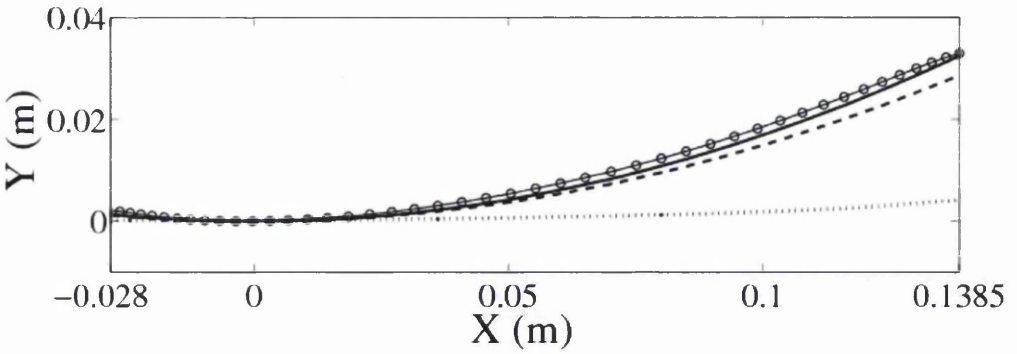

Figure 5.17. Simulated deflection curves during design iterations are compared with the given roll-over shape (ROS) (solid curve with circles) for ESAR_1 design case study. The deflection curve for the initial design is shown by dotted curve and the final design iteration is shown with a solid curve.

It can be noted from Figure 5.17 that the initial material assigned to the front leaf spring was stiffer than the required amount as the corresponding curve hasn't deflected enough to match the given roll-over shape. It was apparent that in order to improve the current results, less stiff material had to be assigned to the front leaf spring in order to allow the foot to deflect. During the first design iteration, as shown in Table 5.5, the material assigned to the front leaf spring was changed to High Strength Carbon Fiber to allow more dorsiflexion. The corresponding deflection curve improved considerably but the results indicated that the stiffness was slightly more than the required amount (Figure 5.17). It was possible to further improve the matching of deflection curve with the given roll-over shape by replacing the material to High Strength Carbon Fiber Epoxy. The simulated data indicated that the deflection curve was approximately equal to the given roll-over shape. In this case study, it was not necessary to change the geometry of the prosthetic foot.

5.4.2 ESAR_2 design case study

In design iteration 1, the materials for the front and real leaf springs of the ESAR_2 foot geometry are changed from Nylon66 (30% carbon fiber) and Ultra high modulus carbon fiber to Syndiotactic polystyrene (10% carbon fiber) and high strength carbon fiber respectively. As shown in Figure 5.19, this design change was not sufficient to

generate a deflection curve that is similar to the given roll-over shape. The thickness of the front leaf spring was reduced with the material properties as given in the design iteration 1 (Figure 5.18). The corresponding deflection curves for original design and design iterations 1 and 2 are shown in Figure 5.19 along with the given roll-over shape.

Table 5.6. Material properties assigned to the finite element model ESAR_2 for each simulation.

Material Properties					
Initial design					
Material	Nylon66 (30% Carbon Fiber)	Ultra High Modulus Carbon Fiber	Structural Steel	Polyethylene	Aluminum
Properties	Front L. Spring	Rear L. Spring	Connector	Foot Sole	Pylon
Density	1280kg/m3	2160kg/m3	7850kg/m3	880kg/m3	3270kg/m3
Young's Modulus	22100Mpa	8.3E+05Mpa	2E+11Pa	550Mpa	3.23E+05MPa
Poisson Ratio	0.3148	0.2	0.3	0.419	0.3
Design iteration 1					
Material	***Syndiotactic Polystyrene (10% Carbon Fiber)***	***High Strength Carbon Fiber***	Structural Steel	Polyethylene	Aluminum
Properties	***Front L. Spring***	***Rear L. Spring***	Connector	Foot Sole	Pylon
Density	***1069kg/m3***	***1630kg/m3***	7850kg/m3	880kg/m3	3270kg/m3
Young's Modulus	***7410Mpa***	***45700Mpa***	2E+11Pa	550Mpa	3.23E+05MPa
Poisson Ratio	***0.3629***	***0.311***	0.3	0.419	0.3

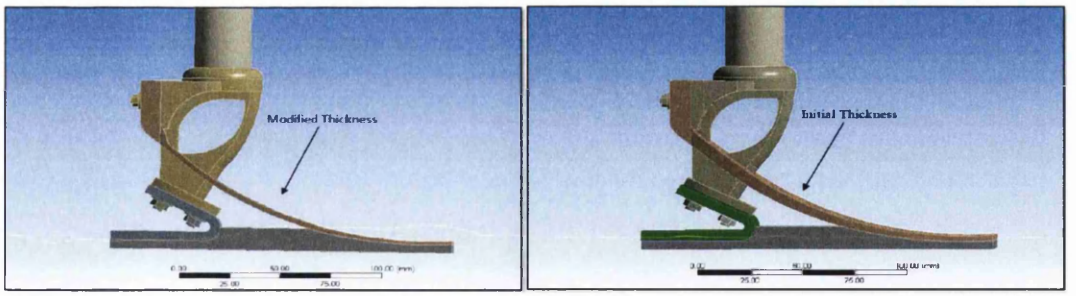

Figure 5.18. Design iteration 2: The thickness of the ESAR_2 foot front leaf spring is reduced.

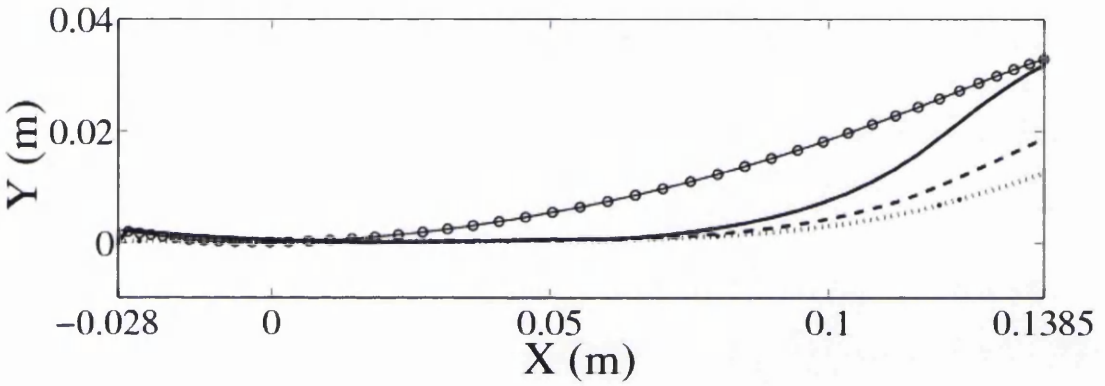

Figure 5.19. Simulated deflection curves during design iterations are compared with the given roll-over shape (ROS) (solid curve with circles) for ESAR_2 design case study. The deflection curve for the initial design is shown by dotted curve and the final design iteration is shown with a solid curve.

The deflection curve obtained by assigning the initial materials to the ESAR_2 foot (Figure 5.19) indicated that the front and rear leaf spring components were stiffer than necessary. In order to increase deflection, more elastic materials (Syndiotactic polystyrene (10% carbon fiber)) and high strength carbon fiber were assigned to the front and rear leaf spring components respectively with properties as displayed in Table 5.6. It was found that by changing the materials, the deflection profile was improved but not to the desired level. In order to increase the deflection even further and improve dorsiflexion, the front leaf spring component was modified by reducing its thickness (see Figure 5.18). It can be noted from the deflection curve for the design iteration 2 in Figure 5.19 that peak deflection was improved and was

approximately equal to the given roll-overs shape. However, despite this design change, the deflection from 0.012m to 0.138m of roll-over distance (plotted on x-axis in Figure 5.19) was limited and as a consequence, the dorsiflexion of the foot is limited in this regions. This may be due to the rigid pylon. This effect did not occur in the ESAR_1 foot geometry. Perhaps, this may be due to fact that the pylon utilised the entire distance to the socket for its function and as a result of this, was able to deflect/deform along its entire length and allow the appropriate amount of dorsiflexion to be achieved.

5.4.3 SACH design case study

In design iteration 1, the Belting material of the SACH foot is changed from Wrought aluminium alloy to Polypropylene (10% calcium carbonate filled) whereas the belting thickness was reduced to lower the stiffness and increase the deflection in the second design iteration. The material properties are shown in Table 5.7 and the design change of belting thickness reduction is shown in Figure 5.20. The corresponding deflection curves for original design and design iterations 1 and 2 are shown in Figure 5.21 along with the given roll-over shape.

Table 5.7. Material properties assigned to the finite element model SACH for each simulation.

Material Properties						
Initial Design						
Material	Polypropylene	Wrought Aluminium Alloy	Polyvinylchloride Foam	Willow Wood	Aluminium	Aluminium
Properties	Heel	Belting	Foot Shell	Keel	Pylon	Pylon's R. Ring
Density	905kg/m3	2699kg/m3	78kg/m3	310kg/m3	3270kg/m3	3270kg/m3
Young's	1000Mp	68000Mpa	80MPa	7100Mp	3.23E+05M	3.23E+05MP

Modulus	a			a	Pa	a
Poisson Ratio	0.4103	0.33	0.31	0.35	0.3	0.3
Design Iteration 1						
Material	Polypropylene	**Polypropylene (10% Calcium Carbonate Filled).**	Polyvinylchloride Foam	Willow Wood	Aluminium	Aluminium
Properties	Heel	**Belting**	Foot Shell	Keel	Pylon	Pylon's R. Ring
Density	905kg/m3	**1060kg/m3**	78kg/m3	310kg/m3	3270kg/m3	3270kg/m3
Young's Modulus	1000Mpa	**2050Mpa**	80MPa	7100Mpa	3.23E+05MPa	3.23E+05MPa
Poisson Ratio	0.4103	**0.3944**	0.31	0.35	0.3	0.3

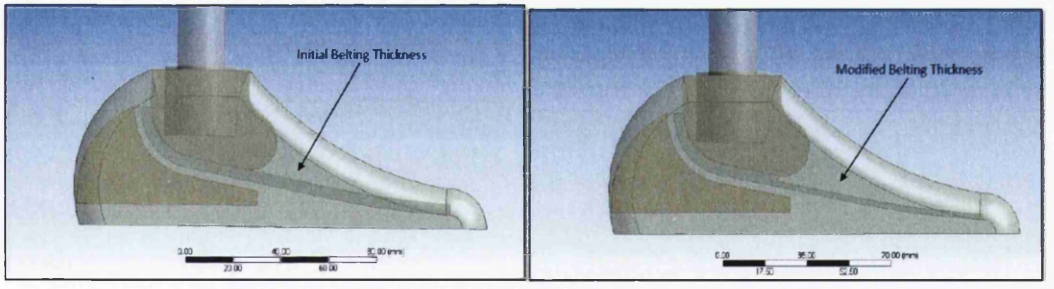

Figure 5.20. The second design iteration for the SACH foot design. The belting thickness is reduced.

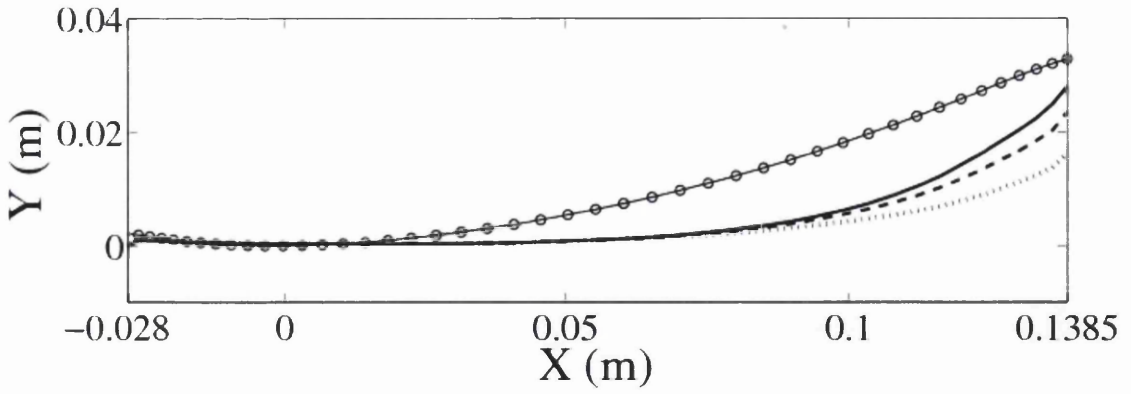

Figure 5.21. Simulated deflection curves during design iterations are compared with the given roll-over shape (ROS) (solid curve with circles) for SACH design case study. The deflection curve for the initial design is shown by dotted curve and the final design iteration is shown with a solid curve.

It is clear that the use of a comparatively pliable material for the belting and the subsequent reduction of the belting thickness have not produced a satisfactory match of the deflection curve with the given roll-over shape.

The reasons for the continued stiff design of a SACH foot may attributed to the rigid pylon that is unable to deflect and allow additional dorsiflexion and also the rigid keel that is attached to the belting restricting deflection due to its length.

5.5 Conclusion

The human foot has complex knee, ankle, muscle and bone structure support that creates a deformation pattern that can be characterised by a roll-over shape and the ground reaction combination. As indicated by the literature review, the biological ankle-foot system maintains a consistent roll-over shape during steady state walking on level ground, and that is considered as invariant with walking speed, added weight and shoe heel height. It is shown that it is possible to predict ground reaction forces computationally for a given roll-over shape data. However, the passive model as described in Chapters 3 and 4 and extended in this Chapter is not sufficient to model the ground reaction forces accurately. Future research incorporating active elements in the computational model is necessary.

Despite the fact that the utility of the roll-over shape has been explored and discussed by many prosthetic researchers, the use of roll-over shapes with corresponding ground reaction forces as a joint design parameter for optimising prosthetic foot has been considered for the first time. It is proposed that the resultant stiffness profile of a prosthetic foot can be optimised to generate a desired deformation pattern in the foot as described by a roll-over shape when subjected to the corresponding set of transient ground reaction forces. Three design guidelines have been proposed and a design flow chart is given to input experimentally determined roll-over shape and ground reaction force information.

The stiffness profile of three design geometries, two Energy storing and returning (ESAR) feet and on SACH foot geometry, was optimised to produce a deflection curve similar to an experimentally determined roll-over shape for a physiological foot of an able bodied person. The prosthetic feet were subjected to the corresponding transient ground reaction forces that were also measured during the experiment. The ESAR_1 geometry was found to be the most suitable design for realising deflections similar to the roll-over shape. Only changes in the material properties were sufficient to optimise the ESAR_1 geometry. However, the finite element analysis suggested that the pylon design of ESAR_2 geometry and the SACH foot did not allow the prosthetic foot to become pliable. ESAR_2 geometry required reduction of spring thickness to improve the deflection curve where as for the SACH foot the reduction in the belting thickness was also not sufficient to make the foot pliable.

It is expected that the proposed novel design methodology is likely to help prosthetic foot designers to gain further insights in the deformation behavior of the prosthetic foot by making them more complaint to their biological counterparts and thus more comfortable and energy efficient for an amputee.

Chapter 6 Conclusion

In this thesis, work has been undertaken in the following areas:

- Computational modelling of bipedal walking based on roll-over shapes.
- Investigation of walking symmetry of lower limp amputees with unbalanced legs mass using the passive bipedal model.
- Optimising and comparing three types of prosthetic feet using finite element analysis.

The following subsections draw out the conclusions and identify possible directions for future work within the topic.

6.1 Computational modelling of bipedal walking with roll-over shape

A computational investigation into the effect of roll-over shape, slope angle, mass ratio and length ratio on bipedal walking stability and gait parameters such as average velocity, mechanical energy, step period and inter-leg angle has been performed. A passive locomotion of a two linked biped with three lumped masses located on legs and hip joint has been studied with a roll-over shape attached to the ankle joint. A roll-over shape characterised all three sections of the stance legs rolling motion viz the heel area (hindfoot), middle of roll-over shape (midfoot) and toe area (forefoot). The roll-over shape was defined by a piecewise polynomial function with three sub functions corresponding to the roll-over shape sections. In order to explore heel to toe rolling motion, the roll-over shape is descritised with multiple pivot points and the hybrid dynamics of a walking step has been described by three different phases namely single support phase, single support leg transition phase and double support transition phase. A nonlinear differential equation has been introduced to analyse the double pendulum motion during the single support phase and the conservation of angular momentum has been used to determine gait

descriptors during transition phases. Rolling motion of a disk on an inclined surface and rolling motion of the bipedal walking for a fixed roll-over shape have been investigated to validate the proposed discrete pivot point model. Convergence of the step period and inter-leg angle were observed for high number of pivot points (e.g. 3000 pivot points). Bifurcation diagrams and the phase plane limit cycle have been introduced to explore the range of symmetric walking and also the effect of changing bipedal parameters (e.g. ground slope angle, mass ratio, length ratio) on gait descriptors (e.g. average velocity, step period, mechanical energy or inter-leg angle). The results from the bipedal model with roll-over shape were compared with point feet model presented by Goswami et al. (1996). The influence of the roll-over shape and bipedal parameters on gait descriptors has been studied. Interestingly, the inter-leg angle [delta] was found to remain almost constant for different roll-over shapes.

6.2 Investigation of walking symmetry of lower limp amputees with unbalanced legs mass using the passive bipedal model

A two link passive bipedal model with a realistic roll-over shape and masses for physiological, prosthetic leg and upper body has been proposed with the aim of exploring the effect of prosthetic foot roll-over shape on symmetry of walking. For this purpose, the hybrid dynamics of bipedal walking has been enhanced to be able to analyse the bipedal gait with different legs mass values and COM. The symmetry of walking has been investigated with a lighter prosthetic leg as compared to the physiological leg. Inter-leg angle and step period values are used for the evaluation of the asymmetry of walking. The results concluded that by decreasing legs mass ratio and length ratio the symmetric walking becomes asymmetric, chaotic and then unstable. It was discovered that by adjusting the roll-over shape, asymmetric walking with unbalanced leg mass becomes symmetric with respect to inter-leg angle or step period but not both at the same time.

Optimal roll-over shapes have been determined with respect to the roll-over gain and the forefoot arc length. Three different body weights (small, mid and large) and two different physiological roll-over gain (1.5 and 2.5) were used to explore the effect of body weight and roll-over gain on the optimum area of the prosthetic foot roll-over

shape respectively. A nonlinear inverse proportion between the roll-over gain and forefoot arc length was observed within an optimum area. Phase plane limit cycle was used to investigate the effect of optimising roll-over shape with reference to the inter-leg angle and the step period on symmetry of walking. It was clearly seen that gait descriptors are more symmetric when the roll-over shape was optimised with respect to the inter-leg angle as compared to the step period.

6.3 Optimising and comparing three types of prosthetic feet using Finite Element Analysis

An experimental work has been performed to measure a roll-over shape of a subject by determining the position of COP with respect to Ankle-Foot coordinate system using force plate data, motion analysis software (Quintic Biomechanics) and MATLAB software. The force plate data captured the position of COP at each time step with reference to the global coordinate system. The kinematics of the ankle and knee joint was analysed by commercial Quintic Biomechanics software that used the data captured by motion cameras. The resulting roll-over shape was finally calculated using a MATLAB script by synchronising the data given by the force plate and Quintic software. Ground reaction forces (GRFs) have been measured at each time step by using a force plate during a walking step.

A novel design process, based on a finite element modelling method, has been illustrated by optimally designing a conventional (SACH) foot and two energy storing and returning (ESAR) feet so that the deflection of the feet under GRFs matches with the measured roll-over shape.

6.4 Future Research

The biped model that was considered in this thesis has been based on a two-linked planar passive model with the rolling motion of the foot contact modelled by a roll-over shape. However, human bodies possess more degrees of freedom (DOF), 3D motion and are able to power their body joints during walking. Therefore, the future

work challenge is to extend the proposed model with a predictive dynamics model that is linked with neuromuscular data and is active but retains as many passive elements as possible to maximise the human energy efficiency. The efficacy of this model can be measured using biomechanical models of human motion involving quantification of ground reaction forces, moments and classification of function based on signals generated *in vivo* during measurement of gait and activities of daily living, along with functional scores. The model can become 'smart' if it is linked with muscles within the intact part of the body using Electromyography (EMG) sensors and signals. Looking ahead, for the active prosthesis to remain light weight and autonomous, novel power harvesting and power management solutions will need to be developed.

Further investigation could also be conducted into the determination of the stiffness and damping of the foot and other body segments during a walking cycle and apply it into the computational model. The passive elements would then be optimised with respect to experimental data for joints kinematics and GRFs. The optimal passive model would be used to reach an optimal control design for a stable bipedal walking.

In Chapter 4, it was shown that optimising the prosthetic foot roll-over shape leads to less asymmetrical walking. Since the optimal roll-over shapes are based on the two-linked passive model, the recommended active model can replace the existing model to obtain more accurate optimal roll-over shape for individual amputees.

More work is also needed in order to reach an optimal prosthetic foot design so that the deflection of the foot under GRFs produce a roll-over shape which is almost identical to the desired shape. Therefore, a natural extension to the research would be incorporation of the dynamics of a bionic feet mechanism into existing finite element method presented in Chapter 5. This would enable the prosthetic foot to adapt with different walking or running situations automatically as characterised by a combination of optimal roll-over shapes and GRFs.

References

ADALARASU, K., JAGANNATH, M. & MATHUR, M. K. 2011. Comparison on Jaipur, SACH and Madras Foot. *INTERNATIONAL JOURNAL OF ADVANCED ENGINEERING SCIENCES AND TECHNOLOGIES,* 4, 187-192.

ADAMCZYK, P. G., COLLINS, S. H. & KUO, A. D. 2006. The advantages of a rolling foot in human walking. *J Exp Biol,* 209, 3953-63.

ALARANTA, H., LEMPINEN, V., HAAVISTO, E., POHJOLAINEN, T. & HURRI, H. 1994. Subjective benefits of energy storing prostheses. *Prosthet Orthot Int,* 18, 92-97.

ANDRYSEK, J. 2010. Lower-limb prosthetic technologies in the developing world: A review of literature from 1994-2010. *Prosthet Orthot Int,* 34, 378-98.

ARMSTRONG , H. G. 1988. *Anthropometry and Mass Distribution for Human Analogues* [Online]. Available: http://www.smf.org/docs/articles/hic/USAARL_88-5.pdf [Accessed 25 June 2013].

ARYA, A., LEES, A., NIRULA, H. & KLENERMAN, L. 1995. A biomechanical comparison of the SACH, Seattle and Jaipur feet using ground reaction forces. *Prosthet Orthot Int,* 19, 37-45.

ASANO, F., ZHI-WEI, L. & YAMAKITA, M. 2005. Biped Gait Generation and Control Based on a Unified Property of Passive Dynamic Walking. *Robotics, IEEE Transactions on,* 21, 754-762.

BAR-COHEN, Y. & BREAZEAL, C. 2003. *Biologically inspired intelligent robots*, SPIE-The International Society for Optical Engineering.

BELLMAN, R. D., HOLGATE, M. A. & SUGAR, T. G. Year. SPARKy 3: Design of an active robotic ankle prosthesis with two actuated degrees of freedom using regenerative kinetics. *In:* Biomedical Robotics and Biomechatronics, 2008. BioRob 2008. 2nd IEEE RAS & EMBS International Conference on, 19-22 Oct. 2008 2008. 511-516.

BERGELIN, B. J. & VOGLEWEDE, P. A. 2012. Design of an Active Ankle-Foot Prosthesis Utilizing a Four-Bar Mechanism. *Journal of Mechanical Design,* 134, 061004-061004.

BONNET, X., PILLET, H., FODE, P., LAVASTE, F. & SKALLI, W. 2012. Finite element modelling of an energy-storing prosthetic foot during the stance phase of transtibial amputee gait. *Proc Inst Mech Eng H,* 226, 70-5.

BURKE, M. J., ROMAN, V. & WRIGHT, V. 1978a. Bone and joint changes in lower limb amputees. *Ann. Rheum. Dis,* 37, 252-254.

BURKE, M. J., ROMAN, V. & WRIGHT, V. 1978b. Bone and joint changes in lower limb amputees. *Annals of the Rheumatic Diseases,* 37, 252-254.

CHAS-A-BLATCHFORD-AND-SONS-LTD. 2013. Chas A Blatchford and Sons Ltd. Available: http://www.endolite.co.uk/products/type/feet [Accessed 25/06 2013].

CHOI, H. S., PARK, H. L. & KIM, Y. H. Year. Foot-Ankle Roll-Over Characteristics in Different Heel Heights during Walking. *In:* Engineering in Medicine and Biology Society, 2005. IEEE-EMBS 2005. 27th Annual International Conference of the, 17-18 Jan. 2006 2005. 6882-6884.

COLLINS, S., RUINA, A., TEDRAKE, R. & WISSE, M. 2005. Efficient Bipedal Robots Based on Passive-Dynamic Walkers. *Science,* 307, 1082-1085.

COLLINS, S. H., WISSE, M. & RUINA, A. 2001. A Three-Dimensional Passive-Dynamic Walking Robot with Two Legs and Knees. *The International Journal of Robotics Research,* 20, 607-615.

CURTZE, C., HOF, A. L., VAN KEEKEN, H. G., HALBERTSMA, J. P. K., POSTEMA, K. & OTTEN, B. 2009. Comparative roll-over analysis of prosthetic feet. *Journal of Biomechanics,* 42, 1746-1753.

CZERNIECKI, J. M., GITTER, A. & WEAVER, K. 1994. Effect of alterations in prosthetic shank mass on the metabolic costs of ambulation in above-knee amputees. *Am J Phys Med Rehabil,* 73, 348-52.

DE LATEUR, B. J., GIACONI, R. M., QUESTAD, K., KO, M. & LEHMANN, J. F. 1991. Footwear and posture. Compensatory strategies for heel height. *Am J Phys Med Rehabil,* 70, 246-54.

DELISA, J. A. 1998. *Gait Analysis in the Science of Rehabilitation,* DIANE.

DONN, J. M., PORTER, D. & ROBERTS, V. C. 1989. The effect of footwear mass on the gait patterns of unilateral below-knee amputees. *Prosthet Orthot Int,* 13, 140-4.

DRONGELEN, S. V. 2000. *Energy storing feet: beneficial?*

ENGSBERG, J. R., LEE, A. G., PATTERSON, J. L. & HARDER, J. A. 1991. External loading comparisons between able-bodied and below-knee-amputee children during walking. *Arch Phys Med Rehabil,* 72, 657-661.

ESPY, D. D., YANG, F., BHATT, T. & PAI, Y. C. 2010. Independent influence of gait speed and step length on stability and fall risk. *Gait & Posture,* 32, 378-382.

FATONE, S. & HANSEN, A. H. 2007. Effect of ankle-foot orthosis on roll-over shape in adults with hemiplegia. *J Rehabil Res Dev,* 44, 11-20.

FREIDOVICH, L. B., METTIN, U., SHIRIAEV, A. S., SPONG, M. W. 2009. A Passive 2-DOF Walker: Hunting for Gaits Using Virtual Holonomic Constraints. *Robotics, IEEE Transactions on*, 25, 1202-1208.

FRIEDMANN, M. D. & LAWRENCE, W. 1972. *Amputations and prostheses in primitive cultures*, Spring.

GAILEY, R., ALLEN, K., CASTLES, J., KUCHARIK, J. & ROEDER, M. 2008. Review of secondary physical conditions associated with lower-limb amputation and long-term prosthesis use. *J Rehabil Res Dev,* 45, 15-29.

GAILEY, R. S., WENGER, M. A., RAYA, M., KIRK, N., ERBS, K., SPYROPOULOS, P. & NASH, M. S. 1994. Energy expenditure of trans-tibial amputees during ambulation at self-selected pace. *Prosthetics and Orthotics International,* 18, 84-91.

GARCIA, M., CHATTERJEE, A., RUINA, A. & COLEMAN, M. 1998. The simplest walking model: stability, complexity, and scaling. *J Biomech Eng,* 120, 281-8.

GARD, S. A. & CHILDRESS, D. S. 2001. What Determines the Vertical Displacement of the Body During Normal Walking? *J Prosthet Orthot,* 13, 64-67.

GENG, T., PORR, B. & WÖRGÖTTER, F. 2006. Fast Biped Walking with a Sensor-driven Neuronal Controller and Real-time Online Learning. *The International Journal of Robotics Research,* 25, 243-259.

GITTER, A., CZERNIECKI, J. & MEINDERS, M. 1997. Effect of prosthetic mass on swing phase work during above-knee amputee ambulation. *Am J Phys Med Rehabil,* 76, 114-21.

GITTER, A., CZERNIECKI, J. M. & DEGROOT, D. M. 1991. Biomechanical analysis of the influence of prosthetic feet on below-knee amputee walking. *Am J Phys Med Rehabil,* 70, 142-148.

GOSWAMI, A. 1999. Postural Stability of Biped Robots and the Foot-Rotation Indicator (FRI) Point. *The International Journal of Robotics Research,* 18, 523-533.

GOSWAMI, A., THUILOT, B. & ESPIAU, B. 1996. *Compass-like biped robot Part I: Stability and bifurcation of passive gaits* [Online]. Available: http://hal.inria.fr/inria-00073701/en/ [Accessed 2013].

GOSWAMI, A., THUILOT, B. & ESPIAU, B. 1998. A Study of the Passive Gait of a Compass-Like Biped Robot: Symmetry and Chaos. *The International Journal of Robotics Research,* 17, 1282-1301.

HAFNER, B. J., SANDERS, J. E., CZERNIECKI, J. M. & FERGASON, J. 2002. Transtibial energy-storage-and-return prosthetic devices: A review of energy concepts and a proposed nomenclature. *Journal of Rehabilitation Research and Developmen,* 39, 1-11.

HANSEN, A. H. 2002. *Roll-over Characteristics of Human Walking with Applications for Artificial Limbs.* PhD, Northwestern University.

HANSEN, A. H. & CHILDRESS, D. S. 2005. Effects of adding weight to the torso on roll-over characteristics of walking. *J Rehabil Res Dev,* 42, 381-90.

HANSEN, A. H. & CHILDRESS, D. S. 2009. Effects of shoe heel height on the roll-over shapes of prosthetic ankle-foot systems: implications for heel-height-adjustable components. *Journal of Prosthetics & Orthotics,* 21, 48-54.

HANSEN, A. H. & CHILDRESS, D. S. 2010. Investigations of roll-over shape: implications for design, alignment, and evaluation of ankle-foot prostheses and orthoses. *Disability Rehabilitation,* 32, 2201-2209.

HANSEN, A. H., CHILDRESS, D. S. & KNOX, E. H. 2000. Prosthetic foot roll–over shapes with implications for alignment of trans–tibial prostheses. *Prosthetics and Orthotics International,* 24, 205-215.

HANSEN, A. H., CHILDRESS, D. S. & KNOX, E. H. 2004a. Roll-over shapes of human locomotor systems: effects of walking speed. *Clinical Biomechanics,* 19, 407-414.

HANSEN, A. H., CHILDRESS, D. S. & MIFF, S. C. 2004b. Roll-over characteristics of human walking on inclined surfaces. *Human Movement Science,* 23, 807-821.

HANSEN, A. H., MEIER, M. R., SAM, M., CHILDRESS, D. S. & EDWARDS, M. L. 2003. Alignment of trans-tibial prostheses based on roll-over shape principles. *Prosthetics and Orthotics International,* 27, 89-99.

HANSEN, A. H., MEIER, M. R., SESSOMS, P. H. & CHILDRESS, D. S. 2006. The Effects of Prosthetic Foot Roll-Over Shape Arc Length on the Gait of Trans-Tibial Prosthesis Users. *Prosthetics and Orthotics International,* 30, 286-299.

HANSON, A. H., CHILDRESS, D. S. & KNOX, E. H. 1999. Roll-over shapes of prosthetic feet. *Gait & Posture,* 9, 126.

HASS, J., HERRMANN, J. M. & GEISEL, T. 2006. Optimal Mass Distribution for Passivity-Based Bipedal Robots. *The International Journal of Robotics Research,* 25, 1087-1098.

HEKMATFARD, M., FARAHMAND, F. & EBRAHIMI, I. 2013. Effects of prosthetic mass distribution on the spatiotemporal characteristics and knee kinematics of transfemoral amputee locomotion. *Gait & Posture,* 37, 78-81.

HITT, J., SUGAR, T., HOLGATE, M., BELLMAN, R. & HOLLANDER, K. 2009. Robotic transtibial prosthesis with biomechanical energy regeneration. *Industrial Robot: An International Journal,* 36, 441-447.

HITT, J. K., BELLMAN, R., HOLGATE, M., SUGAR, T. G. & HOLLANDER, K. W. Year. The SPARKy (Spring Ankle With Regenerative Kinetics) Project: Design and Analysis of a Robotic Transtibial Prosthesis With Regenerative

Kinetics. *In:* In: Proceedings of the ASME 2007 International Design Engineering Technical Conferences & Computers and Information in Engineering Conference IDETC/CIE 2007., 2007. 1587-1596.

HOBBELEN, D. G. E. & WISSE, M. 2008. Controlling the Walking Speed in Limit Cycle Walking. *The International Journal of Robotics Research,* 27, 989-1005.

HSU, M.-J., NIELSEN, D. H., LIN-CHAN, S.-J. & SHURR, D. 2006. The Effects of Prosthetic Foot Design on Physiologic Measurements, Self-Selected Walking Velocity, and Physical Activity in People With Transtibial Amputation. *Archives of Physical Medicine and Rehabilitation,* 87, 123-129.

HUANG, Y., CHEN, B., WANG, Q. & WANG, L. Year. Adding segmented feet to passive dynamic walkers. *In:* Advanced Intelligent Mechatronics (AIM), 2010 IEEE/ASME International Conference on, 6-9 July 2010 2010. 652-657.

HURLEY, G. R. B., MCKENNEY, R., ROBINSON, M., ZADRAVEC, M. & PIERRYNOWSKI, M. R. 1990. The role of the contralateral limb in below-knee amputee gait. *Prosthetics and Orthotics International,* 14, 33-42.

HURMUZLU, Y., GÉNOT, F. & BROGLIATO, B. 2004. Modeling, stability and control of biped robots—a general framework. *Automatica,* 40, 1647-1664.

HURWITZ, D. E., SUMNER, D. R. & BLOCK, J. A. 2001. Bone density, dynamic joint loading and joint degeneration. A review. *Cells Tissues Organs,* 169, 201-9.

ISAKOV, E., KEREN, O. & BENJUYA, N. 2000. Trans–tibial amputee gait: Time–distance parameters and EMG activity. *Prosthetics and Orthotics International,* 24, 216-220.

KIM, C. M. & ENG, J. J. 2004. Magnitude and pattern of 3D kinematic and kinetic gait profiles in persons with stroke: relationship to walking speed. *Gait & Posture,* 20, 140-146.

KLODD, E., HANSEN, A., FATONE, S. & EDWARDS, M. 2010. Effects of prosthetic foot forefoot flexibility on gait of unilateral transtibial prosthesis users. *J Rehabil Res Dev,* 47, 899-910.

KNOX, E. H. 1996. *The Role of Prosthetic Feet in Walking.* PhD PhD, Northwestern University.

KULKARNI, J., GAINE, W. J., BUCKLEY, J. G., RANKINE, J. J. & ADAMS, J. 2005. Chronic low back pain in traumatic lower limb amputees. *Clinical Rehabilitation,* 19, 81-86.

KUO, A. D. 1999. Stabilization of lateral motion in passive dynamic walking. *Int. J. Robot. Res,* 18, 917-930.

KURZ, M. J., JUDKINS, T. N., ARELLANO, C. & SCOTT-PANDORF, M. 2008. A passive dynamic walking robot that has a deterministic nonlinear gait. *Journal of Biomechanics,* 41, 1310-1316.

KWAN, M. & HUBBARD, M. 2007. Optimal foot shape for a passive dynamic biped. *Journal of Theoretical Biology,* 248, 331-339.

LA HERA, P. X. L. M., SHIRIAEV, A. S., FREIDOVICH, L. B., METTIN, U. & GUSEV, S. V. 2013. Stable Walking Gaits for a Three-Link Planar Biped Robot With One Actuator. *Robotics, IEEE Transactions on,* 29, 589-601.

LEE, W. C. C. & ZHANG, M. 2005. Design of monolimb using finite element modelling and statistics-based Taguchi method. *Clinical Biomechanics,* 20, 759-766.

LEHMANN, J., PRICE, R., BOSWELL-BESSETTE, S., DRALLE, A., QUESTAD, K. & DELATEUR, B. 1993. Comprehensive analysis of energy storing prosthetic feet: Flex Foot and Seattle Foot Versus Standard SACH foot. *Arch Phys Med Rehabil,* 74, 1225-31.

LI, J., TIAN, Y., HUANG, X. & CHEN, H. Year. Foot shape for passive dynamic kneed biped robot. *In:* Robotics and Biomimetics (ROBIO), 2010 IEEE International Conference on, 14-18 Dec. 2010 2010. 1281-1286.

MACFARLANE, P. A., NIELSEN, D. H., SHURR, D. G. & MEIER, K. 1991. Gait Comparisons for Below-Knee Amputees Using a Flex-Foot(TM) Versus a Conventional Prosthetic Foot. *J Prosthet Orthot,* 3, 150-161.

MAJOR, M. J., TWISTE, M., KENNEY, L. P. & HOWARD, D. 2011. Amputee Independent Prosthesis Properties--a new model for description and measurement. *J Biomech,* 44, 2572-5.

MARKOWITZ, J., KRISHNASWAMY, P., EILENBERG, M. F., ENDO, K., BARNHART, C. & HERR, H. 2011. Speed adaptation in a powered transtibial prosthesis controlled with a neuromuscular model. *Philosophical Transactions of the Royal Society B: Biological Sciences,* 366, 1621-1631.

MATTES, S. J., MARTIN, P. E. & ROYER, T. D. 2000. Walking symmetry and energy cost in persons with unilateral transtibial amputations: Matching prosthetic and intact limb inertial properties. *Archives of Physical Medicine and Rehabilitation,* 81, 561-568.

MCGEER, T. 1990. Passive Dynamic Walking. *The International Journal of Robotics Research,* 9, 62-82.

MEIER, M. R., STEER, S. A., HANSEN, A. H., M. SAM, D. S. & CHILDRESS. Available: http://www.nupoc.northwestern.edu/nupoc-research/lowerlimb/pdfs/manual_2_core.pdf [Accessed July 2013].

MIZUNO, N., AOYAMA, T., NAKAJIMA, A., KASAHARA, T. & TAKAMI, K. 1992. Functional evaluation by gait analysis of various ankle-foot assemblies used by below-knee amputees. *Prosthet Orthot Int,* 16, 174-82.

NARIOKA, K., TSUGAWA, S. & HOSODA, K. Year. 3D limit cycle walking of musculoskeletal humanoid robot with flat feet. *In:* Intelligent Robots and Systems, 2009. IROS 2009. IEEE/RSJ International Conference on, 10-15 Oct. 2009 2009. 4676-4681.

OMASTA, M., PALOUŠEK, D., NÁVRAT, T. & ROSICKÝ, J. 2012. Finite element analysis for the evaluation of the structural behaviour, of a prosthesis for trans-tibial amputees. *Medical Engineering & Physics,* 34, 38-45.

OPILA-CORREIA, K. A. 1990. Kinematics of high-heeled gait with consideration for age and experience of wearers. *Arch Phys Med Rehabil,* 71, 905-9.

PERRY, J. & SHANFIELD, S. 1993. Efficiency of dynamic elastic response prosthetic feet. *J Rehabil Res Dev,* 30, 137-143.

PLETTENBURG, D. H. Year. Basic requirements for upper extremity prostheses: the WILMER approach. *In:* Engineering in Medicine and Biology Society, 1998. Proceedings of the 20th Annual International Conference of the IEEE, 28 Oct-1 Nov 1998 1998. 2276-2281 vol.5.

POSTEMA, K., HERMENS, H. J., DE VRIES, J., KOOPMAN, H. F. J. M. & EISMA, W. H. 1997. Energy storage and release of prosthetic feet Part 1: Biomechanical analysis related to user benefits. *Prosthetics and Orthotics International,* 21, 17-27.

POWERS, C. M., TORBURN, L., PERRY, J. & AYYAPPA, E. 1994. Influence of prosthetic foot design on sound limb loading in adults with unilateral below-knee amputations. *Arch Phys Med Rehabil,* 75, 825-829.

RADIN, E. L., PARKER, H. G., PUGH, J. W., STEINBERG, R. S., PAUL, I. L. & ROSE, R. M. 1973. Response of joints to impact loading — III: Relationship between trabecular microfractures and cartilage degeneration. *Journal of Biomechanics,* 6, 51-57.

REMY, C. D., BUFFINTON, K. W. & SIEGWART, R. 2009. Stability Analysis of Passive Dynamic Walking of Quadrupeds. *The International Journal of Robotics Research.*

REN, L., HOWARD, D., REN, L., NESTER, C. & TIAN, L. 2010. A generic analytical foot rollover model for predicting translational ankle kinematics in gait simulation studies. *Journal of Biomechanics,* 43, 194-202.

RIHS, D. & POLIZZI, I. 2001. *Prosthetic Foot Design.* Victorian University of Technology.

ROBINSON, J. L., SMIDT, G. L. & ARORA, J. S. 1977. Accelerographic, temporal, and distance gait factors in below-knee amputees. *Phys Ther,* 57, 898-904.

ROMO, H. D. 1999. Specialized Prostheses for Activities: An Update. *Clinical Orthopaedics and Related Research,* 361, 63-70.

ROYER, T. D. & MARTIN, P. E. 2005. Manipulations of Leg Mass and Moment of Inertia: Effects on Energy Cost of Walking. *Medicine & Science in Sports & Exercise,* 37, 649-656.

SAGAWA JR, Y., TURCOT, K., ARMAND, S., THEVENON, A., VUILLERME, N. & WATELAIN, E. 2011. Biomechanics and physiological parameters during gait in lower-limb amputees: A systematic review. *Gait & Posture,* 33, 511-526.

SAM, M., HANSEN, A. H. & CHILDRESS, D. S. 2004. Characterisation of prosthetic feet used in low-income countries. *Prosthetics and Orthotics International,* 28, 132-140.

SAUNDERS, M. M., SCHWENTKER, E. P., KAY, D. B., BENNETT, G., JACOBS, C. R., VERSTRAETE, M. C. & NJUS, G. O. 2003. Finite element analysis as a tool for parametric prosthetic foot design and evaluation. Technique development in the solid ankle cushioned heel (SACH) foot. *Comput Methods Biomech Biomed Engin,* 6, 75-87.

SAWACHA, Z., CRISTOFERI, G., GUARNERI, G., CORAZZA, S., DONA, G., DENTI, P., FACCHINETTI, A., AVOGARO, A. & COBELLI, C. 2009. Characterizing multisegment foot kinematics during gait in diabetic foot patients. *J Neuroeng Rehabil,* 6, 1743-0003.

SINITSKI, E. H., HANSEN, A. H. & WILKEN, J. M. 2012. Biomechanics of the ankle–foot system during stair ambulation: Implications for design of advanced ankle–foot prostheses. *Journal of Biomechanics,* 45, 588-594.

SKINNER, H. B. & BARRACK, R. L. 1990. Ankle weighting effect on gait in able-bodied adults. *Archives of Physical Medicine and Rehabilitation,* 71, 112-115.

SMITH, J. D. & MARTIN, P. E. 2007. Walking patterns change rapidly following asymmetrical lower extremity loading. *Human Movement Science,* 26, 412-425.

SNYDER, R. D., POWERS, C. M., FONTAINE, C. & PERRY, J. 1995. The effect of five prosthetic feet on the gait and loading of the sound limb in dysvascular below-knee amputees. *J Rehabil Res Dev,* 32, 309-315.

SRINIVASAN, S., WESTERVELT, E. R. & HANSEN, A. H. 2009. A Low-Dimensional Sagittal-Plane Forward-Dynamic Model for Asymmetric Gait and Its Application to Study the Gait of Transtibial Prosthesis Users. *Journal of Biomechanical Engineering,* 131, 031003.

UNDERWOOD, H. A., TOKUNO, C. D. & ENG, J. J. 2004. A comparison of two prosthetic feet on the multi-joint and multi-plane kinetic gait compensations in individuals with a unilateral trans-tibial amputation. *Clinical Biomechanics,* 19, 609-616.

VALENTI, T. J. 1990. Experience with Endoflex: A Monolithic Thermoplastic Prosthesis for Below Knee Amputees. *J. Prosthetics and Orthotic* 3, 43-50.

VAN DER LINDE, H., HOFSTAD, C. J., GEURTS, A. C., POSTEMA, K., GEERTZEN, J. H. & VAN LIMBEEK, J. 2004. A systematic literature review of the effect of different prosthetic components on human functioning with a lower-limb prosthesis. *J Rehabil Res Dev,* 41, 555-70.

VENTURA, J. D., KLUTE, G. K. & NEPTUNE, R. R. 2011. The effects of prosthetic ankle dorsiflexion and energy return on below-knee amputee leg loading. *Clinical Biomechanics,* 26, 298-303.

VERSLUYS, R., BEYL, P., DAMME, M. V., DESOMER, A., HAM, R. V. & LEFEBER, D. 2009. Prosthetic feet: State-of-the-art review and the importance of mimicking human ankle–foot biomechanics. *Disability and Rehabilitation: Assistive Technology,* 4, 65-75.

VERSLUYS, R., DESOMER, A., LENAERTS, G., BEYL, P., VAN DAMME, M., VANDERBORGHT, B., VANDERNIEPEN, I., VAN DER PERRE, G. & LEFEBER, D. Year. From conventional prosthetic feet to bionic feet: A review study. *In:* Biomedical Robotics and Biomechatronics, 2008. BioRob 2008. 2nd IEEE RAS & EMBS International Conference on, 19-22 Oct. 2008 2008. 49-54.

VICKERS, D. R., PALK, C., MCINTOSH, A. S. & BEATTY, K. T. 2008. Elderly unilateral transtibial amputee gait on an inclined walkway: a biomechanical analysis. *Gait Posture,* 27, 518-29.

VUKOBRATOVIC, M. & BOROVAC, B. 2004. ZERO-MOMENT POINT — THIRTY FIVE YEARS OF ITS LIFE. *International Journal of Humanoid Robotics,* 01, 157-173.

VUKOBRATOVIC, M. & JURICIC, D. 1969. Contribution to the Synthesis of Biped Gait. *Biomedical Engineering, IEEE Transactions on,* BME-16, 1-6.

WAGNER, J., SIENKO, S., SUPAN, T. & BARTH, D. 1987. Motion analysis of SACH vs Flex-Foot in moderately active below-knee amputees. *Clinical Prosthetics & Orthotics,* 11, 55-62.

WANG, C. C. & HANSEN, A. H. 2010. Response of able-bodied persons to changes in shoe rocker radius during walking: Changes in ankle kinematics to maintain a consistent roll-over shape. *Journal of Biomechanics,* 43, 2288-2293.

WANG, Q., WEI, K., WANG, L. & LV, D. Year. Modeling and stability analysis of human normal walking with implications for the evolution of the foot. *In:* Biomedical Robotics and Biomechatronics (BioRob), 2010 3rd IEEE RAS and EMBS International Conference on, 26-29 Sept. 2010 2010. 479-484.

WATERS, R. L. & MULROY, S. 1999. The energy expenditure of normal and pathologic gait. *Gait & Posture,* 9, 207-231.

WESTERVELT, E. R. 2003. *Toward a Coherent Framework for the Control of Planar Biped Locomotion.* PhD, University of Michigan.

WESTERVELT, E. R., GRIZZLE, J. W., CHEVALLEREAU, C., CHOI, J. H. & MORRIS, B. 2007. *Feedback control of dynamic bipedal robot locomotion*, Taylor & Francis LLC.

WHITTLE, M. W. 1996. Clinical gait analysis: A review. *Human Movement Science,* 15, 369-387.

WILSON, A. B. 1972. *Limb Prosthetcs*, R.E. Krieger Publishing Company

N.Y. Huntington.

WIRTA, R. W., MASON, R., CALVO, K. & GOLBRANSON, F. L. 1991. Effect on gait using various prosthetic ankle-foot devices. *J Rehabil Res Dev,* 28, 13-24.

WISSE, M., HOBBELEN, D. G. E. & SCHWAB, A. L. 2007. Adding an Upper Body to Passive Dynamic Walking Robots by Means of a Bisecting Hip Mechanism. *Robotics, IEEE Transactions on,* 23, 112-123.